INFLUENCE OF BACKUP BEARINGS AND SUPPORT STRUCTURE DYNAMICS ON THE BEHAVIOR OF ROTORS WITH ACTIVE SUPPORTS

Final Report for Research Grant Number NAG3-1507

submitted to:

National Aeronautics and Space Administration
Lewis Research Center
Cleveland, Ohio 44135

by

George T. Flowers, Ph.D.
Associate Professor

Department of Mechanical Engineering
Auburn University
Auburn University, AL 36849-5341
Phone: (334) 844-3330

October, 1996

Final Report

This report presents a synopsis of the research work performed under grant number NAG3-1507. The goals of the research effort, as described in the grant proposal, have been fulfilled. Specific accomplishments are itemized below.

1. Experimental facilities have been developed. This includes a magnetic bearing test rig and an auxiliary bearing test rig. In addition, components have been designed, constructed, and tested for use with a rotordynamics test rig located at NASA Lewis Research Center. Photographs of the specific articles are shown in Appendix A.

2. The tasks performed under Grant No. NAG3-157 are detailed below. Papers that document the accomplishments of the research effort are included in Appendix B.

    i. A study of the rotordynamics of an auxiliary bearing supported T-501 engine model was performed. A paper documenting this work was presented at the *Symposium on Nonlinear and Stochastic Dynamics*, held at the *1994 ASME Winter Annual Meeting*, November 13-18, 1994, Chicago, Illinois. The paper has also been submitted to the *ASME Journal of Vibration and Acoustics*. An additional paper that discusses some of the work using the T-501 engine model has been presented at the *First Industry/University Symposium on High Speed Civil Transport Vehicles*, December 4-6, 1994, Greensboro, North Carolina.

    ii. An experimental/simulation study of auxiliary bearing rotordynamics has been performed. A paper that documents this work was presented at the *40th ASME International Gas Turbine and Aeroengine Conference*, June 5-8, 1995, Houston, Texas. An additional paper will be presented at the *ASME International Mechanical Engineering Conference and Exposition*, Nov. 17-22, 1996, Atlanta, Georgia.

    iii. A rotordynamical model for a magnetic bearing supported rotor system, including auxiliary bearing effects has been developed and simulation studies performed. A paper that documents this work was presented at the *ASME 15th Biennial Conference on Vibration and Sound*, Boston, Massachusetts, Sept. 17-21, 1995.

    iv. A finite element model for a foil bearing has been developed and studies of a rotor supported by foil bearings have been performed. A paper that documents the work was presented at the *1996 SDM Conference*, held in Salt Lake City, Utah, April 15-17, 1996.

3. Two students affiliated with this project have graduated with M.S. degrees - April M. Free and James L. Lawen, Jr. Ms Free is currently employed by Pratt and Whitney Aircraft Engines, Inc. (West Palm Beach, Florida) and Mr. Lawen is employed by the General Electric Corporate Research and Development Center (Schenectady, New York).

Bibliography

1. Flowers, G.T., and Wu, Fangsheng, "Disk/Shaft Vibration Induced by Bearing Clearance Effects: Analysis and Experiment," presented at *the Second Biennial European Joint Conference on Engineering Systems, Design, and Analysis (ESDA)*, July 4-7, London, England; also published in *ASME Journal of Vibration and Acoustics*, Vol. 118, pp. 204-208, April, 1996.

2. Flowers, G.T., Xie, Huajun, and Lawrence, C., "Steady-State Dynamic Behavior of an Auxiliary Bearing Supported Rotor System," presented at the *Symposium on Nonlinear and Stochastic Dynamics*, held at the *1994 ASME Winter Annual Meeting*, November 13-18, 1994, Chicago, Illinois; also submitted to the *ASME Journal of Vibration and Acoustics*.

3. Flowers, G.T., Xie, H., and Sinha, S.C., "Dynamic Behavior of a Magnetic Bearing Supported Jet Engine Rotor with Auxiliary Bearings," presented at the *First Industry/University Symposium on High Speed Civil Transport Vehicles*, Greensboro, North Carolina, December 4-6, 1994.

4. Lawen, James L., Jr., and Flowers, George T., "Synchronous Dynamics of a Coupled Shaft/Bearing/Housing System With Auxiliary Support From a Clearance Bearing: Analysis and Experiment," presented at the *40th ASME International Gas Turbine and Aeroengine Conference*, June 5-8, 1995; also accepted for publication in the *ASME Journal of Engineering for Gas Turbines and Power*.

5. Free, A., Flowers, George T., and Trent, Victor S., "Rotordynamic Modelling and Response Characteristics of a Magnetic Bearing Rotor System," presented at the *ASME 15th Biennial Conference on Vibration and Noise*, Sept. 17-21, 1995, Boston, Massachusetts; also, submitted to the *Journal of Vibration and Control*.

6. Li, Feng, and Flowers, George T., "Nonlinear Dynamics of a Foil Bearing Supported Rotor System: Simulation and Analysis," presented at the *37th AIAA/ASME/ASCE/AHS/ASC Structures, Structural Dynamics, and Materials Conference*, April 15-17, 1996, Salt Lake City, Utah.

7. Lawen, James L., Jr., and Flowers, George T., "Interaction Dynamics Between Flexible Rotor and an Auxiliary Clearance Bearing," to be presented at the *ASME International Mechanical Engineering Conference and Exposition,* Nov. 17-22, 1996; also submitted to the *ASME Journal of Vibration and Acoustics*, July 1996.

Appendix A - Photographs of Experimental Facilities

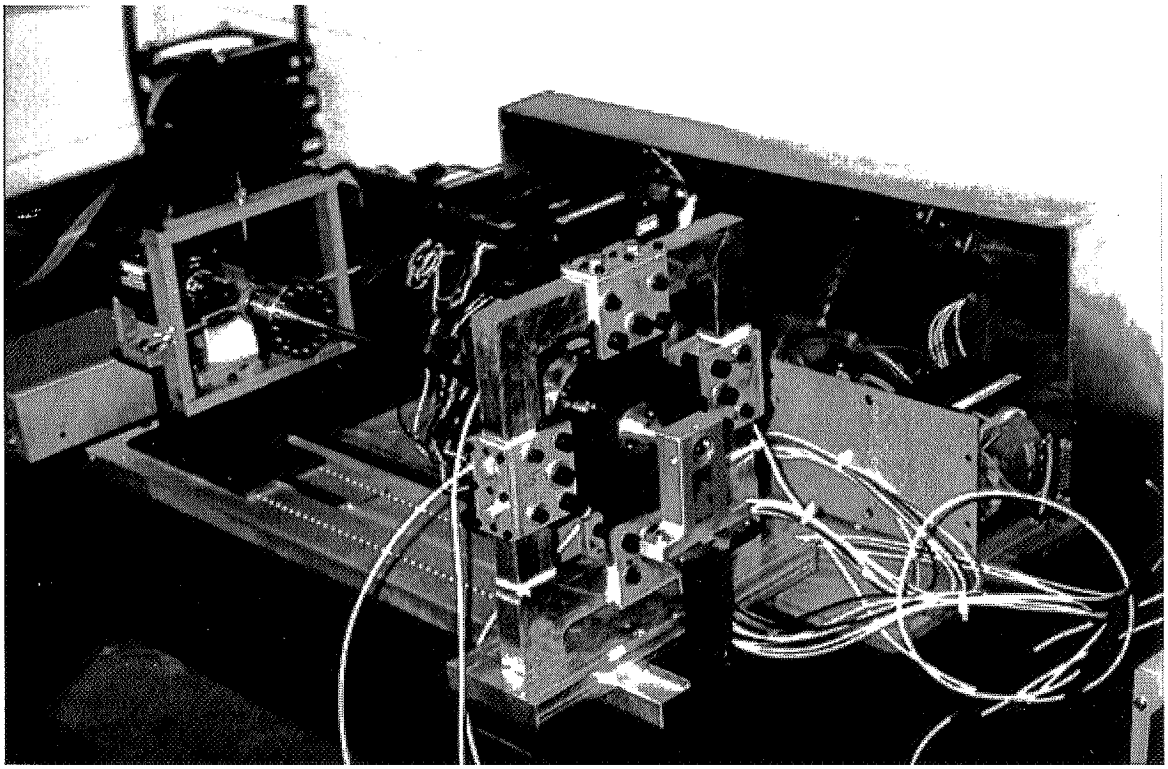

Figure 1: Magnetic Bearing Supported Rotor Test Rig

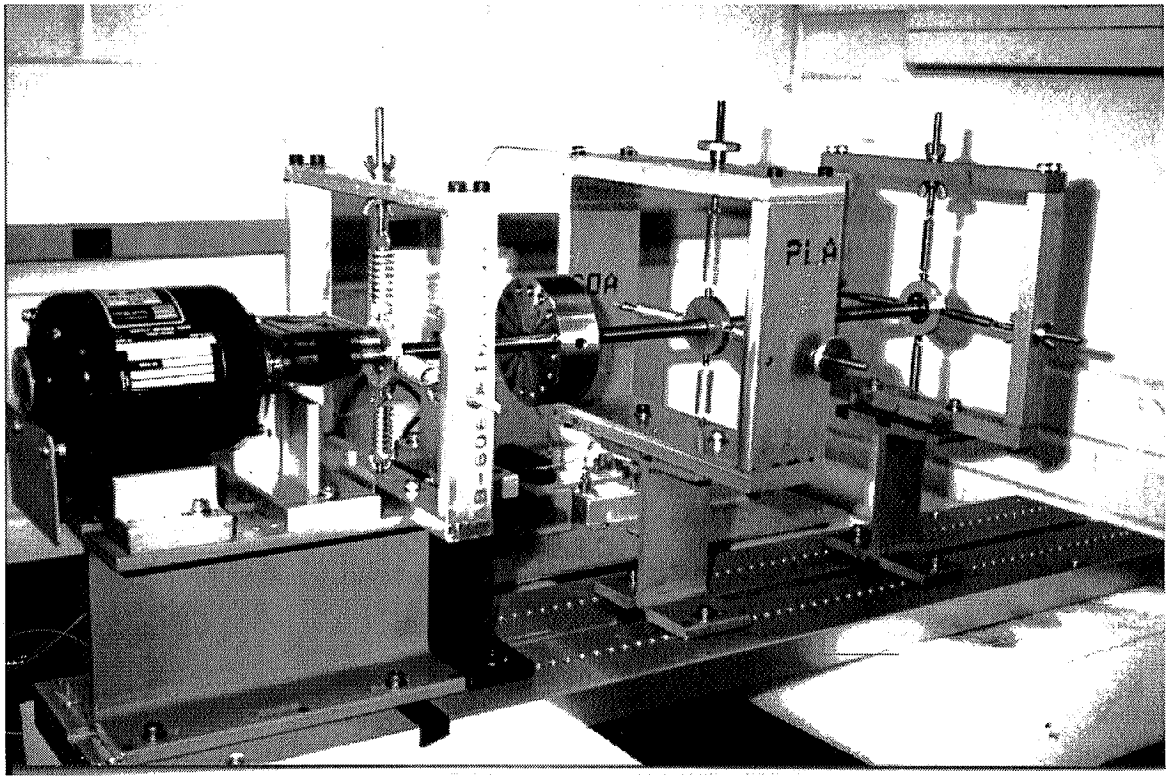

Figure 2: Auxiliary Bearing Rotor Test Rig

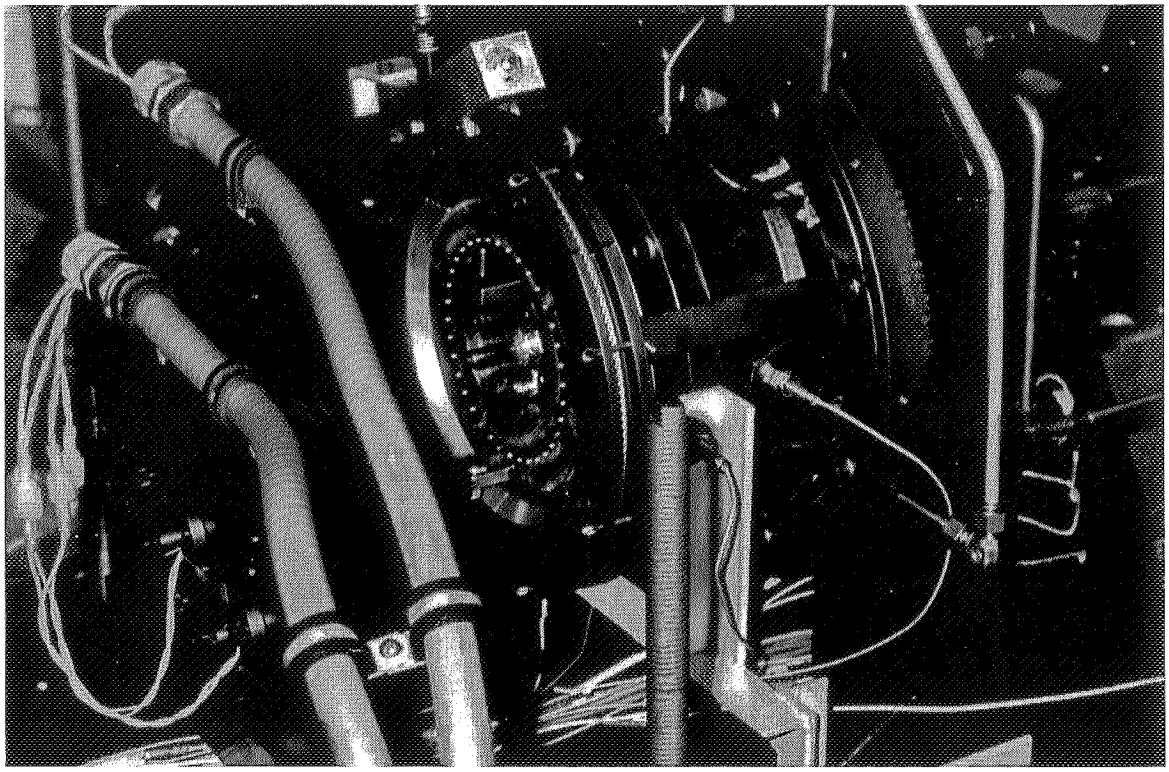

Figure 3.a: Auxiliary Bearing Test Component for use with NASA/Lewis Rotordynamics Test Rig (Overall View)

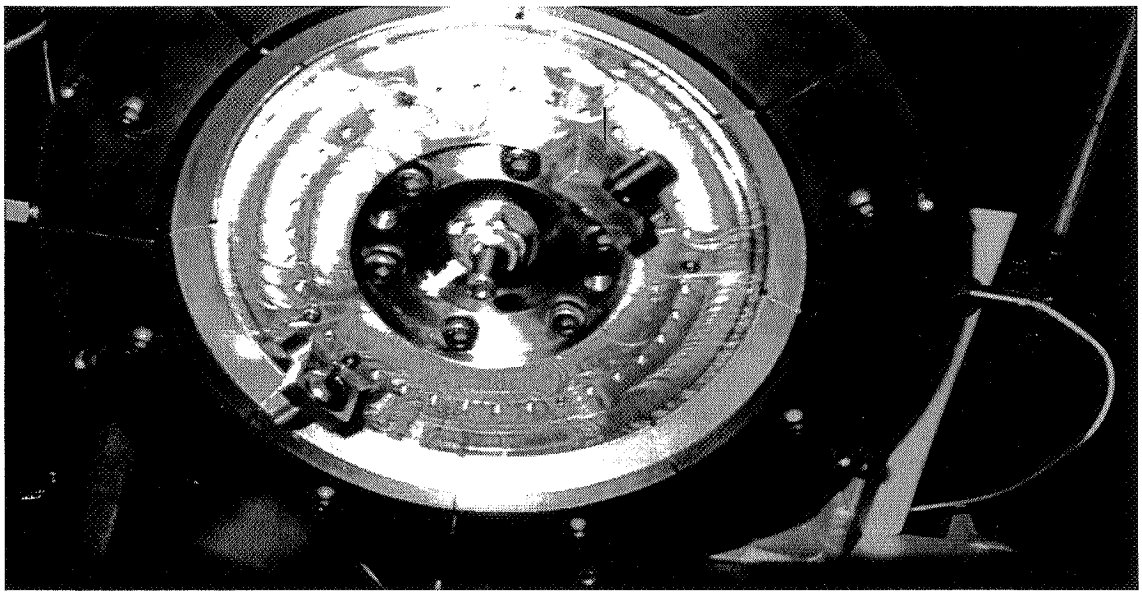

Figure 3.b: Auxiliary Bearing Test Component for use with NASA/Lewis Rotordynamics Test Rig (Close-up View)

Appendix B - Research Publications

Disk/Shaft Vibration Induced by Bearing Clearance Effects: Analysis and Experiment

G. T. Flowers

Fangsheng Wu

Department of Mechanical Engineering,
Auburn University,
Auburn, AL

This study presents an investigation of the dynamics of a rotor system with bearing clearance. Of particular interest is the influence of such effects on coupled disk/shaft vibration. Experimental results for a rotor system with a flexible disk are presented and compared to predictions from a simulation model. Some insights and conclusions are obtained with regard to the conditions under which such vibration may be significant.

Background and Motivation

Rotor systems typically consist of a shaft with one or more bladed disks attached. Disk and blade vibration are issues of important concern for stress analysts. Complex finite element models are developed to assess the dynamic stresses in such components and insure the integrity of the design. However, models for rotordynamical analyses are typically developed assuming that disk flexibility effects are negligible. It is generally presumed that the disk is sufficiently rigid so as to not significantly impact rotor vibration over the operating region.

There is a fairly large body of work documented in the literature concerning studies of disk flexibility on rotors and turbomachinery. A discussion of this previous work with regard to linear rotor systems is presented in Flowers and Ryan (1991). An excellent source for a comprehensive review of work in this area is presented by Davis (1989).

Previous investigators into the area of coupled rotor/disk vibration have noted that disk flexibility has little effect on critical speeds but that it may significantly influence higher natural frequencies of the rotor system (Chivens and Nelson, 1975). One can draw the conclusion from these results that synchronous vibration due to imbalance will be little affected by disk flexibility. However, there are sources of higher frequency excitation that could serve to excite these natural frequencies. Perhaps the most obvious are multi-synchronous effects corresponding to the blade pass frequency (from fluid forces impinging on the rotor blades). Another potential source is from nonlinearities that may be present in the system. For example, nonlinear bearing forces due to clearance effects may result in supersynchronous rotor vibration. There are quite a number of studies in the literature concerning the effects of bearing clearance (and the related phenomena of rubbing) on rotordynamical behavior. Some of the works that have most influenced the current study were conducted by Johnson (1962), Black (1968), Ehrich (1966), and Childs (1978), and Muszynska (1984).

Advanced designs for many types of high speed rotating machinery that use magnetic bearings for support have been proposed and are in the development and construction stages. There are a number of such systems already in commercial use. Rotor systems supported by magnetic bearings must have backup bearings to provide support under overload conditions or if the magnetic bearing fails. Backup bearings are characterized by a clearance between the rotor and the bearing such that contact does not occur under normal operating conditions. As a result, issues related to the effects of bearing clearance on rotordynamical behavior are of current concern. The objective of the present work is to develop an understanding of possible coupling between the dynamics of disk and shaft that may be induced by bearing clearance effects and to provide guidance to designers concerned with such systems.

Experimental Model

In order to investigate whether bearing clearance can lead to significant coupling between rotor and disk vibration, experimental tests were performed with a rotor test rig. A drawing of the test rig is shown in Fig. 1.

The rotor used in this study has two basic components: a flexible disk and a shaft. The steel shaft is 0.375 in. diameter and 16.0 inches long. The flexible disk is a circular aluminum plate 0.0125 inches thick and 14.0 inches in diameter. The natural frequency of its lowest one nodal diameter bending mode is about 40 Hz. It is attached with four bolts to a 2.0 inch diameter hub mounted with a press fit to the center of the shaft.

The rotor shaft is supported by bushings at two ends. The left end of the shaft is placed directly in the bushing base. This support provides a force but only a minimal couple so that the shaft is effectively free to pivot about this point. The right bearing is supported by a special device, which is designed to provide stiffness and to simulate bearing clearance. A diagram for this device is shown in Fig. 2. It has two sets of springs. The softer springs are to support the weight of the rotor, and the harder springs act as the main stiffness for the system. The stiffness in the x and y directions of each spring set may be different. The clearance is adjustable by turning the inner tapered ring in or out. In this experiment, the spring constant of

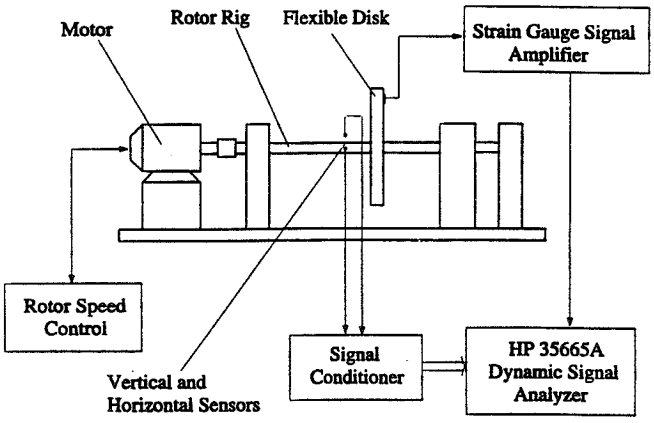

Fig. 1 Experimental test apparatus

Contributed by the Technical Committee on Vibration and Sound for publication in the JOURNAL OF VIBRATION AND ACOUSTICS. Manuscript received Feb. 1994. Associate Technical Editor: M. Ahmadian

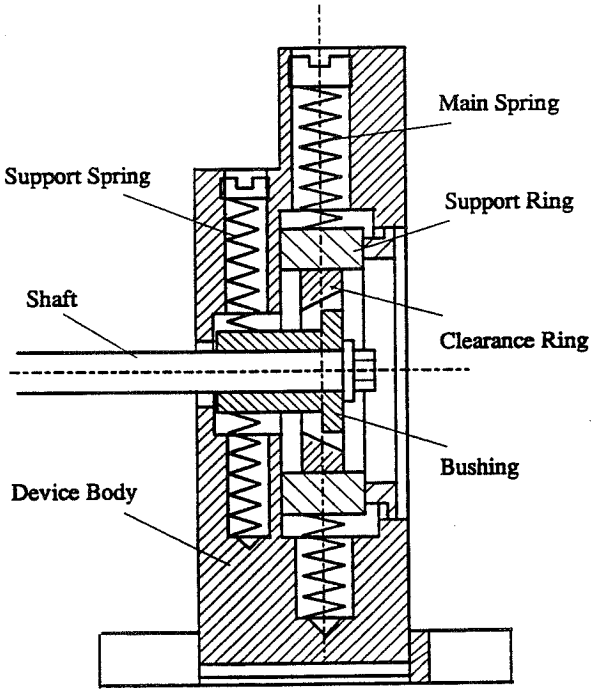

Fig. 2 Shaft right end support device

the soft spring is 1.9 lb/in. The spring constant of the hard spring is 8.1 lb/in. in the x_1 (horizontal) direction and 19.7 lb/in. in the x_2 (vertical) direction.

The rotor is driven by a speed adjustable motor. The speed of the rotor can be controlled by turning the speed control knob on the front panel of the control box. Shaft vibration was measured using eddy current proximity displacement sensors fixed so as to measure displacement in the vertical and horizontal directions. Strain gages mounted to the disk were used to measure the disk vibration. The strain gage signals were transmitted from the rotating disk to the signal conditioner using a set of slip rings affixed to the shaft. The displacement signals of the shaft and disk were recorded and analyzed with a signal analyzer.

Simulation Model

The simulation model is similar to that developed in an earlier study (Flowers and Wu, 1993). The primary differences are that rotational stiffening of the disk have been taken into account and that damping is included in the bearing support forces. A schematic diagram of the model is shown in Fig. 3. It consists of a rigid shaft, a rigid hub, a flexible disk and a support with a symmetric clearance. The equation development is based on the following considerations:

(1) The disk is assumed to flex only in the lateral direction.
(2) Only rotational vibration is considered. This is because only the rotational motion is coupled with the lateral disk vibration. One nodal diameter disk vibration is assumed.

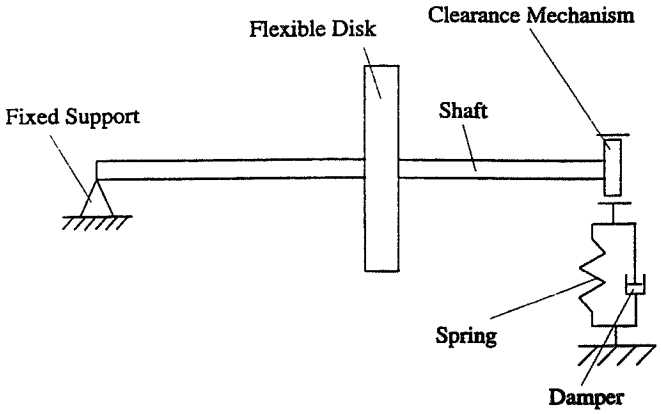

Fig. 3 Simulation model

(3) The rotor speed is constant.

After some mathematical manipulations, the dimensionless equations of motion for the whole system can be obtained as

$$\ddot{x}_1 + r_1\ddot{x}_2 + r_2\ddot{x}_3 + 2r_2\dot{x}_4 + f_{n1} = \cos\tau \quad (1)$$

$$\ddot{x}_2 - r_1\ddot{x}_1 + r_2\ddot{x}_4 - 2r_2\dot{x}_3 + f_{n2} = \sin\tau \quad (2)$$

$$\ddot{x}_3 + 2\dot{x}_4 + 2\xi_3\omega_3\dot{x}_3 + (\omega_3^2 - 1)x_3 = -(\ddot{x}_1 + 2\dot{x}_2) \quad (3)$$

$$\ddot{x}_4 - 2\dot{x}_3 + 2\xi_3\omega_3\dot{x}_4 + (\omega_3^2 - 1)x_4 = -(\ddot{x}_2 - 2\dot{x}_1) \quad (4)$$

$$f_{n1} = -\phi\left[\left(1 - \frac{\delta}{\sqrt{x_1^2 + x_2^2}}\right)(\omega_1^2 x_1) + 2\xi_1\omega_1\dot{x}_1\right]$$

$$f_{n2} = -\phi\left[\left(1 - \frac{\delta}{\sqrt{x_1^2 + x_2^2}}\right)(\omega_2^2 x_2) + 2\xi_2\omega_2\dot{x}_2\right]$$

$$\delta = \frac{\Delta}{e}$$

$$\phi = 1 \quad \text{if } \sqrt{x_1^2 + x_2^2} > \delta$$

$$0 \quad \text{otherwise}$$

In the above equations, x_1, x_2, x_3 and x_4 are scaled by e, the imbalance eccentricity. Time is scaled by the rotor speed, Ω. f_{n1} and f_{n2} are the nonlinear moments due to contacting between the rotor and the bearings.

The effective stiffness of a spinning disk can be strongly influenced by the spin speed. Based upon earlier work (Wu and Flowers, 1992), the lowest natural frequency of such a disk can be written as

$$\omega_3^2 = \frac{19 + \nu}{16} + \frac{\omega_{30}^2}{\Omega^2}$$

where ω_{30} is the natural frequency of the nonspinning disk. This expression is used in Eqs. (3) and (4) to account for spin stiffening effects.

Nomenclature

e = imbalance eccentricity
f_{n1}, f_{n2} = nonlinear bearing forces
r_1 = gyroscopic mass influence ratio
r_2 = disk mass influence ratio
x_1, x_2 = shaft degrees of freedom
x_3, x_4 = disk degrees of freedom
Δ = bearing clearance
Ω = rotor speed
ω_1 = natural frequency of rotor support in x_1 direction
ω_2 = natural frequency of rotor support in x_2 direction
ω_3 = natural frequency of rotor disk
$\tau = \Omega t$
ξ_1 = damping ratio of rotor support in x_1 direction
ξ_2 = damping ratio of rotor support in x_2 direction
ξ_3 = damping ratio of rotor disk
$(\dot{\ }) = \frac{d}{d\tau}$

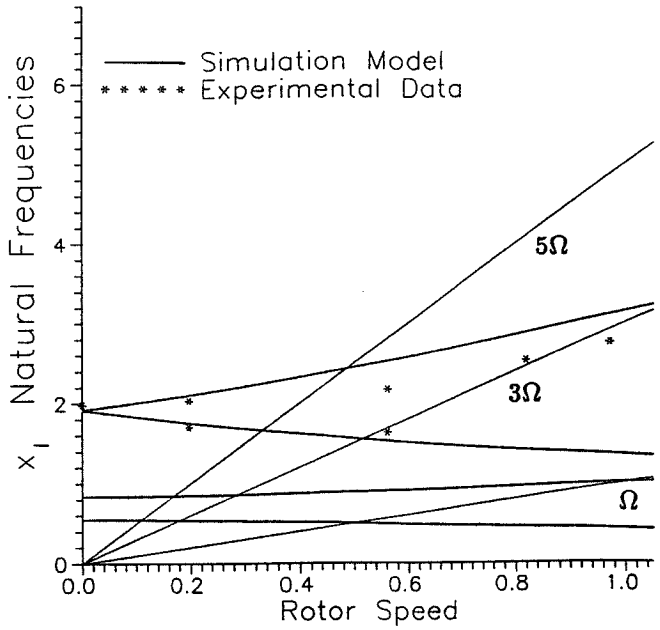

Fig. 4 Rotor natural frequencies

Comparison of Experiment and Simulation

A number of tests were conducted using the experimental setup described in the previous section. In addition, studies for differing parametric configurations have been conducted using the simulation model described above. The basic results are very similar to those obtained by Flowers and Wu (1993). The results presented here are typical. The following discussion is directed at comparing the predictions of the simulation model with experimentally observed responses, with the objective of obtaining insight into the behavior of flexible disk rotor systems with bearing clearance effects.

First, the linear characteristics of the system were examined. Figure 4 shows experimental data of the natural frequencies for the coupled disk/shaft vibration mode as a function of rotor speed obtained using the impulse excitation method. Using the data from such tests and additional measurements and calculations, the linear stiffness, damping, and mass characteristics of the experimental rotor system were identified. The numerical values are shown in Table 1.

Figure 4 also shows the natural frequencies as a function of rotor speed obtained from the simulation model. These results agree relatively well with the experimentally obtained data and serve to validate the structural parameters selected for the simulation model. Ω, 3Ω, and 5Ω lines are also shown on the figure. The intersections of these lines with the natural frequency curve provides significant insight into the nonlinear behavior of the flexible disk rotor system, as is discussed below.

Next, the nonlinear behavior of the system was investigated. A clearance value was selected and the rotor speed was slowly increased over a range of rotor speeds, with the resulting response amplitudes and frequencies measured and recorded.

It is important to note that many vibration frequencies are possible. During the course of the study, 1Ω − 6Ω frequency components were observed for certain parametric configurations. In addition, frequency components that are fractions of the rotor speed were observed for certain speed ranges and initial conditions. However, for a rotor with a symmetric clearance and minimal frictional effects, the odd integer multiples of the rotor speed appear to generally be the primary supersynchronous frequency components. The current discussion will concentrate on those frequencies. However, the basic conclusions should be directly applicable to other supersynchronous vibration frequencies as well.

Figure 5 shows the experimentally measured amplitudes of the Ω, 3Ω, and 5Ω components of the shaft response for various rotor speeds. Simulation results are also shown on Fig. 5. These results were obtained using the harmonic balance method and were verified at selected points through direct numerical integration of the equations of motion. There is relatively good agreement between the simulation results and the corresponding experimental data. Certainly the basic trends match quite well.

An important observation that can be made from examination of these figures is that the peaks of the respective components correspond to the intersections of the Ω, 3Ω, and 5Ω lines with the natural frequency curves. It appears that the nonlinear effects are serving to excite the coupled modes of the rotor/disk system. This is true for both the forward and backward whirl modes of the rotor system.

The peaks occurring at a rotor speed of 0.51 correspond to the intersections of the 3Ω line with the natural frequency curve. They relate to a backward whirl mode. The peaks occurring at rotor speeds of 0.33 and 0.485 correspond to the intersections of the 5Ω line with the natural frequency curve. Those occurring at 0.33 relate to a backward whirl mode and those occurring at 0.485 relate to a forward whirl mode. Note that the amplitudes of the supersynchronous components associated with the forward whirl mode of the disk/shaft vibration are much lower than those associated with the backward whirl mode. This result was observed for all the parametric configurations examined in the course of this study.

The Ω, 3Ω, and 5Ω components contribute (more or less significantly) to the overall response at the corresponding intersection point. However, it is important to note that the Ω component is increased rather dramatically at the intersection points as a result of the presence of disk flexibility. Apparently, the nonlinear coupling between the various frequency components serves to produce this effect.

Conclusions

A study of disk/shaft vibration induced by bearing clearance effects has been presented. Both experimental tests and simulation results have been presented. The responses predicted by the simulation model and those observed experimentally agree quite well. The behavior of both the experimental test rig and the simulation model was quite sensitive to changes in parametric configuration. As a result it is quite difficult to predict exactly how a certain system is going to behave in the presence of a bearing clearance effect, i.e., whether or not coupled disk/shaft vibration will be significantly excited. However, a few general conclusions and guidelines can be drawn from this study.

1. An understanding of the mechanism for coupled disk/shaft vibration induced by clearance effects has been obtained. The nonlinear effects have served to produce

Table 1 Simulation model parameters

Parameter	Value
r_1	0.5
r_2	0.1
ξ_1	0.06
ξ_2	0.06
ξ_3	0.01
ω_1	0.55
ω_2	0.85
ω_3	1.8
ν	0.3
δ	1.2

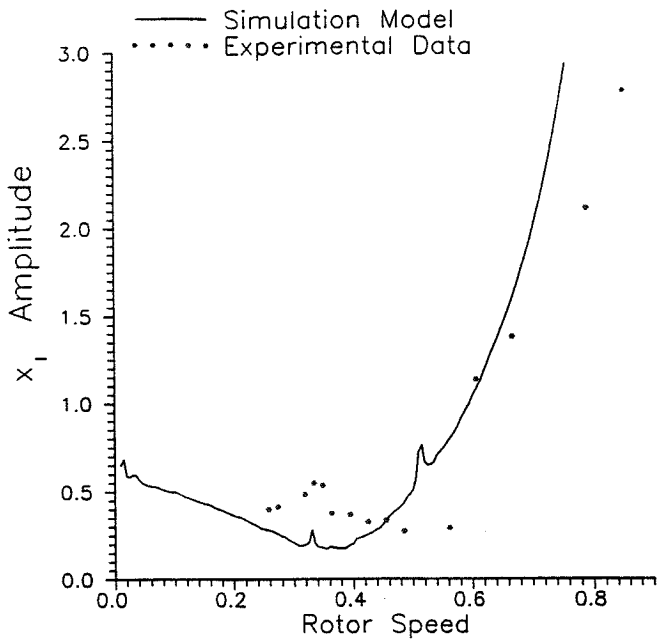

Fig. 5(*a*) Ω component of shaft vibration response

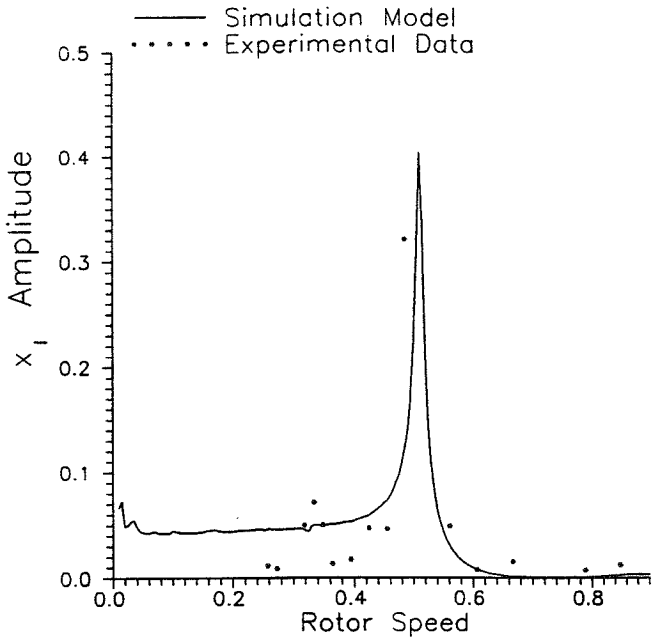

Fig. 5(*b*) 3Ω component of shaft vibration response

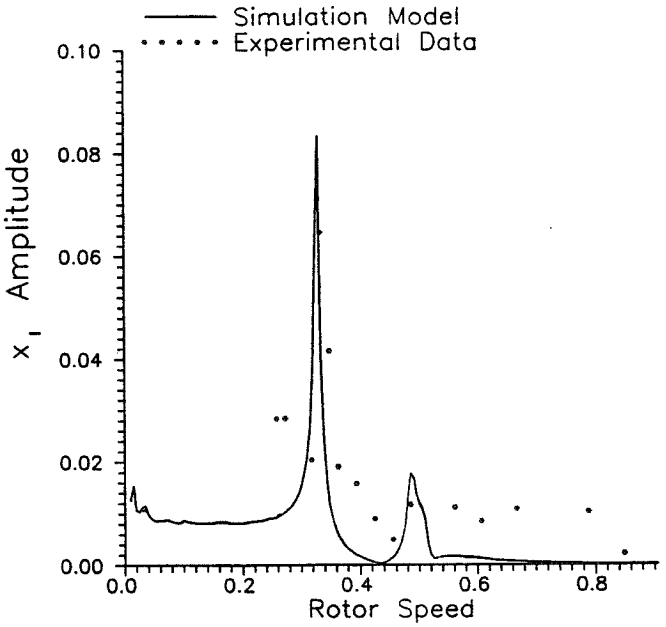

Fig. 5(*c*) 5Ω component of shaft vibration response

superharmonics that excite coupled disk shaft modes. Conversely, the additional degree of freedom provided by the disk flexibility has served to exaggerate the frequency components of the response, resulting in higher amplitudes at the rotor speeds corresponding to the respective natural frequency/multi-synchronous line intersection points.

2. Bearing clearance effects primarily serve to excite backward whirl modes for coupled disk/shaft vibration. Forward whirl modes may be excited but the associated amplitudes appear to be much lower.
3. The bearing support stiffnesses used in this study were not symmetric. These nonsymmetries, together with the clearance, have served to produce the supersynchronous vibration that excites the coupled disk/shaft vibration modes. Please note that the influence of nonsymmetrical stiffnesses and bearing clearance in this regard has been discussed in further detail by Flowers and Wu (1993).
4. From a design perspective, the Campbell diagram is a useful tool to predict when such behavior may occur. The intersections of the corresponding supersynchronous line with the coupled disk/shaft vibration mode frequency curve will indicate at what rotor speeds peak responses for that frequency component are likely to occur. Whether or not such behavior will actually occur and the relative significance of such effects depends very strongly on the imbalance, clearance, damping, and stiffness values.
5. It appears to be relatively difficult to excite coupled disk/shaft vibration with bearing clearance effects. The occurrence of such behavior was very sensitive to rotor speed, as judged by the relative difficulty encountered during

the experimental work in obtaining the peak amplitude responses. This conclusion is verified by the simulation work that indicates that the behavior occurs only over a very limited range of rotor speed. The supersynchronous frequency must almost exactly coincide with a natural frequency in order to excite the behavior.

Acknowledgment

This work was partially supported by the National Science Foundation under Grant No. MSS-9110051 and partially by the National Aeronautics and Space Administration under Grant No. NAG3-1507. The Government has certain rights in this material. Special appreciation is expressed to Dr. Charles Lawrence of NASA/Lewis Research Center.

References

Black, H. F., "Forced Subrotative Speed Dynamic Action of Rotating Machines," *Journal of Mechanical Engineering Science*, Vol. 10, No. 4, pp. 1–12.

Chivens, D. R., and Nelson, H. D., 1975, "The Natural Frequencies and Critical Speeds of a Rotating, Flexible Shaft-Disk System," ASME *Journal of Engineering for Industry*, Vol. 97, August, pp. 881–886.

Childs, D. W., 1978, "Rub-Induced Parametric Excitation in Rotors," ASME Paper No. 78-WA/DE-14, Presented at the 1978 ASME Winter Annual Meeting.

Davis, R. R., 1989, "Practical Nonlinear Simulation of Rotating Machinery Dynamics with Application to Turbine Blade Rubbing," Ph.D. Dissertation, Department of Mechanical Engineering, University of California, Davis, June.

Ehrich, F. F., 1966, "Subharmonic Vibrations of Rotors in Bearing Clearance," ASME Paper 66-MD-1, Design Engineering Conference and Show, Chicago, Ill, May 9–12.

Flowers, G. T., and Ryan, S. G., 1993, "Development of a Set of Equations for Incorporating Disk Flexibility Effects in Rotordynamical Analyses," ASME *Journal of Engineering for Gas Turbines and Power*, Vol. 115, No. 2, pp. 227–233.

Flowers, G. T., and Wu, F. S., 1993, "A Study of the Influence of Bearing Clearance on Lateral Coupled Shaft/Disk Rotordynamics," ASME *Journal of Engineering for Gas Turbines and Power*, Vol. 115, No. 2, pp. 279–286.

Johnson, D. C., 1962, "Synchronous Whirl of a Vertical Shaft Having a Clearance in One Bearing," *Journal of Mechanical Engineering Science*, Vol. 4, No. 1, pp. 85–93.

Lamb, H., and Southwell, R. V., 1921, "The Vibrations of a Spinning Disk," *Proceedings of the Royal Society of London*, Series A, Vol. 99, July, pp. 272–280.

Muszynska, A., 1984, "Synchronous and Self-Excited Vibrations Caused by Full Annular Rub," presented at *Eigth Machinery Dynamics Seminar*, Halifax, Nova Scotia, Canada, Oct. 1–2.

Wu, F. S., and Flowers, G. T., 1992, "A Transfer Matrix Technique for Evaluating the Natural Frequencies and Critical Speeds of a Rotor with Multiple Flexible Disks," ASME *Journal of Vibration and Acoustics*, Vol. 114, No. 2, pp. 242–248.

95N 32691

DYNAMIC BEHAVIOR OF A MAGNETIC BEARING SUPPORTED JET ENGINE ROTOR WITH AUXILIARY BEARINGS

G.T. Flowers
H. Xie
S.C. Sinha

Department of Mechanical Engineering
Auburn University
Auburn, Alabama

ABSTRACT

This paper presents a study of the dynamic behavior of a rotor system supported by auxiliary bearings. The steady–state behavior of a simulation model based upon a production jet engine is explored over a wide range of operating conditions for varying rotor imbalance, support stiffness and damping. Interesting dynamical phenomena, such as chaos, subharmonic responses, and double–valued responses, are presented and discussed.

KEYWORDS: magnetic bearings, auxiliary bearings, nonlinear rotordynamics.

NOMENCLATURE

C_B = auxiliary bearing support damping, lb.s/in.
F_n = normal force, lb
$\mathbf{F}_X$ = external force vector acting on the rotor in X direction
$\mathbf{F}_Y$ = external force vector acting on the rotor in Y direction
$\mathbf{I}_a$ = rotor inertia matrix
K_B = auxiliary bearing support stiffness, lb/in.
K_C = contact stiffness, lb/in.
M_B = auxiliary bearing mass, lb.s^2/in.
M_k = mass of kth rotor element, lb.s^2/in.
N = total number of modes considered
N_{B1} = node number at auxiliary bearing #1
N_{B2} = node number at auxiliary bearing #2
$\mathbf{Q}_X$ = rotor modal coordinate vector in X direction
$\mathbf{Q}_Y$ = rotor modal coordinate vector in Y direction
R_B = radius of auxiliary bearing bore, in.
R_R = radius of rotor journal, in.
$\mathbf{X}_R$ = rotor physical coordinate vector in X direction
$\mathbf{Y}_R$ = rotor physical coordinate vector in Y direction
e = rotor imbalance eccentricity, in.
g = gravitational acceleration, in./s^2
t = time, s
Δ = deformation at the contact point, in.
$\mathbf{\Gamma} = \mathbf{\Psi}^T \mathbf{I}_a \mathbf{\Psi}$
$\mathbf{\Psi}$ = rotor free-free modal rotation matrix
Ω = rotor operating speed, rad/s
$\mathbf{\Phi}$ = rotor free-free modal displacement matrix
$\delta = R_B - R_R$, auxiliary bearing clearance, in.

ζ = modal damping coefficient

INTRODUCTION

Active magnetic bearings are one of the most innovative recent developments in the turbomachinery field. This technology provides the potential for significant improvements over other types of rotor support, including elimination of wear and bearing friction-related energy losses as well as a means of actively suppressing rotor vibration. A critical component of any magnetic bearing design is the auxiliary bearing, which protects the soft iron core of the magnetic bearing and provides rotor support in case of overload or failure of the primary (magnetic) bearing. Magnetic bearing systems appear to provide particularly great promise for use in aeronautical applications. In this regard, current effort is directed toward developing jet engines with rotors supported by magnetic bearings. For such applications, safety is an important concern. Toward this end, it is desirable to design the system to operate with auxiliary bearing support for an extended period of time.

A number of different bearing types have been suggested as auxiliary bearings. These include bushings, rolling element bearings, and various types of journal bearings. The most commonly considered are rolling element bearings. The major disadvantage associated with using rolling element bearings (or bushings) is the requirement of a clearance between the rotor and the inner race of the bearing, without which many of the advantages associated with using magnetic bearings would be reduced or eliminated. This clearance introduces a nonlinear dynamical feature which may significantly impact the behavior of the rotor.

There are quite a number of studies in the literature concerned with nonlinear rotordynamics. Yamamoto (1954) conducted a systematic study of rotor responses involving bearing clearance effects. Black (1968) studied the rotor/stator interaction with a clearance. Ehrich (1966, 1988 and 1991), Bently (1974), Muszynska (1984) and Childs (1979 and 1982) observed and studied subharmonic responses associated with clearance effects. While this work has served to greatly enhance the understanding of such systems, more detailed study is needed. Much of this earlier work was conducted from the perspective that the clearance is a result of manufacturing error or misfitting and is best eliminated. However, in a rotor system fitted with magnetic bearings and auxiliary bearings, the clearance becomes a design parameter rather than an irregularity. From this point of view, it is important to develop a better understanding of the expected dynamic responses. Such knowledge will provide guidelines for the selection of auxiliary bearing parameters.

There has been relatively little work available in the open literature that is specifically concerned with auxiliary bearings. Two papers that are directly related to research on auxiliary bearings are Gelin et al., (1990) and Ishii and Kirk (1991). Both of these papers are mainly concerned with transient responses. The current work is specifically concerned with developing a better understanding of the expected steady-state dynamical behavior for an auxiliary bearing supported rotor. Simulation results for a rotor based upon a production jet engine are presented and discussed.

The model used in the current study has two principal components - the rotor and the auxiliary bearings. The rotor is modelled using the free-free bending mode shapes and natural frequencies obtained through finite element analysis. The finite element code uses 34 stations and the first four modes (two rigid body and two flexible modes) are included in the simulation model. Figure 1 shows a schematic diagram of the finite element model. The rotor equations of motion can be expressed in terms of modal coordinates as:

$$\ddot{\mathbf{Q}}_X + 2\zeta\omega_n\dot{\mathbf{Q}}_X + \Omega\Gamma\dot{\mathbf{Q}}_Y + \omega_n^2\mathbf{Q}_X + 2\Omega\zeta\omega_n\mathbf{Q}_Y = \Phi^T\mathbf{F}_X, \tag{1.a}$$

$$\ddot{\mathbf{Q}}_Y + 2\zeta\omega_n\dot{\mathbf{Q}}_Y - \Omega\Gamma\dot{\mathbf{Q}}_X + \omega_n^2\mathbf{Q}_Y - 2\Omega\zeta\omega_n\mathbf{Q}_X = \Phi^T\mathbf{F}_Y. \tag{1.b}$$

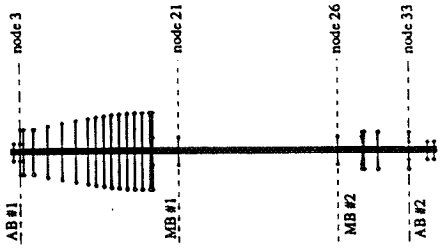

FIGURE 1 DIAGRAM OF THE FINITE ELEMENT MODEL

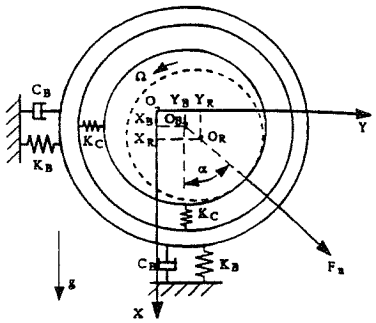

FIGURE 2 AUXILIARY BEARING MODEL

where

$$\mathbf{F}_X = \{F_{X1}, F_{X2}, \ldots, F_{Xm}\}^{-T},$$
$$\mathbf{F}_Y = \{F_{Y1}, F_{Y2}, \ldots, F_{Ym}\}^{-T},$$
$$\mathbf{Q}_X = \Phi^{-1}\mathbf{X}_R,$$
$$\mathbf{Q}_Y = \Phi^{-1}\mathbf{Y}_R,$$
$$\omega_n = \begin{pmatrix} \omega_{n_1} & 0 & \ldots & 0 \\ 0 & \omega_{n_2} & \ldots & 0 \\ \ldots & \ldots & \ldots & \ldots \\ 0 & 0 & \ldots & \omega_{n_N} \end{pmatrix}$$

with

$$\mathbf{X}_R = \{X_{R1}, X_{R2}, \ldots, X_{Rm}\}^{-T},$$
$$\mathbf{Y}_R = \{Y_{R1}, Y_{R2}, \ldots, Y_{Rm}\}^{-T}.$$

(m = total number of nodes)

The physical displacements of the rotor at the two auxiliary bearing locations can be obtained using the following coordinate transformation:

$$X_{Rk} = \sum_{i=1}^{N} \Phi_{ki} Q_{Xi}, \qquad (k = N_{B1}, N_{B2})$$
$$Y_{Rk} = \sum_{i=1}^{N} \Phi_{ki} Q_{Yi},$$

The model for the auxiliary bearings is shown in Figure 2. The governing equations of motion are:

$$M_{Bk}\ddot{X}_{Bk} + C_{Bk}\dot{X}_{Bk} + K_{Bk}X_{Bk} = F_{nk}\cos\alpha_k + M_{Bk}g, \qquad (2.a)$$
$$M_{Bk}\ddot{Y}_{Bk} + C_{Bk}\dot{Y}_{Bk} + K_{Bk}Y_{Bk} = F_{nk}\sin\alpha_k, \qquad (2.b)$$

where

$$\alpha_k = tan^{-1} \frac{Y_{Rk} - Y_{Bk}}{X_{Rk} - X_{Bk}}.$$
$$(k = N_{B1}, N_{B2})$$

$$F_{Xk} = - F_{nk} \cos \alpha_k + M_k \, g + M_k \, e \, \Omega^2 \cos(\Omega t),$$
$$F_{Yk} = - F_{nk} \sin \alpha_k + M_k \, e \, \Omega^2 \sin(\Omega t).$$

The rotor/bearing interaction is represented with the normal force F_{nk}

$$F_{nk} = \begin{cases} K_C \delta_k, & \Delta_k > 0, \\ 0, & \Delta_k \leq 0, \end{cases} \tag{3}$$

where

$$\Delta_k = (X_{Rk} - X_{Bk}) \cos \alpha_k + (Y_{Rk} - Y_{Bk}) \sin \alpha_k - \delta_k.$$

DISCUSSION OF RESULTS

The model described in the previous section was used to study the steady–state dynamic behavior of such a system using direct numerical integration of the equations and a harmonic balance code. Studies were performed for varied values of imbalance, support stiffness, and support damping, respectively. For the purposes of the current work, the two auxiliary bearings are located at nodes 3 and 33, respectively. It is assumed that they are identical in terms of stiffness, damping and friction characteristics. The nominal system parameters used for the simulation study are M_{B1}=0.0023, M_{B2}=0.0024, K_C=2.855e+6, and ζ=0.03. All the results that are presented correspond to node 3, the location of bearing 1.

The dynamical behavior of a rotor supported by bearings with clearance coupled with the nonsymmetry resulting from gravitational effects can be quite complex. The harmonic balance method is first used to investigate the synchronous behavior for small imbalance values. (Please note that the complex frequency contents associated with medium and large imbalance values makes it a formidable task to apply the harmonic balance method for other cases.) Figure 3 is a typical plot of the steady state response amplitudes as functions of the rotor speed with and without bearing clearance. The nonsymmetric effects resulting from gravity loading is similar to what occurs for a rotor supported by nonsymmetric bearing stiffnesses with regard to influence on critical speeds. The first critical speed splits into two distinct values. For the X direction, the gravity force tends to keep the rotor in contact with the bearing at low operating speed. The apparent stiffness in this direction is approximately the same as K_B and the resulting critical speed about the same as the critical speed for the linear case (δ=0). For the Y direction, the clearance results in a lower apparent stiffness and a lower critical speed. Several higher order pseudo-critical speeds are also created in the operating speed range (about 1500 rad./sec). It should be noted that the response in the X direction also departs from the linear case at high operating speed. This is because the imbalance force becomes dominant at high rotor speed which in turn makes the gravity force less significant and the clearance effect more important.

Figure 4(a) shows some typical results for varying imbalance. Some of the more dynamically interesting results occur for cases of relatively large imbalance. It is observed that imbalance may influence the frequency content of the rotor responses quite dramatically at certain operating speeds. There exists as many as eight ranges of imbalance values that result in eight different types of rotor responses. In fact, subharmonic responses from $\Omega/2$ through $\Omega/10$ are observed. Those subharmonics are not directly related to the system's natural frequencies as were the cases with other researchers' findings (such as Ehrich, 1988). Moreover, several types of subharmonic responses may occur for identical parametric configurations, but different imbalance values.

Figures 4(b) and 4(c) show typical results using K_B or C_B as the variable parameter. Clear routes to chaos are observed. As K_B increases beyond certain value, a period-doubling bifurcation always

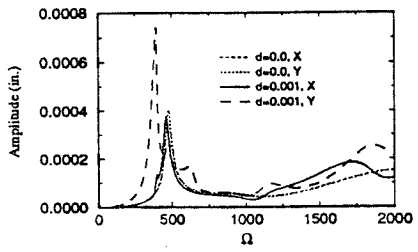

FIGURE 3 INFLUENCE OF CLEARANCE ON CRITICAL SPEEDS (e=0.0001, C_B=150.0, K_B=0.313x10^6)

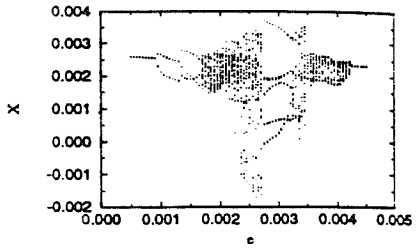

FIGURE 4(a) BIFURCATION DIAGRAM WITH IMBALANCE AS THE VARIABLE PARAMETER (Ω=1000, δ=0.002, C_B=150, K_B=0.313x10^6)

takes place. As C_B decreases below certain value, the responses always become chaotic. However, the bifurcation type is not well defined as for varied K_B. It should be pointed out that even though a lower K_B may leads to a better system response, it may also fail to protect the magnetic bearings due to the fact that it could result in a larger rotor orbit-center offset. In addition, higher bearing damping does not necessarily result in synchronous responses. It is observed that, with small imbalance ($e \leq 0.0005$), the responses are always synchronous for all speeds in the speed range considered ($\leq$ 1800) if C_B is large enough (C_B=250.0) and the clearance is small enough ($\delta \leq 0.001$). As with the other cases, higher bearing damping or lower bearing stiffness or lower imbalance tends to increase the probability of synchronous responses.

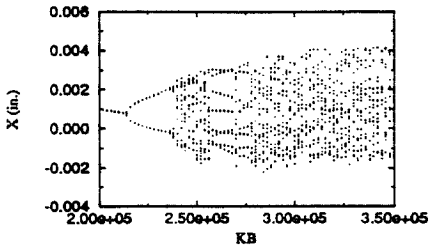

FIGURE 4(b) BIFURCATION DIAGRAM WITH BEARING STIFFNESS AS THE VARIABLE PARAMETER (Ω=1500, δ=0.002, C_B=150, e=0.0008)

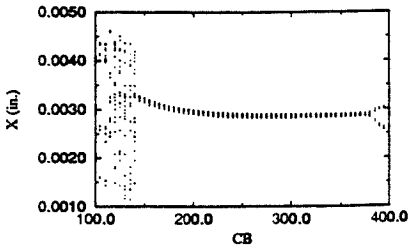

FIGURE 4(c) BIFURCATION DIAGRAM WITH BEARING DAMPING AS THE VARIABLE PARAMETER (Ω=1500, δ=0.002, e=0.0015, K_B=0.313x10^6)

CONCLUSIONS

As a summary of the results discussed above, the following conclusions can be drawn:

1. Imbalance may serve to dramatically alter the frequency contents of the rotor responses at certain operating speeds. This is particularly evident for cases of large clearance, high bearing stiffness and low bearing damping.
2. For sufficiently high imbalance:
   i. There is a threshold level of damping below which complex dynamical behavior can be expected.
   ii. There is a threshold level of stiffness above which complex dynamical behavior can be expected.
3. Clear routes to chaos are observed. As bearing stiffness increases beyond a certain value, a period-doubling bifurcation takes place which leads to chaos. As bearing damping decreases below a certain value, chaos also tends to occur but the bifurcation type is not so clearly defined.

ACKNOWLEDGEMENT

The authors would like to express their gratitude to S. A. Klusman of the Allison Engine Company for many helpful discussions and practical advice.
This work was supported by NASA under Grant No. NAG3-1507. The Government has certain rights in this material.

REFERENCES

Bently, D. E., 1974, "Forced Subrotative Speed Dynamic Action of Rotating Machinery," ASME Paper No. 74-PET-16.

Black, H. F., 1968, "Interaction of a Whirling Rotor With a Vibrating Stator Across a Clearance Annulus," *Journal of Engineering Science*, Vol. 10, No. 1, pp. 1-12.

Childs, D. W., 1979, "Rub-Induced Parametric Excitation in Rotors," ASME *Journal of Mechanical Design*, Vol. 101, pp. 640-644.

Childs, D. W., 1982, "Fractional-Frequency Rotor Motion Due to Nonsymmetric Clearance Effects," ASME *Journal of Engineering for Power*, Vol. 104, pp. 533-541.

Ehrich, F. F., 1966, "Subharmonic Vibration of Rotors in Bearing Clearance," ASME Paper 66-MD-1.

Ehrich, F. F., 1988, "High Order Subharmonic Response of High Speed Rotors in Bearing Clearance," ASME *Journal of Vibration, Acoustics, Stress, and Reliability in Design*, Vol. 110, pp. 9-16.

Ehrich, F. F., 1991, "Some Observations of Chaotic Vibration Phenomena in High-Speed Rotordynamics," ASME *Journal of Vibration, Acoustics, Stress, and Reliability in Design*, Vol. 113, pp. 50-57.

Gelin, A., Pugnet, J. M., and Hagopian, J. D., 1990, "Dynamic Behavior of Flexible Rotors with Active Magnetic Bearings on Safety Auxiliary Bearings," *Proceedings of 3rd International Conference on Rotordynamics*, Lyon, France, pp. 503-508.

Ishii, T., and Kirk, R. G., 1991, "Transient Response Technique Applied to Active Magnetic Bearing Machinery During Rotor Drop," *DE- Vol. 35, Rotating Machinery and Vehicle Dynamics, ASME*, pp.191-199.

Muszynska, A., 1984, "Partial Lateral Rotor to Stator Rubs, " IMechE Paper No. C281/84.

Yamamoto, T. T., 1954, "On Critical Speeds of a Shaft," *Memoirs of the Faculty of Engineering*, Nagoya University (Japan), Vol. 6, No. 2.

THE AMERICAN SOCIETY OF MECHANICAL ENGINEERS
345 E. 47th St., New York, N.Y. 10017

95-GT-216

SYNCHRONOUS DYNAMICS OF A COUPLED SHAFT/BEARING/HOUSING SYSTEM WITH AUXILIARY SUPPORT FROM A CLEARANCE BEARING: ANALYSIS AND EXPERIMENT

James L. Lawen, Jr.
Auburn University
Auburn, AL 36849

George T. Flowers
Auburn University
Auburn, AL 36849

ABSTRACT

This study examines the response of a flexible rotor supported by load sharing between linear bearings and an auxiliary clearance bearing. The objective of the work is to develop a better understanding of the dynamical behavior of a magnetic bearing supported rotor system interacting with auxiliary bearings during a critical operating condition. Of particular interest is the effect of coupling between the bearing/housing and shaft vibration on the rotordynamical responses. A simulation model is developed and a number of studies are performed for various parametric configurations. An experimental investigation is also conducted to compare and verify the rotordynamic behavior predicted by the simulation studies. A strategy for reducing sychronous shaft vibration through appropriate design of coupled shaft/bearing/housing vibration modes is identified. The results are presented and discussed.

NOMENCLATURE

C = damping, N-sec/m
K = stiffness, N/m
M_b = auxiliary bearing mass, kg.
M_h = housing mass, kg.
N = total number of modes considered
N_{b1} = node number at leftmost bearing
N_{b2} = node number at rightmost bearing
N_{b3} = node number at auxiliary clearance bearing
$\mathbf{Q}_x$ = rotor modal coordinate vector in X direction
$\mathbf{Q}_y$ = rotor modal coordinate vector in Y direction
t = time, s
X_r = rotor physical coordinate vector in X direction, m
Y_r = rotor physical coordinate vector in Y direction, m
X_b = auxiliary bearing physical coordinate vector in X direction, m
Y_b = auxiliary bearing physical coordinate vector in Y direction, m
X_h = housing physical coordinate vector in X direction, m
Y_h = housing physical coordinate vector in Y direction
Δ = radial clearance in auxiliary bearing, m
$\mathbf{I}_a$ = rotor polar mass inertia matrix, kg-m^2
Ψ = rotor free-free modal rotation matrix
Φ = rotor free-free modal displacement matrix
$\Gamma = \Psi^T \mathbf{I}_a \Psi$
Ω = rotor operating speed, rad/s
ω_n = matrix of rotor free–free natural frequencies, rad/s
ψ = imbalance vector

Subscripts

bx = auxiliary bearing, x-direction
by = auxiliary bearing, y-direction
c = contact
hx = housing, x-direction
hx = housing, y-direction
xr = rightmost bearing, x-direction
xl = leftmost bearing, x-direction
yr = rightmost bearing, y-direction
yl = leftmost bearing, y-direction

Presented at the International Gas Turbine and Aeroengine Congress & Exposition
Houston, Texas - June 5-8, 1995
This paper has been accepted for publication in the Transactions of the ASME
Discussion of it will be accepted at ASME Headquarters until September 30, 1995

INTRODUCTION

In recent years, the use of active magnetic bearings for supporting turbomachinery has been an area of interest for both academic researchers and turbomachinery users in industry. Magnetic bearings provide the potential for significant improvements over other types of rotor support, including elimination of wear and bearing friction-related energy losses as well as a means of actively suppressing rotor vibration. However, their use has been significantly limited due to a number of technical problems. A particular area of concern is the auxiliary bearing, which protects the soft iron core of the magnetic bearing and provides rotor support in case of overload or failure of the magnetic bearing.

Typically, the auxiliary bearings have relatively small clearances so that magnetic bearing rotor/stator contact does not occur during bearing failure or power loss. Due to these small clearances, contact between the rotor system and the auxiliary bearings can occur during standard operation of the magnetic bearings. When this occurs, load sharing between the magnetic bearings and the auxiliary bearings results, and the rotor system interacts with its auxiliary bearings. The dynamics of such an occurrence must be understood in order to properly design the auxiliary bearing system for a magnetic bearing supported rotor.

A number of different bearing types have been suggested as auxiliary bearings. These include bushings, rolling element bearings, and various types of journal bearings. The most commonly considered are rolling element bearings. The major disadvantage associated with using rolling element bearings (or bushings) is the requirement of a clearance between the rotor and the inner race of the bearing, without which many of the advantages associated with using magnetic bearings would be reduced or eliminated. This clearance introduces a nonlinear dynamical feature which may significantly impact the behavior of the rotor.

There are quite a number of studies in the literature concerned with nonlinear rotordynamics. Ehrich (1965 and 1967) studied the rotor/stator interaction with a clearance and found zones of bistable synchronous behavior. Black (1968) also found these bistable interaction zones. Ehrich extended this research by predicting subharmonic behavior (1966 and 1988), superharmonic behavior (1992), and chaotic responses (1991). Bently (1974), Muszynska (1984), and Childs (1979 and 1982) also observed and studied subharmonic responses due to clearance effects.

There is relatively little work available in the open literature that is specifically concerned with the dynamics between the rotor system and the auxiliary bearings. The research that has been performed to date is primarily concerned with the transient behavior of rotor drop on the auxiliary bearings due to power faliure or inoperative magnetic bearings. Two papers with this focus are Gelin et al., (1990) and Ishii and Kirk (1991).

The present work is concerned with developing an understanding of the dynamic behavior of a rotor system supported by load sharing between the linear bearings and an auxiliary bearing with clearance. Of particular interest is the influence of coupled shaft/bearing/housing vibration modes on the rotordynamical behavior of such a system.

SIMULATION MODEL

Figure 1 shows the simulation model used for this investigation. It consists of a flexible rotor supported at both ends by magnetic bearings. A rigid disk with adjustable imbalance is placed at the midpoint of the bearing span. As a simplification, the magnetic bearings are modeled as spring and dashpot systems and interaction with a single auxiliary bearing is considered. The auxiliary bearing was modeled as an antifriction bearing with a clearance and a mass attached to a housing. The housing in turn has a mass, stiffness, and damping. Figure 2 shows the auxiliary bearing model used in the simulation.

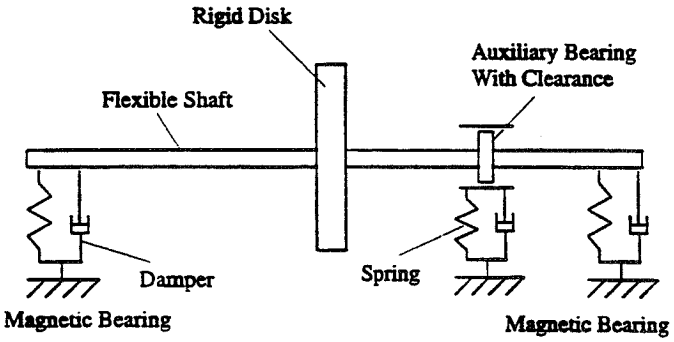

Figure 1 Schematic Diagram of Simulation Model

The rotor is modelled using the free–free bending mode shapes and natural frequencies obtained through finite element analysis. The finite element code uses 19 stations and the first four modes (two rigid body and two flexible modes) are included in the simulation model.

Using these simplifications, the equations of motion for the system can be written as follows:

$$\ddot{\mathbf{Q}}_x + \Omega\Gamma\dot{\mathbf{Q}}_y + \omega_n^2\mathbf{Q}_x + \Phi^T(F_{x,lin} + F_{x,nl})$$

$$= \Phi^T F_{x,imb}, \quad (1.a)$$

$$\ddot{\mathbf{Q}}_y - \Omega\Gamma\dot{\mathbf{Q}}_x + \omega_n^2 \mathbf{Q}_y + \Phi^T(F_{y,lin} + F_{y,nl}) = \Phi^T F_{y,imb}, \quad (1.b)$$

$$M_b\ddot{X}_b + \frac{C_{bx}}{\Omega}(\dot{X}_b - \dot{X}_h) + K_{bx}(X_b - X_h) = F_{x,nl}, \quad (1.c)$$

$$M_b\ddot{Y}_b + \frac{C_{by}}{\Omega}(\dot{Y}_b - \dot{Y}_h) + K_{by}(Y_b - Y_h) = F_{y,nl}, \quad (1.d)$$

$$M_h\ddot{X}_h + (\frac{C_{bx}}{\Omega} + \frac{C_{hx}}{\Omega})\dot{X}_h + (K_{bx} + K_{hx})X_h = C_{bx}\dot{X}_b + K_{bx}X_b, \quad (1.e)$$

$$M_h\ddot{Y}_h + (\frac{C_{by}}{\Omega} + \frac{C_{hy}}{\Omega})\dot{Y}_h + (K_{by} + K_{hy})Y_h = \frac{C_{by}}{\Omega}\dot{Y}_b + K_{by}Y_b, \quad (1.f)$$

where

$$\mathbf{F}_{x,lin} = \Phi_{N_{b1}}(K_{xl}\mathbf{Q}_x + \frac{C_{xl}}{\Omega}\dot{\mathbf{Q}}_x) + \Phi_{N_{b2}}(K_{xr}\mathbf{Q}_x + \frac{C_{xr}}{\Omega}\dot{\mathbf{Q}}_x)$$

$$\mathbf{F}_{y,lin} = \Phi_{N_{b1}}(K_{yl}\mathbf{Q}_y + \frac{C_{yl}}{\Omega}\dot{\mathbf{Q}}_y) + \Phi_{N_{b2}}(K_{yr}\mathbf{Q}_y + \frac{C_{yr}}{\Omega}\dot{\mathbf{Q}}_y)$$

$$\mathbf{F}_{x,imb} = \psi\Omega^2 cos\Omega t,$$

$$\mathbf{F}_{y,imb} = \psi\Omega^2 sin\Omega t,$$

$$\mathbf{F}_{x,nl} = \phi K_c(\delta - \Delta)(\frac{\Phi\mathbf{Q}_x - X_b}{\delta})$$

$$\mathbf{F}_{y,nl} = \phi K_{cont}(\delta - \Delta)(\frac{\Phi\mathbf{Q}_y - Y_b}{\delta})$$

$$\delta = \sqrt{(\Phi\mathbf{Q}_x - X_b)^2 + (\Phi\mathbf{Q}_y - Y_b)^2},$$

$$\phi = 1 \; if \; \delta > \Delta$$

$$0 \; otherwise$$

$$\mathbf{Q}_x = \Phi^{-1}\mathbf{X}_r,$$

$$\mathbf{Q}_y = \Phi^{-1}\mathbf{Y}_r,$$

with

$$\mathbf{X}_r = \{X_{r1}, X_{r2}, \ldots, X_{rm}\}^T,$$

$$\mathbf{Y}_r = \{Y_{r1}, Y_{r2}, \ldots, Y_{rm}\}^T.$$

(m = total number of nodes)

The physical displacements of the rotor at the auxiliary bearing or magnetic bearing locations can be obtained using the following coordinate transformation:

$$X_{rk} = \sum_{i=1}^{N} \Phi_{ki} Q_{xi}, \qquad (k = N_{b1}, N_{b2}, N_{b3})$$

$$Y_{rk} = \sum_{i=1}^{N} \Phi_{ki} Q_{yi},$$

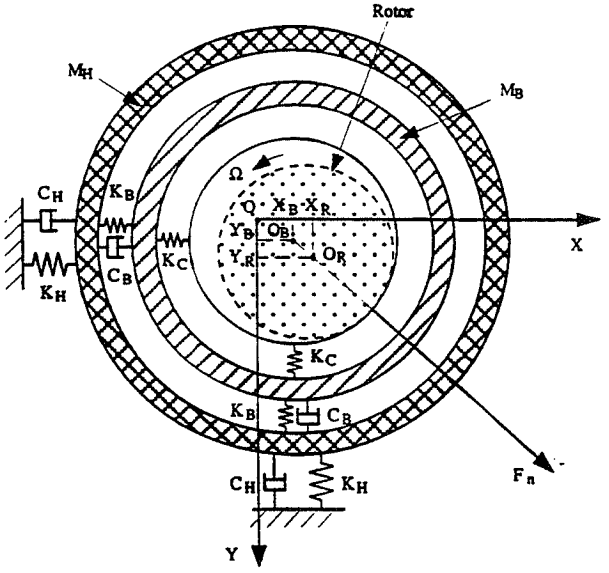

Figure 2 Auxiliary Bearing Model

EXPERIMENTAL MODEL

Experimental tests were performed in order to validate the behavior predicted by the simulation model and to gain some insight into the dynamical responses that are to be expected. A schematic diagram of the rotor test rig that was used in the experimental work is shown in Figure 3.

The rotor used in this study has two basic components: a flexible shaft and an auxiliary clearance bearing. The shaft is made of steel and is 0.374 inches in diameter and 18.0 inches in length. It is supported at 1.0 inch from the right end by ball bearings suspended in a frame by four springs and at 1.0 inch from the left end by a bushing with a tight clearance. These supports

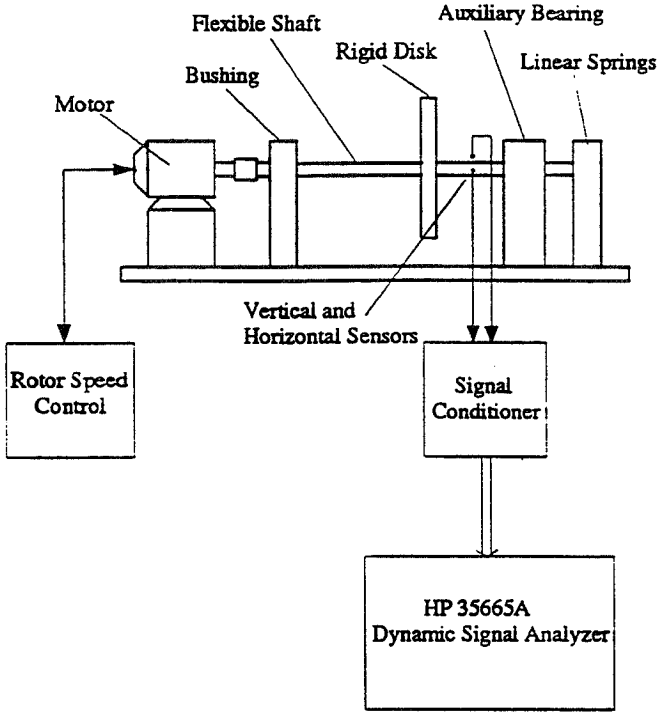

Figure 3 Experimental Model

represent the magnetic bearings. The stiffness of the left support is 17511 N/m (101.5 lb/in) for both the horizontal and vertical directions. It is used to somewhat isolate the rotor from the effects of the flexible coupling which attaches the rotor to the motor and to enforce low amplitude vibration at this location to protect the motor. The stiffness of the right support, for both horizontal and vertical directions, is 2539 N/m (14.5 lb/in). This lower stiffness allows for significant vibration of the rotor in the speed range of the motor. A rigid disk with an adjustable imbalance is placed at the midpoint of the bearing span. The auxiliary clearance bearing/housing consists of a bushing suspended in a frame by four springs (Figure 4). It is situated at the right end of the rotor. The clearance is adjustable by changing the bushing. The auxiliary bearing/housing stiffnesses are varied by interchanging the springs.

The rotor is driven by an adjustable speed motor with feedback speed controller. Shaft vibration is measured using eddy current proximity displacement sensors fixed so as to measure displacement in the vertical and horizontal directions. The displacement signals were recorded and analyzed with a signal analyzer.

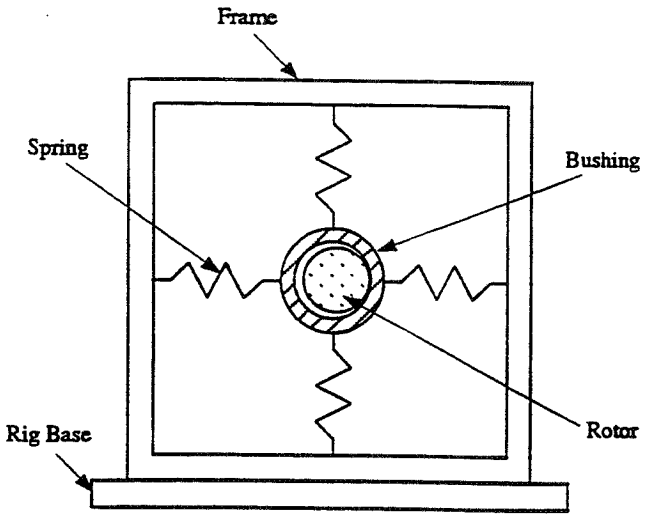

Figure 4 Auxiliary Clearance Bearing

DISCUSSION

A series of parallel studies were conducted using the simulation and experimental models discussed in the preceding sections. The following discussion is aimed at comparing the predictions of the simulation model with experimentally observed responses, with the objective of obtaining insight into the behavior of flexible rotor system dynamics due to load sharing between the magnetic bearings and an auxiliary bearing.

Using the data from measurements and calculations, the stiffness, damping, and mass characteristics of the experimental rotor system were identified. The imbalance configuration consists of 3.0 x 10^{-6} kg-m located at the left end of the rotor shaft (from the flexible coupling to the electric motor) and a variable imbalance located on the rigid disk. Linear, hysteretic, and coulomb friction damping models were considered. The support damping appears to result principally from hysteresis. If synchronous vibration is assumed, this results in a damping coefficient scaled by the rotor speed. The numerical values are given in Table 1.

The governing parameters for an auxiliary bearing are stiffness, mass, damping, clearance, and axial location. The axial location generally is fixed by other considerations, such as space requirements and the need to be close to the magnetic bearing to better protect it. This study focusses on the remaining design parameters. For the system studied, significant nonsynchronous vibration occured only for the 2ω component and for a limited rotor speed range. Figure 5 illustrates the observed behavior for various imbalance values. The amplitudes are quite small and, interestingly, virtually independent of imbalance. The remainder of this discussion will focus on the synchronous response amplitudes.

Parameter	Value	Units
K_b	471	N/m
K_h	$1.8x10^7$	N/m
K_c	87,557	N/m
K_{lx}, K_{ly}	17,510	N/m
K_{rx}, K_{ry}	2,539	N/m
C_{lx}, C_{ly}	1,000	N/m
C_{rx}, C_{ry}	500	N/m
C_{ly}, C_{ly}	1,000	N/m
C_{ry}, C_{ry}	500	N/m
C_{bx}, C_{by}	2,000	N/m
C_{hx}, C_{hy}	0	N/m
M_b	0.033	kg
M_h	0.296	kg
ψ_1	3.0×10^{-6}	kg-m
ψ_{10}	2.5×10^{-5}	kg-m
Δ	$5.0x10^{-5}$	m

Table 1 Simulation Model Parameters

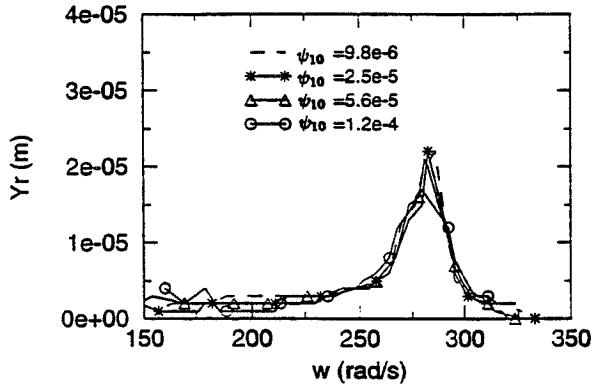

Figure 5 Experimental Results for 2ω Component

The simulation responses discussed below were determined from a single-term harmonic balance analysis that was numerically implemented and verified at selected points using direct numerical integration of the governing equations of motion. The harmonic balance procedure is described by Nayfeh and Mook (1979). Figures 6.a - 6.e show the response amplitudes predicted from the simulation study for the parameters of Table 1. Figures 7.a - 7.c show some corresponding experimental results. The rotor speed range extends to above the second critical speed, with the first critical speed primarily a rotational mode and the second critical speed primarily a translational mode.

Figures 6.a presents simulation results for varying auxiliary bearing stiffness and Figure 7.a shows the corresponding experimental values. There is relatively good agreement between the actual and predicted responses except for the peak values which are very sensitive to damping. At lower rotor speeds, the stiffness effect from the auxiliary bearing tends to dominate and serves to increase the effective lower critical speed. At higher rotor speeds, the inertial effects of the bearing tend to dominate and the added mass serves to lower the effective second critical speed. This effect is balanced somewhat for higher stiffnesses (as is expected), as can be seen for the case with K_b=2,625 N/m. The damping added to the system from the auxiliary bearing serves to attenuate the peak response amplitudes for both critical speeds. The response amplitudes between the two response peaks are affected little by the auxiliary bearing, with the rotor and bearing/housing vibrations tending to decouple for response amplitudes below the clearance. Above the second critical speed, the presence of the auxiliary bearing serves to reduce the response amplitudes for the remainder of the plot. For this region, there is significant coupling between the rotor/bearing/housing vibration and the response amplitudes are below the clearance for speeds greater than about 550 rad/sec. The rotor speed ranges for which coupling of the rotor/bearing/housing vibration will occur depend upon the phase of the combined system response, as described by Black (1968). For the purposes of this study, K_b=471 N/m is chosen as a reasonable value and variations of other parameters are performed with this auxiliary bearing stiffness.

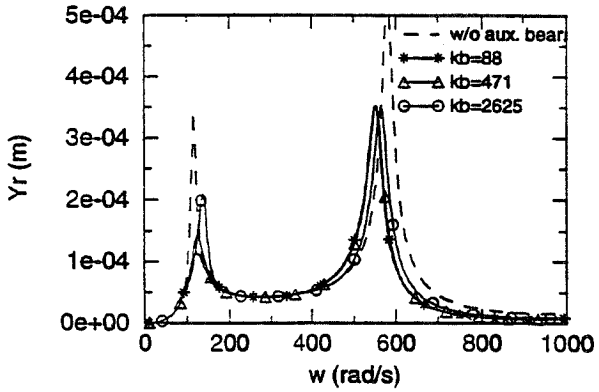

Figure 6.a Simulation Results for Varying Auxiliary Bearing Stiffness

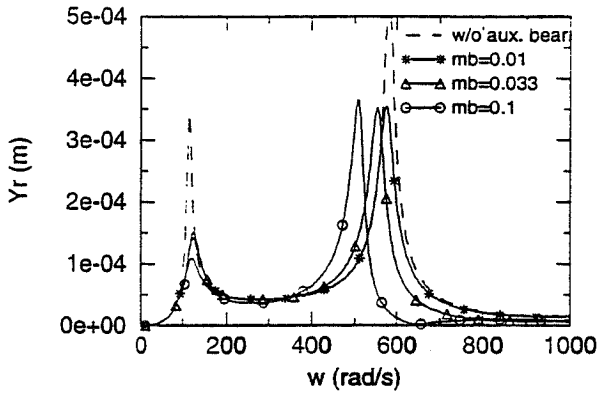

Figure 6.b Simulation Results for Varying Auxiliary Bearing Mass

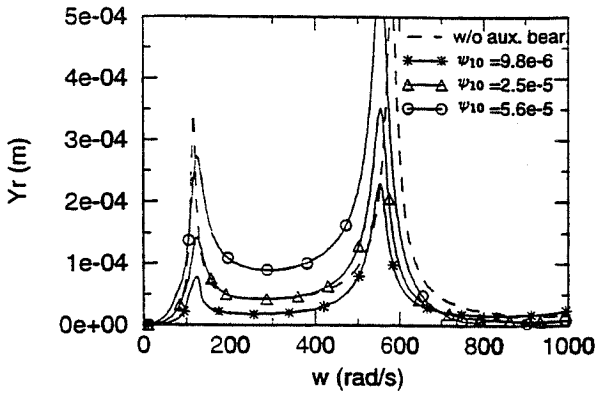

Figure 6.d Simulation Results for Varying Imbalance

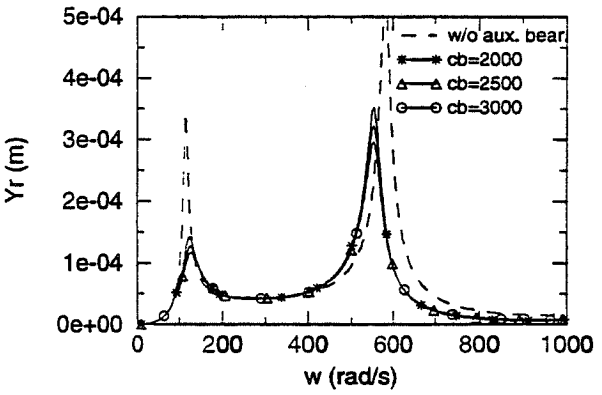

Figure 6.c Simulation Results for Varying Auxiliary Bearing Damping

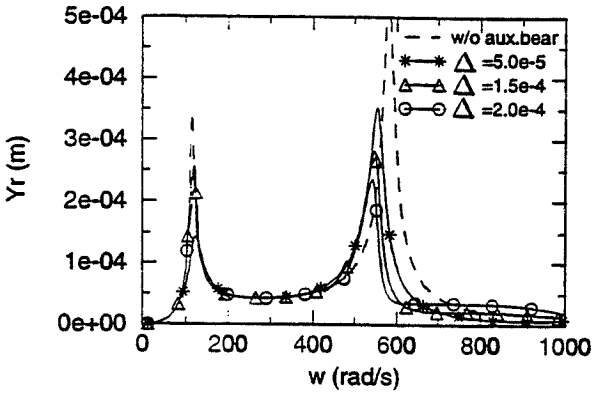

Figure 6.e Simulation Results for Varying Auxiliary Bearing Clearance

Figures 6.b shows the predicted rotor response for the parameters of Table 1 with the bearing mass varied. These results show that the more massive bearing/housing configurations can result in much lower amplitude rotor responses. In fact, for sufficiently high mass values, the response amplitude is dramatically reduced for the rotor speed range from about 600 rad/sec to about 780 rad/sec where it merges with other amplitude response curves. Figure 6.c shows the effect of auxiliary bearing damping on the rotor response. While the response amplitudes remain relatively unchanged for the majority of rotor speeds, higher damping does serve to significantly reduce the rotor response amplitudes through the critical speeds. Damping also effects the phase characteristics of the combined rotor/bearing/housing system and changes the rotor speed ranges for which coupled responses occur. Figures 6.d and 7.b show the rotor response for the parameters of Table 1 with the imbalance varied. As expected, the response amplitudes increase with increasing imbalance. Figures 6.e and 7.c show the rotor response amplitudes with the auxiliary bearing clearance varied. As the clearance increases, the dynamics of the combined rotor/bearing/housing vibration tend to decouple over a wider speed range between the two critical speeds. Again, such behavior is expected from the analysis work for a rotor operating in an annular clearance performed by Black (1968).

Close examination of the above results reveals a very interesting trend. Turbomachine are designed to operate at rotor speeds between the various system critical speeds so as to minimize synchronous

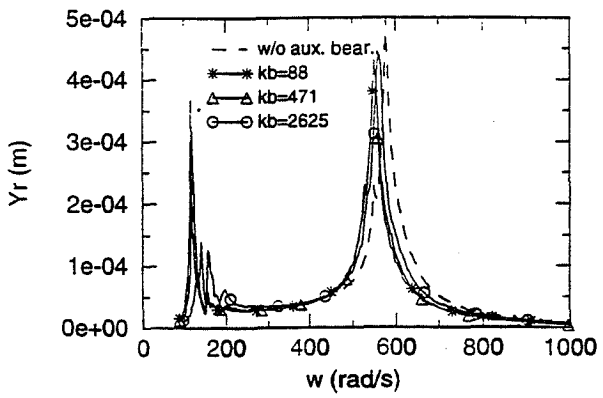

Figure 7.a Experimental Results for Varying Auxiliary Bearing Stiffness

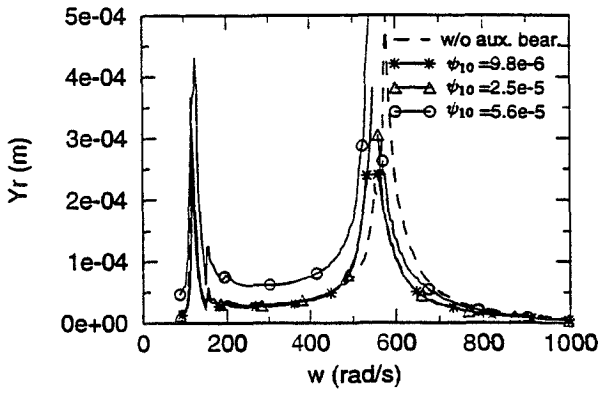

Figure 7.b Experimental Results for Varying Imbalance

response amplitudes. For the present system, the lowest amplitude responses (for operation above the second critical speed) occur for the auxiliary bearing configurations where there is the largest decrease of the second effective critical speed, which is due to a coupling of rotor/stator/housing vibration. While not really suprising, this result indicates an interesting strategy for the design of auxiliary support using clearance bearings. Selection of combined shaft/auxiliary bearing/housing vibration characteristics such that the effective critical speeds nearest the operating speed (directly above and below) shift away from it should result in lower amplitude rotor vibration and provide the best opportunity to protect the magnetic bearing. However, the phase characteristics of the combined system must be such that vibration coupling occurs

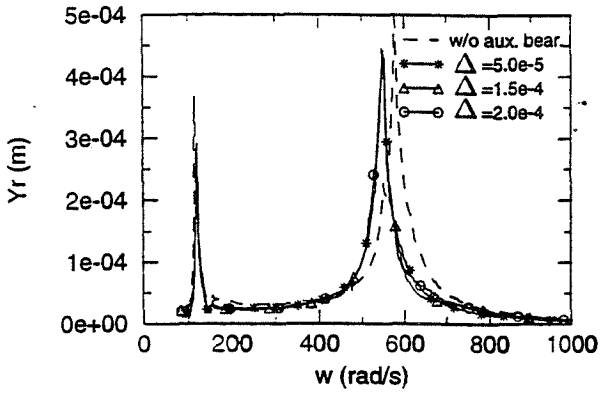

Figure 7.c Experimental Results for Varying Auxiliary Bearing Clearance

and care must be taken to ensure that this is the case if the maximum benefit is to be derived from the auxiliary bearing.

CONCLUSIONS

A study of the dynamical behavior of a flexible rotor supported by linear bearings (representing a set of magnetic bearings) and an auxiliary bearing with clearance has been presented. Parallel simulation and experimental studies have been performed for a variety of parametric configurations. The influence of bearing mass, stiffness, damping, clearance, and imbalance were examined. It was observed that the dynamic behavior of a rotor interacting with an auxiliary bearing depends very strongly on the structural parameters of the auxiliary bearing and associated housing. Appropriate selection of these parameters is critical if acceptable vibration characteristics are to be obtained for such systems. In general, one must carefully consider the influence of housing/bearing dynamics and how to best take advantage of favorable coupled modes of vibration in the development of auxiliary bearing designs.

ACKNOWLEDGEMENT

This work was supported by NASA under Grant No. NGT-70312 and Grant No. NAG3-1507. The Government has certain rights in this material. Appreciation is expressed to S.C. Sinha, S.G. Ryan and A.F. Kascak for their advice and assistance in this research effort.

REFERENCES

Bently, D. E., 1974, "Forced Subrotative Speed Dynamic Action of Rotating Machinery," ASME Paper No. 74-PET-16.

Black, H. F., 1968, "Interaction of a Whirling Rotor With a Vibrating Stator Across a Clearance Annulus," *Journal Mechanical Engineering Science*, Vol. 10, No 1, pp. 1–12.

Childs, D. W., 1979, "Rub-Induced Parametric Excitation in Rotors," *ASME Journal of Mechanical Design*, Vol. 101, pp. 640–644.

Childs, D. W., 1982, "Fractional-Frequency Rotor Motion Due to Nonsymmetirc Clearance Effects," *ASME Journal of Engineering for Power*, Vol. 104, pp. 533–541.

Ehrich, F. F., 1965, "Bistable Vibrations of Rotors in Bearing Clearance," ASME Paper 65–WA/MD–1.

Ehrich, F. F., 1988, "High Order Subharmonic Response of High Speed Rotors in Bearing Clearance," *ASME Journal of Vibration, Acoustics, Stress, and Reliability in Design*, Vol. 110, pp. 9–16.

Ehrich, F. F., 1992, "Observatons of Subcritical Superharmonic and Chaotic Response in Rotordynamics," *ASME Journal of Vibration and Acoustics*, Vol. 114, pp. 93–100.

Ehrich, F. F., 1991, "Some Observatons of Chaotic Vibration Phenonema in High-speed Rotordynamics," *ASME Journal of Vibration, Acoustics, Stress, and Reliability in Design*, Vol. 113, pp. 50–57.

Ehrich, F. F., 1966, "Subharmonic Vibration of Rotors in a Bearing Clearance," ASME Paper 66-MD-1.

Ehrich, F. F., and O'Conner, J. J., 1967, "Stator Whirl with Rotors in Bearing Clearance," *ASME Journal of Engineering for Industry*, August, pp. 381–390.

Gelin, Al, Pugnet, J. M., and Hagopina, J. D., 1990, "Dynamic Behavior of Flexible Rotors with Active Magnetic Bearings of Safety Auxiliary Bearings," *Proceedings of 3rd International Conference on Rotordynamics*, Lyon, France, pp. 503–508.

Ishii, T., and Kirk, R. G., 1991, "Transient Response Technique Applied to Active Magnetic Bearing Machinery During Rotor Drop," *DE-Vol. 35, Rotating Machinery and Vehicle Dynamics, ASME*, pp. 191–199.

Muszynska, A., 1984, "Partial Lateral Rotor to Stator Rubs," IMechE Paper No. C281/84.

Nayfeh, A.H., and Mook, D.T., 1979, Nonlinear Oscillations, John Wiley and Sons. pp. 59–61.

Ryan, S.G., 1991, "Limit Cycle Vibrations in Turbomachinery," NASA Technical Paper 3181.

STEADY–STATE DYNAMIC BEHAVIOR OF A FLEXIBLE ROTOR WITH AUXILIARY SUPPORT FROM A CLEARANCE BEARING

Huajun Xie, George T. Flowers, and Li Feng

Department of Mechanical Engineering
Auburn University
Auburn, Alabama

Charles Lawrence

NASA Lewis Research Center
Cleveland, Ohio

ABSTRACT

This paper investigates the steady-state responses of a rotor system supported by auxiliary bearings in which there is a clearance between the rotor and the inner race of the bearing. A simulation model based upon the rotor of a production jet engine is developed and its steady–state behavior is explored over a wide range of operating conditions for various parametric configurations. Specifically, the influence of rotor imbalance, clearance, support stiffness and damping is studied. Bifurcation diagrams are used as a tool to examine the dynamic behavior of this system as a function of the afore mentioned parameters. The harmonic balance method is also employed for synchronous response cases. The observed dynamical responses is discussed and some insights into the behavior of such systems are presented.

NOMENCLATURE

C_B = auxiliary bearing support damping, lb.s^2/in.
F_n = normal force, lb
$\mathbf{F}_X$ = external force vector acting on the rotor in X direction
$\mathbf{F}_Y$ = external force vector acting on the rotor in Y direction
$\mathbf{I}_a$ = rotor inertia matrix
K_B = auxiliary bearing support stiffness, lb/in.
K_C = contact stiffness, lb/in.
M_B = auxiliary bearing mass, lb.s^2/in.
M_k = mass of kth rotor element, lb.s^2/in.
N = total number of modes considered
$NB1$ = node number at auxiliary bearing #1
$NB2$ = node number at auxiliary bearing #2
$\mathbf{Q}_X$ = rotor modal coordinate vector in X direction
$\mathbf{Q}_Y$ = rotor modal coordinate vector in Y direction
R_B = radius of auxiliary bearing bore, in.
R_m = radius of auxiliary bearing pitch, in.
R_R = radius of rotor journal, in.
$\mathbf{X}_R$ = rotor physical coordinate vector in X direction
$\mathbf{Y}_R$ = rotor physical coordinate vector in Y direction
e = rotor imbalance eccentricity, in.
g = gravitational acceleration, in./s^2
t = time, s
Δ = deformation at the contact point, in.
$\mathbf{\Gamma} = \mathbf{\Psi}^T \mathbf{I}_a \mathbf{\Psi}$
$\mathbf{\Psi}$ = rotor free-free modal rotation matrix
Ω = rotor operating speed, rad/s
ω_n = rotor natural frequency, rad/s
$\mathbf{\Phi}$ = rotor free-free modal displacement matrix
$\delta = R_B - R_R$, auxiliary bearing clearance, in.
μ = dynamic friction coefficient
μ_ψ = rolling friction coefficient
ψ_B = angular displacement of auxiliary bearing inner-race
ζ = modal damping coefficient

INTRODUCTION

One of the most innovative developments in the turbomachinery field involves the use of active magnetic bearings (AMB) for rotor support. This technology provides the potential for significant improvements in the dynamic behavior of rotor systems, allowing for loading, eccentricity, shaft position and vibration to be continuously monitored and controlled. In order to protect the soft iron cores of the magnetic bearings and to provide rotor support in the event of failure of the bearing or during an overload situation, auxiliary (or backup) bearings are usually included in the rotor design. There are a number of auxiliary bearing configurations that have been considered. Typically a clearance bearing (bushing or rolling element bearing), in which there is a gap between the rotor and the inner race of the bearing, is used. The clearance introduces a nonlinear dynamical feature which may significantly impact the behavior of the rotor.

There are a number of studies in the literature concerned with the dynamics of rotors with clearance effects. Yamamoto (1954) conducted a systematic study of rotor responses involving bearing clearance effects. Black (1968) studied the rotor/stator interaction with a clearance. He concluded that rotor/stator interactions may occur in a variety of forms and circumstances, including jump phenomena. Ehrich (1966) reported the first identification of a second order subharmonic vibration phenomenon in a rotor system associated with bearing clearance (1966). Bently (1974) published experimental observations of second and third order subharmonic vibration in a rotor system. Later, Muszynska (1984) cited the occurrence of second, third, and fourth order subharmonic responses in a rotor rubbing case and Ehrich (1988 and 1991) observed eighth and ninth order subharmonic vibration as well as chaotic vibration in a high speed turbomachine. Childs (1979 and 1982) published two papers to explain the mechanism for the second and third order subharmonic responses noted above. Choi and Noah (1994) investigated the influence of bearing clearances on rotordynamic responses, including bifurcation behavior and chaos. This paper also contains an excellent review and list of additional references on the topic.

There has been quite a bit of recent work that is specifically concerned with auxiliary bearings in magnetic bearing supported rotor systems. Gelin et al. (1990) studied the transient dynamic behavior of rotors on auxiliary bearings during the coast down. Ishii and Kirk (1991) and Kirk and Ishii (1993) investigated the transient responses of a flexible rotor during the rotor drop after the magnetic bearings become inactive. Schweitzer, et al. (1994) presents a good discussion of issues related to the touch–down dynamics of rotors on auxiliary bearings. While these studies have greatly enhanced the understanding of the dynamics of rotors supported by auxiliary clearance bearings, most of them have been performed from the perspective that the rotor will be shut down if failure of one or more of the magnetic bearings occurs. As a result, work in this area has concentrated on transient dynamical behavior for a rotor with a decreasing spin speed. From a practical perspective, such an assumption is appropriate for noncritical applications, such as power generators and compressors. However, magnetic bearing systems appear to provide particularly great promise for use in aeronautical and aerospace applications. There are active programs at many of the major jet engine manufacturers to develop engines supported by magnetic bearings. Safety is a major concerns in any aeronautical design. In particular, it is desirable for an aircraft to be able to return to its base and land if the magnetic bearing(s) fail. In addition, flywheel energy storage systems which require extended operation of the rotor on auxiliary bearings are being considered for space applications. Toward this end, it is desirable to design the rotor system to take maximum advantage of the backup bearings and use them as true auxiliary bearings to provide support during critical situations in a safe and consistent manner. If clearance bearings are to be used for such applications, an important concern in this regard is the dynamic behavior of the rotor when it is in contact with the auxiliary bearing. If safe and effective operation is to be ensured during these periods, it is essential that designers have a very good understanding of the steady–state dynamics of rotor systems with clearance effects.

In the current paper, simulation studies are performed for a complex rotor system supported by auxiliary bearings with clearance at each end of the rotor. This work is specifically concerned with systems in which the clearances are quite small (on the order of a few mils), which is appropriate for applications in which the backup bearing is acting to provide rotor support on a consistent basis. The influence of rotor imbalance, clearance, support stiffness and support damping are investigated using direct numerical integration of the governing equations of motion and the harmonic balance method. Some insights are obtained with regard to the frequency and amplitude behavior of the steady–state vibration of such a system. Based upon these results, some design guidelines and suggestions are presented.

SIMULATION MODEL

The rotor is modelled using free–free normal mode shapes and natural frequencies obtained through finite element analysis. The model data is representative for the rotor of a jet engine. Fig. 1 shows a schematic diagram of the FEM rotor model. The torsional motion of the shaft is not considered in this paper. Using state space representation and modal coordinates, the equations of motion for the rotor are expressed as

$$\ddot{\mathbf{Q}}_X + 2\zeta\omega_n\dot{\mathbf{Q}}_X + \Omega\mathbf{\Gamma}\dot{\mathbf{Q}}_Y + \omega_n^2\mathbf{Q}_X + 2\Omega\zeta\omega_n\mathbf{Q}_Y = \mathbf{\Phi}^T\mathbf{F}_X, \quad (1.a)$$

$$\ddot{\mathbf{Q}}_Y + 2\zeta\omega_n\dot{\mathbf{Q}}_Y - \Omega\mathbf{\Gamma}\dot{\mathbf{Q}}_X + \omega_n^2\mathbf{Q}_Y - 2\Omega\zeta\omega_n\mathbf{Q}_X = \mathbf{\Phi}^T\mathbf{F}_Y, \quad (1.b)$$

where

$$\mathbf{F}_X = \{F_{X1}, F_{X2}, \ldots, F_{Xm}\}^{-1},$$
$$\mathbf{F}_Y = \{F_{Y1}, F_{Y2}, \ldots, F_{Ym}\}^{-1},$$
$$\mathbf{Q}_X = \mathbf{\Phi}^{-1}\mathbf{X}_R,$$
$$\mathbf{Q}_Y = \mathbf{\Phi}^{-1}\mathbf{Y}_R,$$

with

$$\mathbf{X}_R = \{X_{R1}, X_{R2}, \ldots, X_{Rm}\}^{-1},$$
$$\mathbf{Y}_R = \{Y_{R1}, Y_{R2}, \ldots, Y_{Rm}\}^{-1}.$$

(m = total number of nodes)

The physical displacements of the rotor at the two auxiliary bearing locations can be obtained using the following coordinate transformation:

$$X_{Rk} = \sum_{i=1}^{N} \Phi_{ik}\, Q_{Xi}, \qquad (k = NB1, NB2)$$
$$Y_{Rk} = \sum_{i=1}^{N} \Phi_{ik}\, Q_{Yi},$$

The equations of motion for the auxiliary bearings are derived using the model shown in Fig. 2

$$M_{Bk}\ddot{X}_{Bk} + C_{Bk}\dot{X}_{Bk} + K_{Bk}X_{Bk} = F_{nk}\cos\alpha_k - F_{tk}\sin\alpha_k + M_{Bk}\,g, \quad (2.a)$$

$$M_{Bk}\ddot{Y}_{Bk} + C_{Bk}\dot{Y}_{Bk} + K_{Bk}Y_{Bk} = F_{nk}\sin\alpha_k + F_{tk}\cos\alpha_k, \quad (2.b)$$

$$J_{Bk}\ddot{\psi}_{Bk} + C_{B\psi k}\dot{\psi}_{Bk} = F_{tk}R_{Bk} - \mu_\psi F_{nk}R_{mk}, \quad (2.c)$$

where

$$\alpha_k = tan^{-1}\frac{Y_{Rk} - Y_{Bk}}{X_{Rk} - X_{Bk}}. \qquad (k = NB1, NB2)$$

The forces resulting from gravity, imbalance, and rotor/bearing contact are expressed as follows.

$$F_{Xk} = -F_{nk}\cos\alpha_k + F_{tk}\sin\alpha_k + M_k\,g + M_k\,e\,\Omega^2\cos(\Omega t),$$
$$F_{Yk} = -F_{nk}\sin\alpha_k - F_{tk}\cos\alpha_k + M_k\,e\,\Omega^2\sin(\Omega t).$$

The rotor/bearing interaction is represented with the normal force F_{nk}

$$F_{nk} = \begin{cases} K_C\delta_k, & \Delta_k < 0, \\ 0, & \Delta_k \geq 0, \end{cases} \quad (3.a)$$

where

$$\Delta_k = (X_{Rk} - X_{Bk})\cos\alpha_k + (Y_{Rk} - Y_{Bk})\sin\alpha_k - \delta_k$$

and the Coulomb friction force F_{tk}. As long as there exists slip at the contact point, the friction force obeys

$$F_{tk} = \mu F_{nk}. \quad (3.b)$$

However, when there is no slip at the contact point, the friction forces are solved from equations (1) and (2) using the kinematic constraint that the circumferential velocities of the rotor and the inner-race of the back-up bearing at the contact point equal to each other. At the same time, if this solved friction force exceeds the maximum static friction force ($= \mu_s F_{nk}$), equation (3.b) applys again.

DISCUSSION OF RESULTS

The rotor is modeled with 34 stations (as shown in Figure 1) and the first four modes (two rigid body and two flexible modes) are included in the simulation model. The two auxiliary bearings are located at nodes 3 and 33, respectively. This arrangement is taken to represent one of the most technically feasible configurations in that it greatly simplifies bearing maintenance. It is assumed that the two auxiliary bearings are identical in terms of stiffness, damping and friction characteristics. Some nominal system parameters used for the simulation study are M_B=0.0023, K_C=2.855e+6, and ζ=0.03. To avoid excessive cluttering of the plots, all the results that are presented in this paper correspond to the location of the first bearing, which is node number 3.

The primary design parameters for an auxiliary clearance bearing are stiffness, damping, clearance, and load level (imbalance). It is fairly obvious that rotor responses involving nonsymmetric bearing clearance effects are very complex problems and it is quit difficult to obtain a global picture of the system responses with numerical integration alone. In the first phase of the present work, the harmonic balance method is used to investigate the global system behavior. Please note that the complex frequency contents associated with medium and large imbalance values makes it a formidable task to apply the harmonic balance method for configurations other than for purely synchronous behavior. However, an adequately balanced rotor system should have very small imbalance under normal conditions and, thus, should exhibit primarily synchronous responses.

Variation of rotor response amplitudes with rotor speed for the system with and without bearing clearance is shown in Figure 3(a). Examination of the response curves indicates that the effect of nonsymmetries resulting from gravitational loading, coupled with bearing clearance, is similar to that of asymmetric support stiffnesses with regards to critical speeds. The first critical speed actually splits into two pseudo–critical speeds. In the X direction, the gravity force tends to keep the rotor in contact with the bearing at low operating speed. Thus, the apparent stiffness is almost the same as K_B and the pseudo-critical speed is nearly the same as the critical speed for the linear case ($\delta = 0$). In the Y direction, the clearance results in a lower apparent stiffness and, consequently, an additional lower-value pseudo-critical speed. It is seen that several higher order additional pseudo-critical speeds are created in the operating speed range in addition to the 1st additional pseudo-critical speed. The response in the X direction also departs from the linear case at high operating speed. This is because the imbalance force becomes dominant at high rotor speed which in turn makes the gravity force less significant and the clearance effect more important. An interesting phenomena that can result as the clearance is increased is that of double–valued responses. Figure 3(b) shows double–valued responses in the Y direction for four different values of clearance. It is seen that a larger clearance results in wider rotor speed range of double–valued responses. It is also observed that as clearance increases, the apparent stiffness decreases and the first pseudo–critical speed shifts to a lower value. Figure 3(c) shows the double–valued responses in the X direction. Even though the jumps themselves are smaller in magnitude, they are more obvious in trend. Notice how little the change is for the first pseudo-critical speed in the X direction. The system behaviors for higher operating speed range are not shown in Figures 3.b and 3.c so that the jump phenomena can be more clearly illustrated. The system responses in the high operating speed range with the same parameters exhibit primarily amplitude changes.

In the second phase of this study, bifurcation diagrams are constructed using the steady–state system responses obtained through direct numerical integration of the governing equations of motion. Such an approach allows for the study of medium and high imbalance cases for which non-synchronous responses may occur. Near–zero initial conditions were used, simulating situations where the AMBs are functioning properly prior to a system failure. Bifurcation diagrams for varying bearing stiffness, bearing damping, and clearance are shown.

Bifurcation diagrams with bearing stiffness as the variable parameter are shown in Figure 4 and bifurcation diagrams with bearing damping as the variable parameter are shown in Figure 5. These response characteristics are typical for a quite wide range of configurations. There is a threshold stiffness value (about 2.5 x 10^5 for the particular case shown) above which the behavior is always multi–frequency. Conversely, there is a threshold damping value (about 150 for the particular case shown) below which the behavior tends to always be multi–frequency. Figure 6 shows bifurcation diagrams with clearance as the variable parameter. Two values of imbalance are shown. For the lower value (Figure 6.a and Figure 6.b), the responses are synchronous over a wide range of clearance. However, there is a region ($0.002 \leq \delta$ 0.0032) for which the behavior is chaotic. However, for the larger value of imbalance (Figure 6.c and Figure 6.d) it is observed that the there is a threshold value of imbalance ($\delta >$ 0.0024) for which the behavior is always chaotic. Studies were also conducted using rotor imbalance as the variable parameter. The variation in response characteristics for this case is quite similar to that for the case of varied clearance and are not shown for the purpose of brevity.

A common feature among all of the observed responses is that for very small imbalance, the responses are always synchronous. The imbalance range that result in synchronous dominated responses depends on several system parameters. For low back-up bearing stiffness (such as K_B = 0.213e+6) and moderate damping (C_B = 157.0), the responses are almost always synchronous. Only $\Omega/2$ subharmonic are observed at a few operating speeds with a very narrow range of imbalance. It should be noted that even though a lower K_B may leads to a better system response, it may also fail to protect the magnetic bearings due to the fact that it could result in a larger rotor orbit-center offset. However, the dramatic response changes discussed above may occur again if the damping becomes small (such as C_B = 50.0) even though the stiffness still remains small. On the other hand, increasing the damping C_B alone may not be able to eliminate those dramatic changes. It is observed that those changes can still occur for C_B being as large as 700.0. Reducing the size of clearance δ may not eliminate the multi–frequency behavior at certain speeds, but it does tend to narrow the operating speed range where those changes occur. For example, multi–frequency behavior is eliminated for $\Omega \geq 1500$ when δ is reduced from 0.002 to 0.001 with all other parameters remaining the same, but such behavior may still occur for $\Omega \leq 1400$.

CONCLUSIONS

The harmonic balance method and direct numerical integration has been used to study the response characteristics of a jet engine rotor supported by bearings with a clearance. Variations of bearing stiffness, bearing damping , clearance, and rotor imbalance were considered. The dynamic reponses are described in some detail and some suggestions are provided with regard to the design of an appropriate auxiliary

bearing configuration for this rotor system. The basic observations are generally applicable to any rotor system. In summary, the following observations have been made.

1. A close examination of the rotor behavior reveals three basic response modes. The first is primarily synchronous oscillation at the bottom of the bearing dominated by gravitional loading holding the rotor against the bearing. As vibration amplitudes increase, the motion transitions to a a bouncing mode with multiple frequency components. Finally as the vibration amplitudes become sufficiently large, the motion transitions back to purely synchronous whirling.
2. Steady–state synchronous, multi–synchronous, sub– synchronous, and chaotic responses may occur and are observed. Gravitational effects produce a side force on the rotor (a nonsymmetric effect) that may be beneficial (by keeping the rotor in contact with the bearing inner race) or may be harmful (by encouraging the development of multi-frequency vibrations/chaos) depending upon the particular system configuration. Such effects are certainly present in real rotors and need careful consideration in design analyses for such systems.
3. Imbalance may serve to dramatically alter the frequency contents of the rotor responses at certain operating speeds. This is particularly evident for cases of large clearance, high bearing stiffness and low bearing damping. Generally, auxiliary bearing designs with low clearance, low support stiffnesses, and high support damping tend to discourage the development of multi–frequency/chaotic behavior and provide the most favorable rotordynamic behavior. However other requirements, most particularly the requirement that no contact occur between the soft iron components of the AMB, may impose additional constraints that must be considered.

ACKNOWLEDGEMENT

The authors would like to express their gratitude to S. A. Klusman of Allison Turbine Engine Company for many helpful discussions and practical advice.

This work was supported by NASA under Grant No. NAG3–1507. The Government has certain rights in this material.

REFERENCES

Bently, D. E., 1974, "Forced Subrotative Speed Dynamic Action of Rotating Machinery," ASME Paper No. 74-PET-16.

Black, H. F., 1968, "Interaction of a Whirling Rotor With a Vibrating Stator Across a Clearance Annulus," *Journal of Engineering Sci ence*, Vol. 10, No. 1, pp. 1-12.

Chen, P. Y. P, Hahn, E. J., and Wang, G. Y., 1993, "Subharmonic Oscillations in Squeeze Film Damped Rotor Bearing Systems Without Centralizing Springs," ASME Paper 93-GT-428.

Childs, D. W., 1979, "Rub-Induced Parametric Excitation in Rotors," ASME *Journal of Mechanical Design*, Vol. 101, pp. 640-644.

Childs, D. W., 1982, "Fractional-Frequency Rotor Motion Due to Nonsymmetric Clearance Effects," ASME *Journal of Engineering for Power*, Vol. 104, pp. 533-541.

Choi, Sang–Kyu, and Noah, Sherif T., 1994, "Mode Locking and Chaos in a Jeffcott Rotor with Bearing Clearances," *Journal of Applied Mechanics*, Vol.61, No. 1, pp. 131–138.

Cunningham, W. J., 1958, *Introduction to Nonlinear Analysis*, McGraw-Hill Book Co., New York, NY.

Ehrich, F. F., 1966, "Subharmonic Vibration of Rotors in Bearing Clearance," ASME Paper 66-MD-1.

Ehrich, F. F., 1988, "High Order Subharmonic Response of High Speed Rotors in Bearing Clearance," ASME *Journal of Vibration, Acousti cs, Stress, and Reliability in Design*, Vol. 110, pp. 9-16.

Ehrich, F. F., 1991, "Some Observations of Chaotic Vibration Phenomena in High-Speed Rotordynamics," ASME *Journal of Vibration, Acoustics, Stress, and Reliability in Design*, Vol. 113, pp. 50-57.

Feeny, B.F., "Stability of Cylindrical and Conical Motions of a Rigid Rotor in Retainer Bearings," *Proceedings of the Fourth Internation Symposium on Magnetic Bearings*, August 1994, ETH Zurich, pp. 219-224.

Gelin, A., Pugnet, J. M., and Hagopian, J. D., 1990, "Dynamic Behavior of Flexible Rotors with Active Magnetic Bearings on Safety Auxiliary Bearings," *Proceedings of 3rd International Conference on Rotordynamics*, Lyon, France, pp. 503-508.

Kirk, R. G., and Ishii, T., 1993, "Transient Rotor Drop Analysis of Rotors Following Magnetic Bearing Power Outage," *Proceedings of MAG'93*, June, pp. 53-61.

Muszynska, A., 1984, "Partial Lateral Rotor to Stator Rubs, " IMechE Paper No. C281/84.

Schweitzer, G., Blueler, HH., and Traxler, A., 1994, Active Magnetic Bearings, VDF, Zurich, pp. 141-146.

Yamamoto, T. T., 1954, "On Critical Speeds of a Shaft," *Memoirs of the Faculty of Engineering*, Nagoya University (Japan), Vol. 6, No. 2.

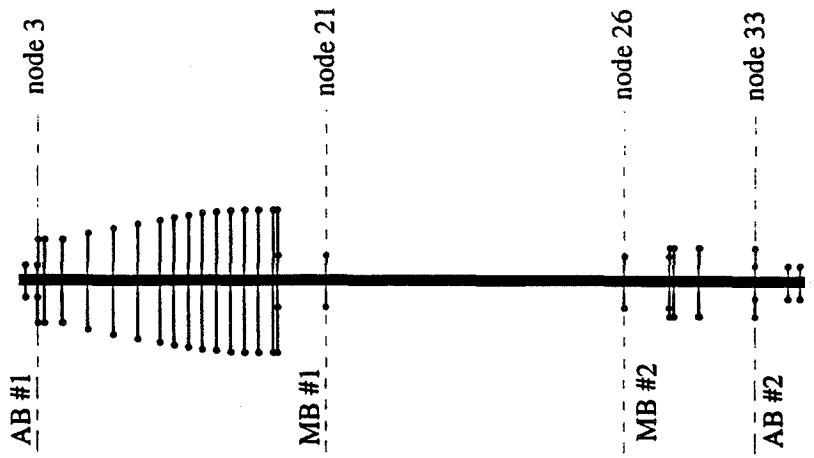

Figure 1: Diagram of Finite Element Rotor Model

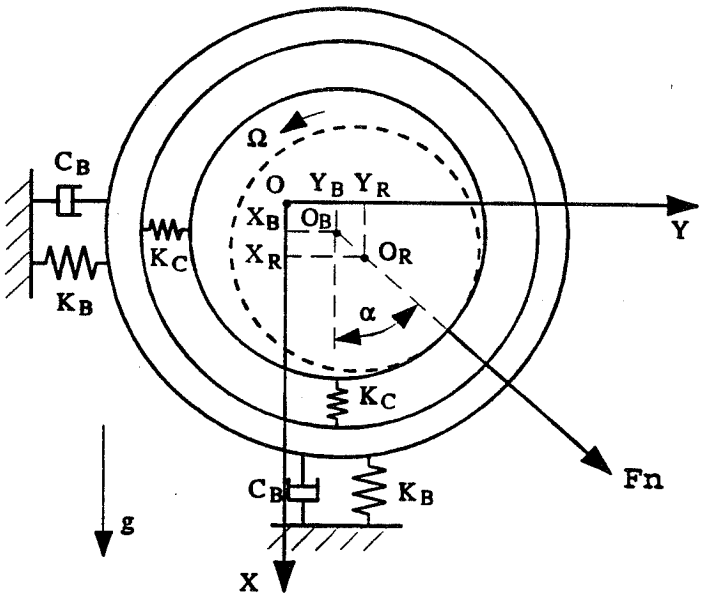

Figure 2: Auxiliary Bearing Model

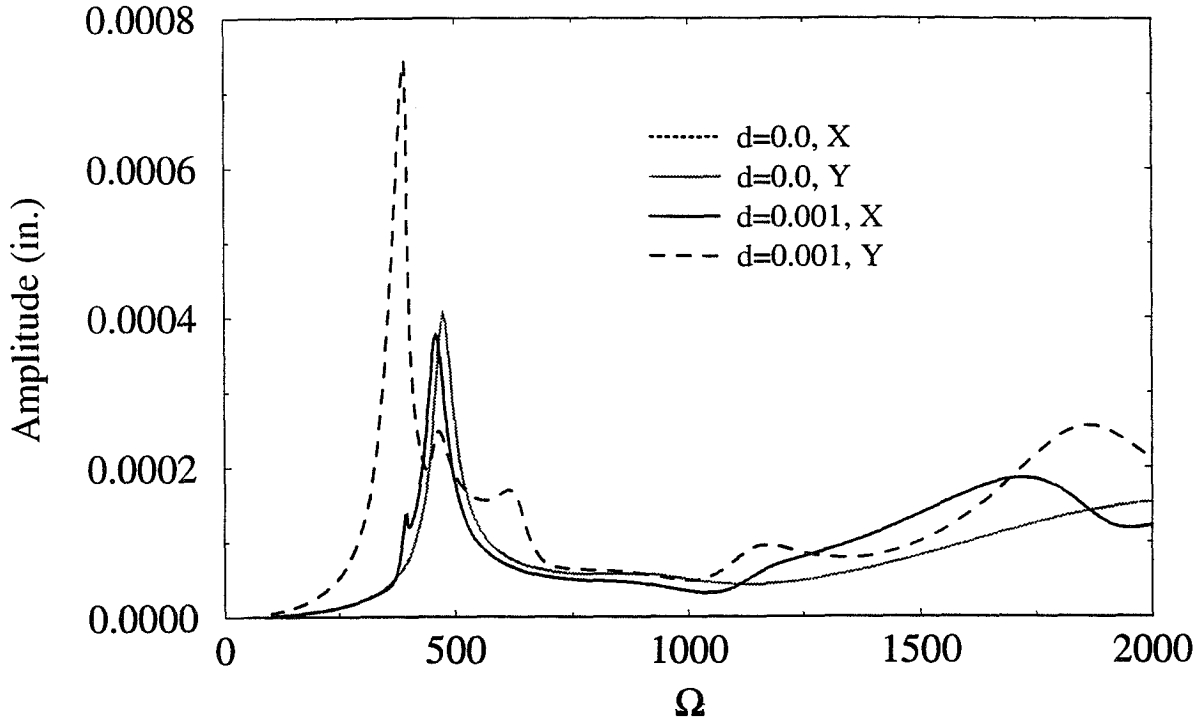

Figure 3.a: Synchronous Response Amplitudes with Auxiliary Bearing Clearance as the the Variable Parameter
$C_B = 150,\ e = 0.0001,\ K_B = 0.313e6$

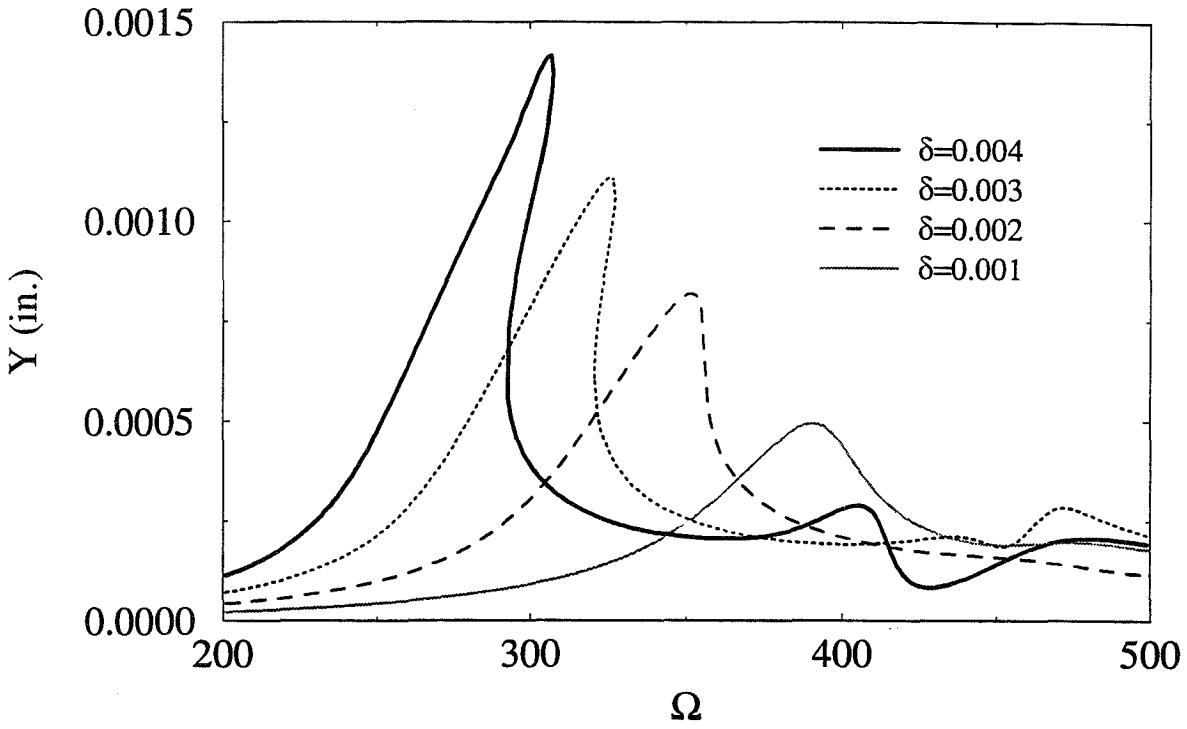

Figure 3.b: Synchronous Response Amplitudes with Auxiliary Bearing Clearance as the the Variable Parameter
$C_B = 300,\ e = 0.0001,\ K_B = 0.313e6$

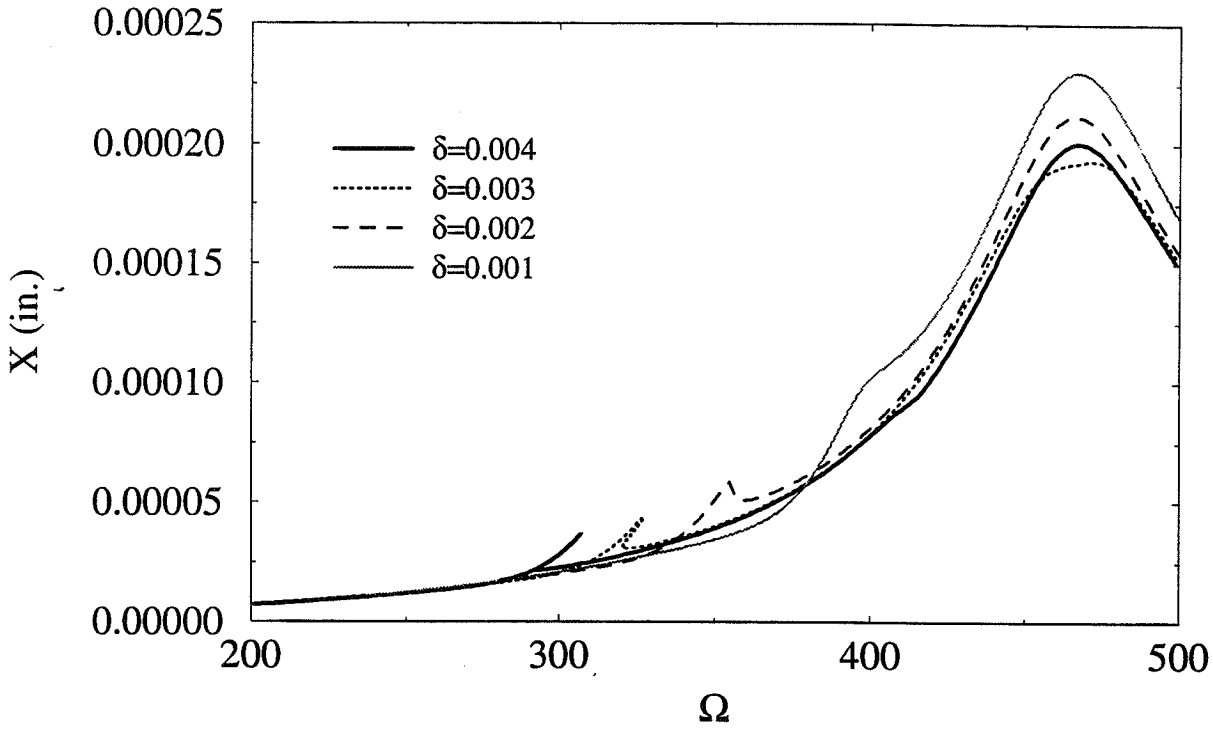

Figure 3.c: Synchronous Response Amplitudes with Auxiliary Bearing Clearance as the the Variable Parameter
$C_B = 300,\ e = 0.0001,\ K_B = 0.313e6$

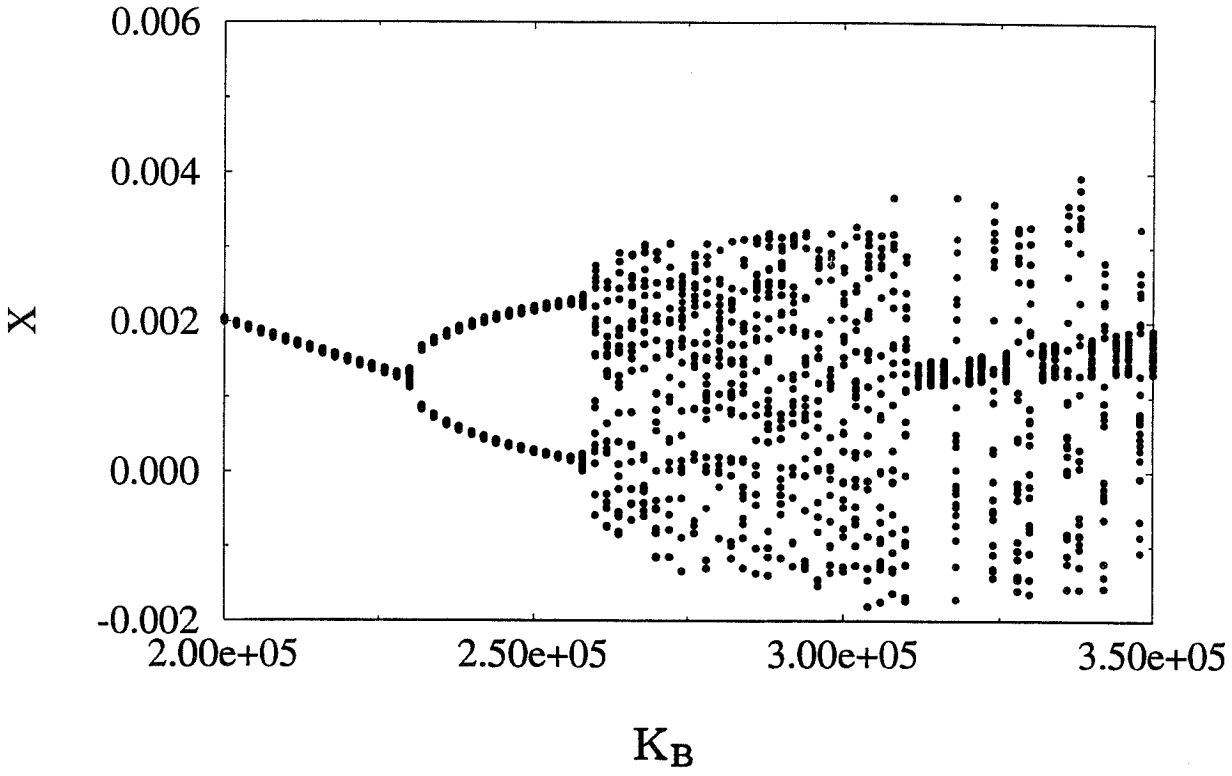

Figure 4.a: Bifurcation Diagram with Auxiliary Bearing Stiffness as the Variable Parameter
$C_B = 250,\ \omega = 1500,\ e = 0.0008,\ d = 0.002$

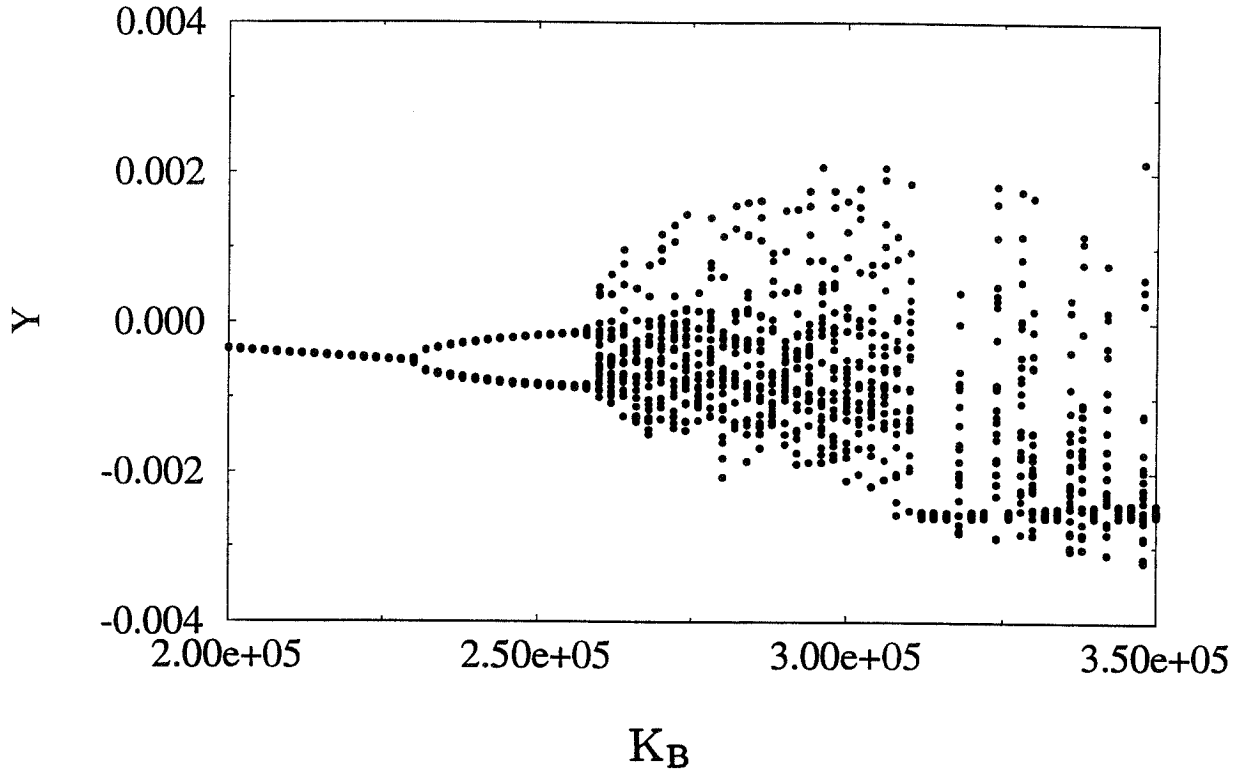

Figure 4.b: Bifurcation Diagram with Auxiliary Bearing Stiffness as the Variable Parameter
$C_B = 250,\ \omega = 1500,\ e = 0.0008\ d = 0.002$

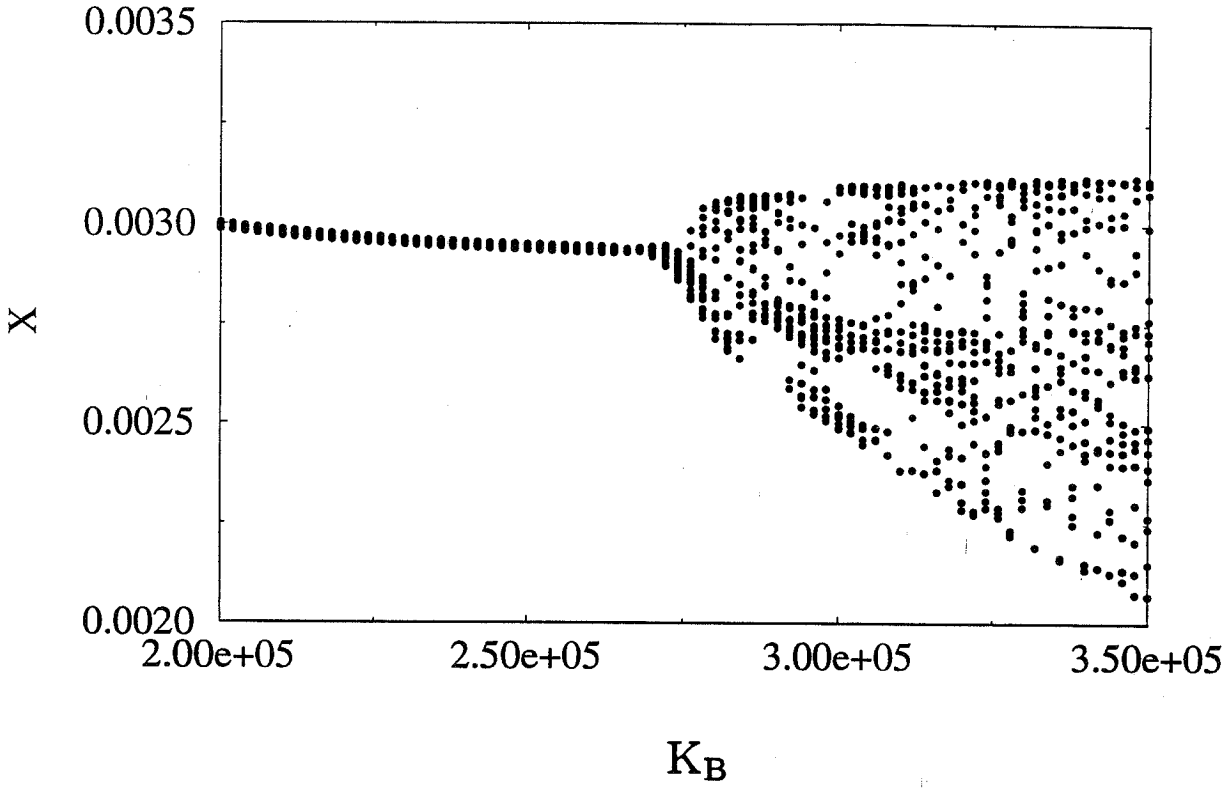

Figure 4.c: Bifurcation Diagram with Auxiliary Bearing Stiffness as the Variable Parameter
$C_B = 250,\ \omega = 1500,\ e = 0.0004\ d = 0.002$

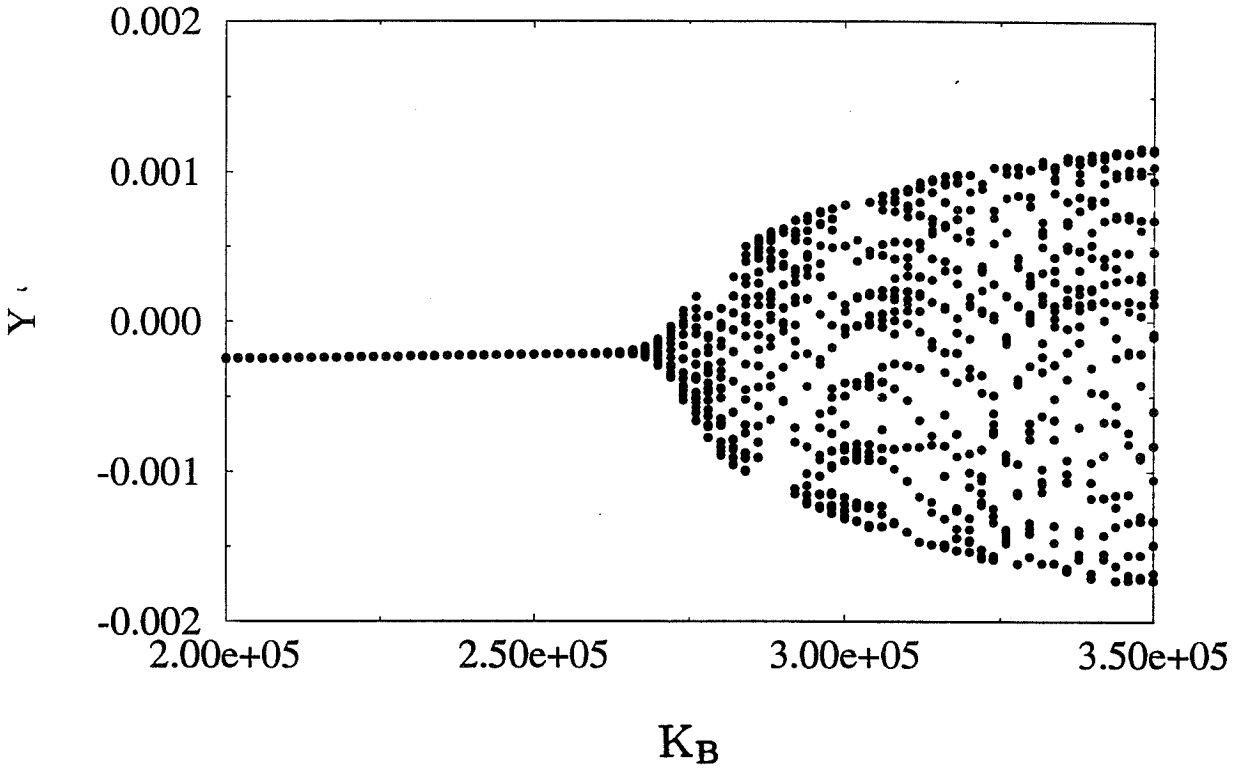

Figure 4.d: Bifurcation Diagram with Auxiliary Bearing Stiffness as the Variable Parameter
$C_B = 250,\ \omega = 1500,\ e = 0.0004\ d = 0.002$

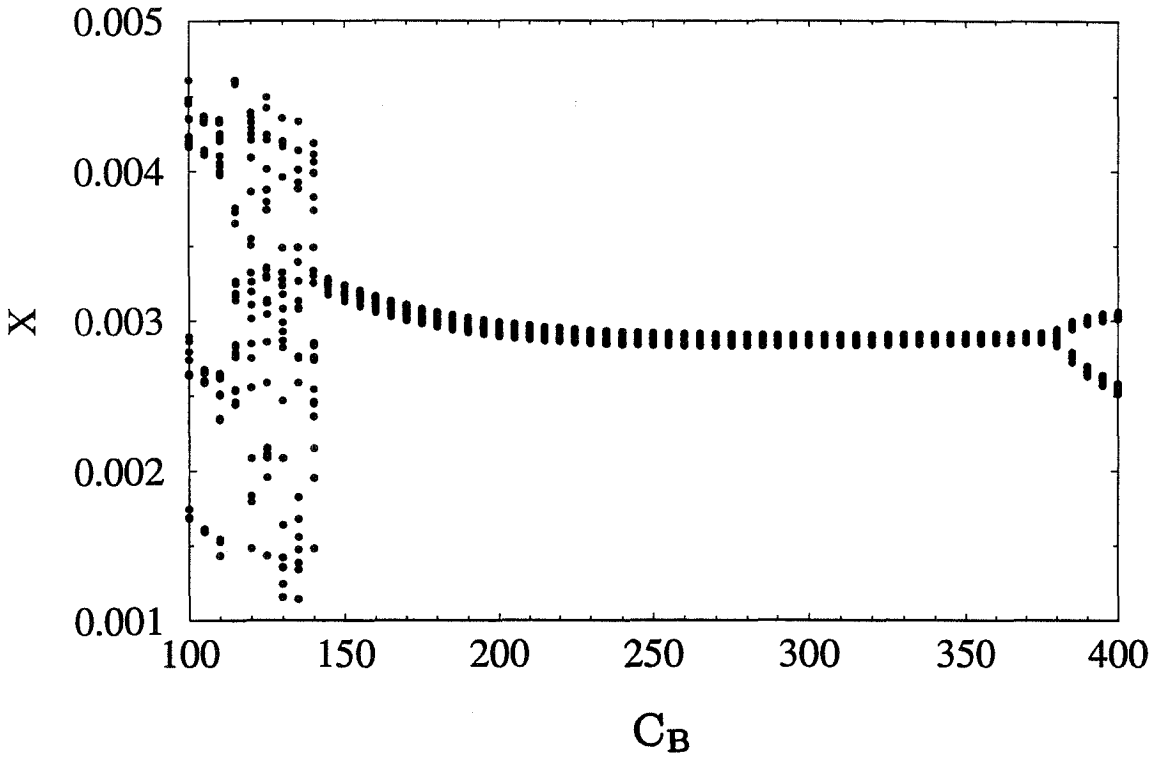

Figure 5.a: Bifurcation Diagram with Auxiliary Bearing Damping as the Variable Parameter
$K_B = 0.313e6,\ \omega = 1500,\ e = 0.0015\ d = 0.002$

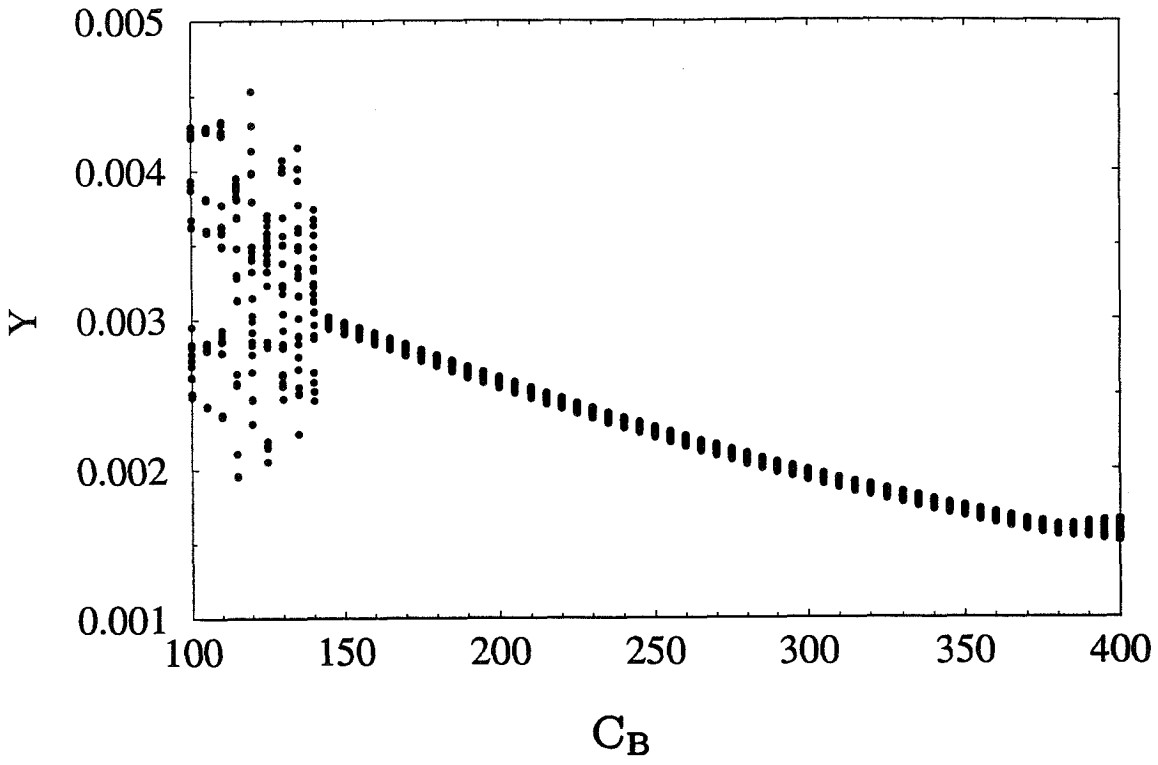

Figure 5.b: Bifurcation Diagram with Auxiliary Bearing Damping as the Variable Parameter
$K_B = 0.313e6,\ \omega = 1500,\ e = 0.0015\ d = 0.002$

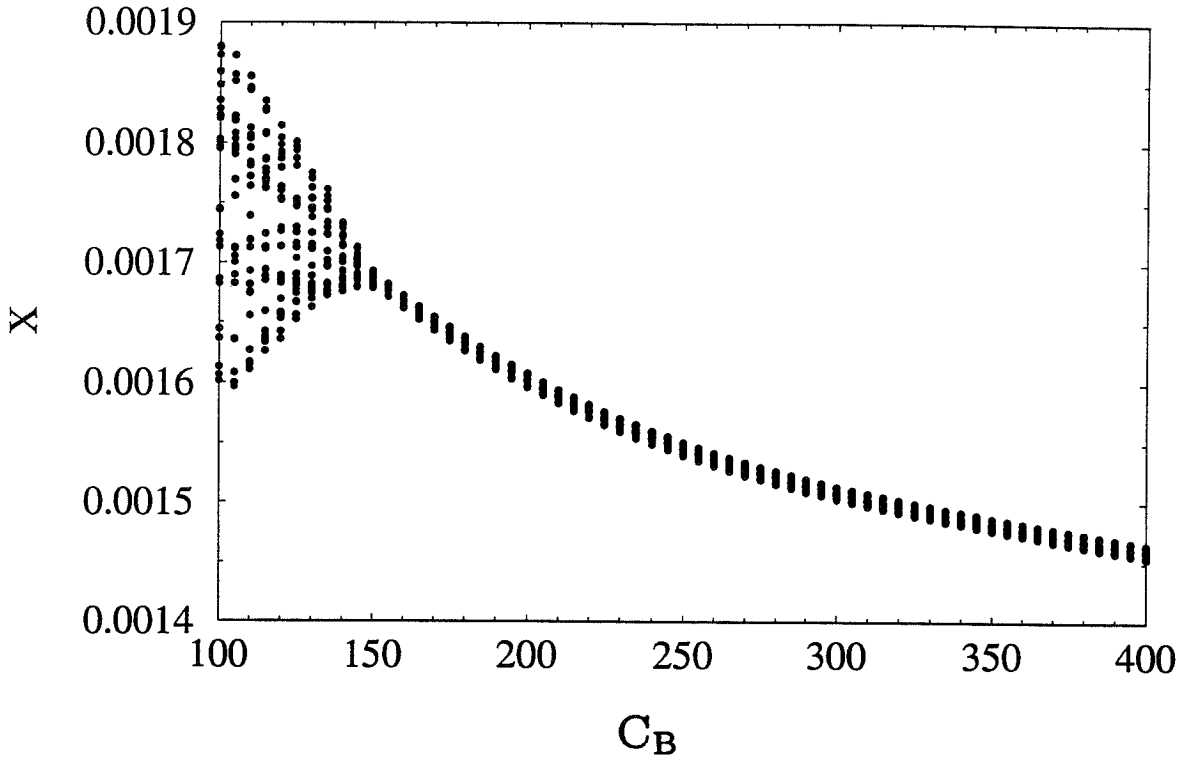

Figure 5.c: Bifurcation Diagram with Auxiliary Bearing Damping as the Variable Parameter
$K_B = 0.313e6$, $\omega = 1000$, $e = 0.0015$ $d = 0.001$

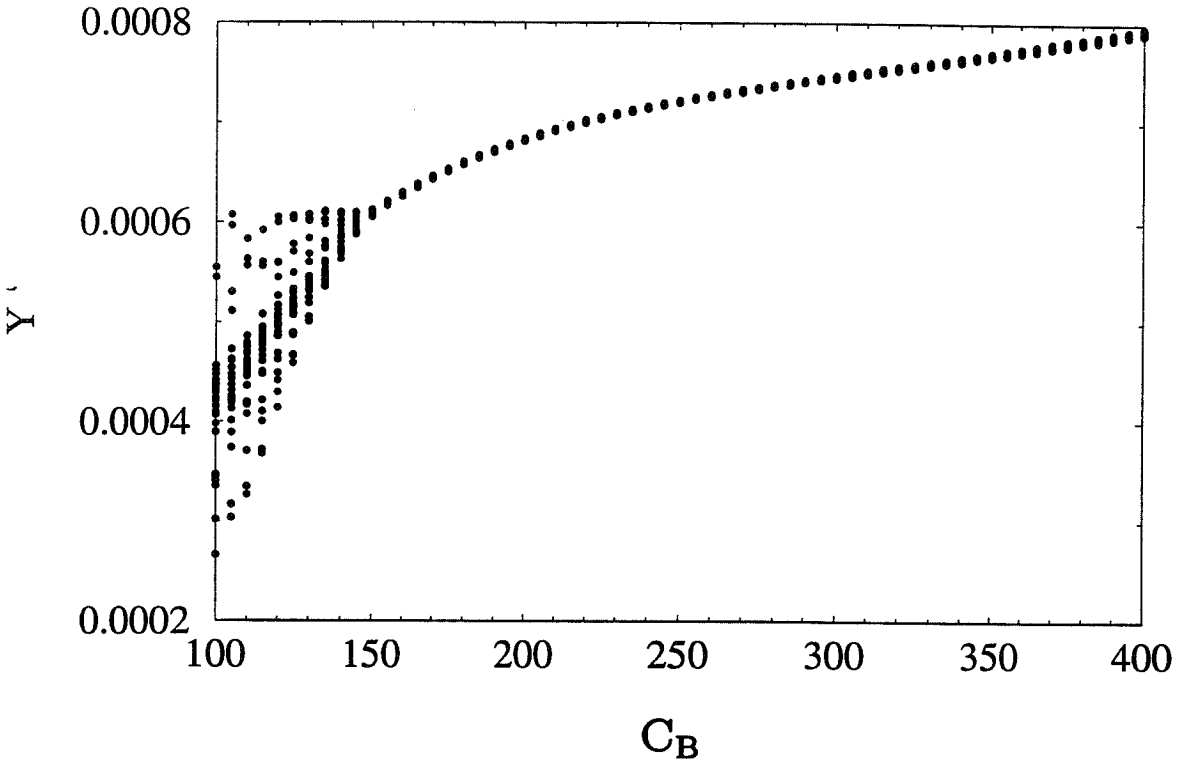

Figure 5.d: Bifurcation Diagram with Auxiliary Bearing Damping as the Variable Parameter
$K_B = 0.313e6$, $\omega = 1000$, $e = 0.0015$ $d = 0.001$

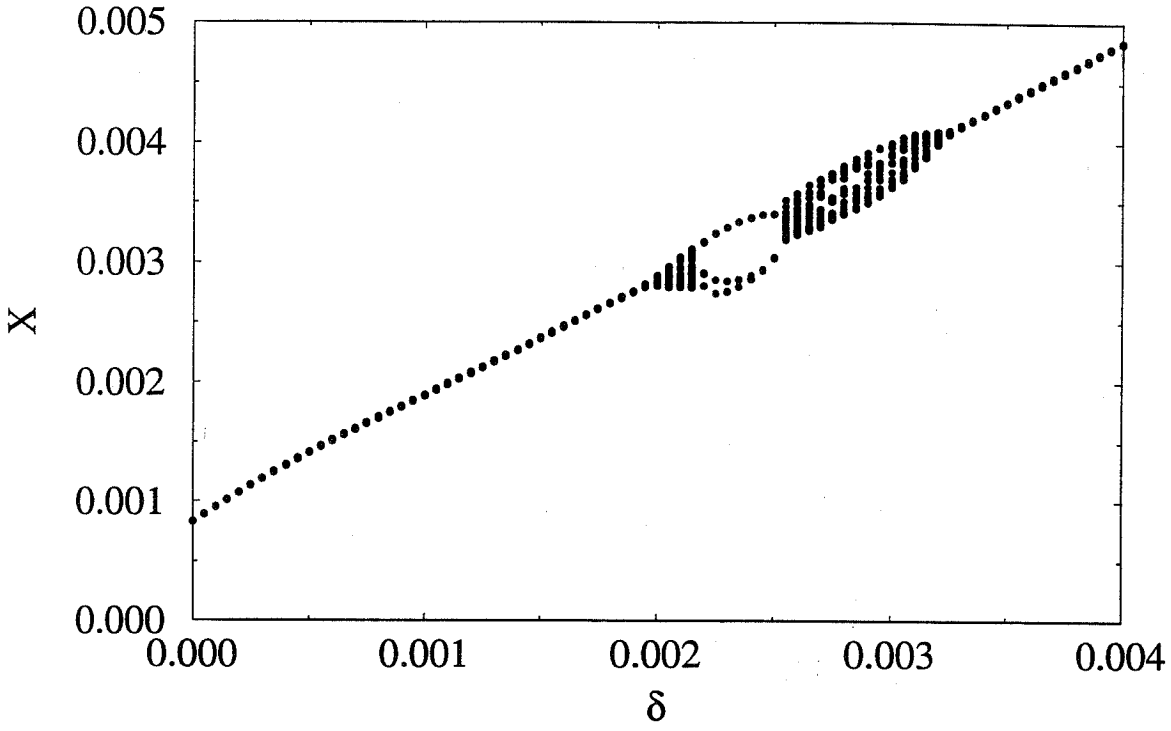

Figure 6.a: Bifurcation Diagram with Auxiliary Bearing Clearance as the Variable Parameter
$C_B = 250,\ K_B = 0.313e6,\ \omega = 1500,\ e = 0.0005$

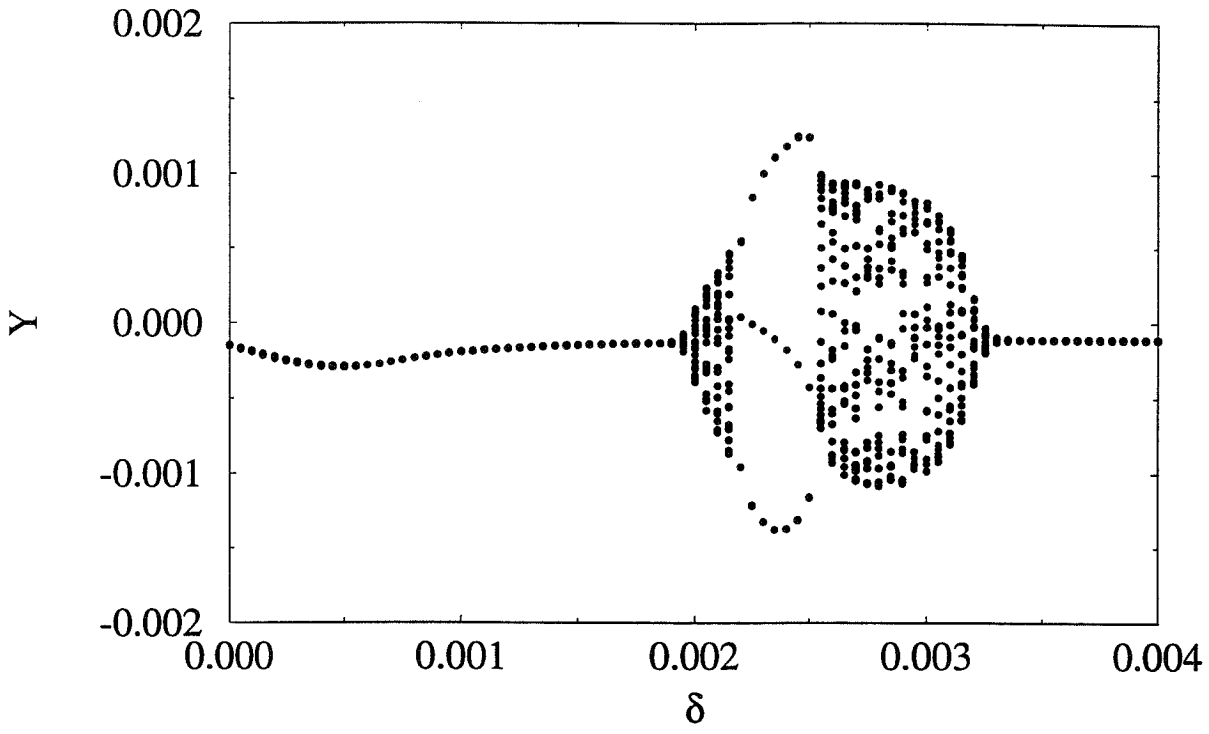

Figure 6.b: Bifurcation Diagram with Auxiliary Bearing Clearance as the Variable Parameter
$C_B = 250,\ K_B = 0.313e6,\ \omega = 1500,\ e = 0.0005$

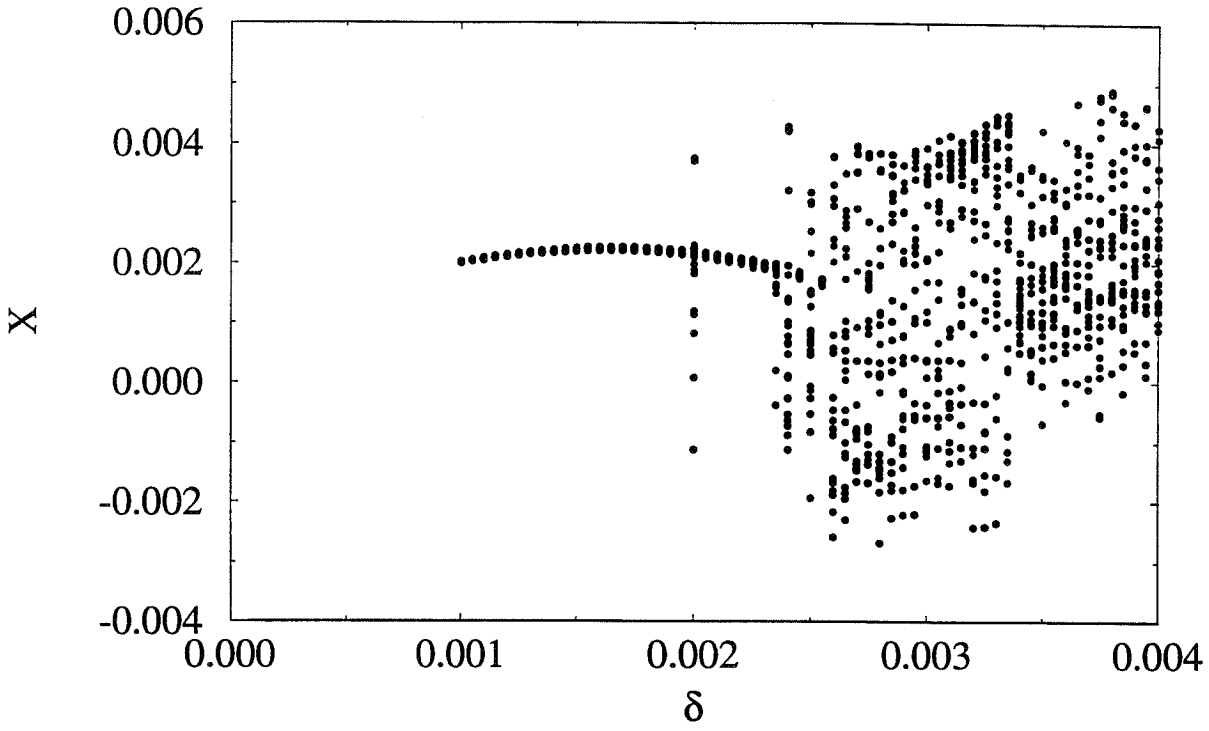

Figure 6.c: Bifurcation Diagram with Auxiliary Bearing Clearance as the Variable Parameter
$C_B = 250,\ K_B = 0.313e6,\ \omega = 1500,\ e = 0.0010$

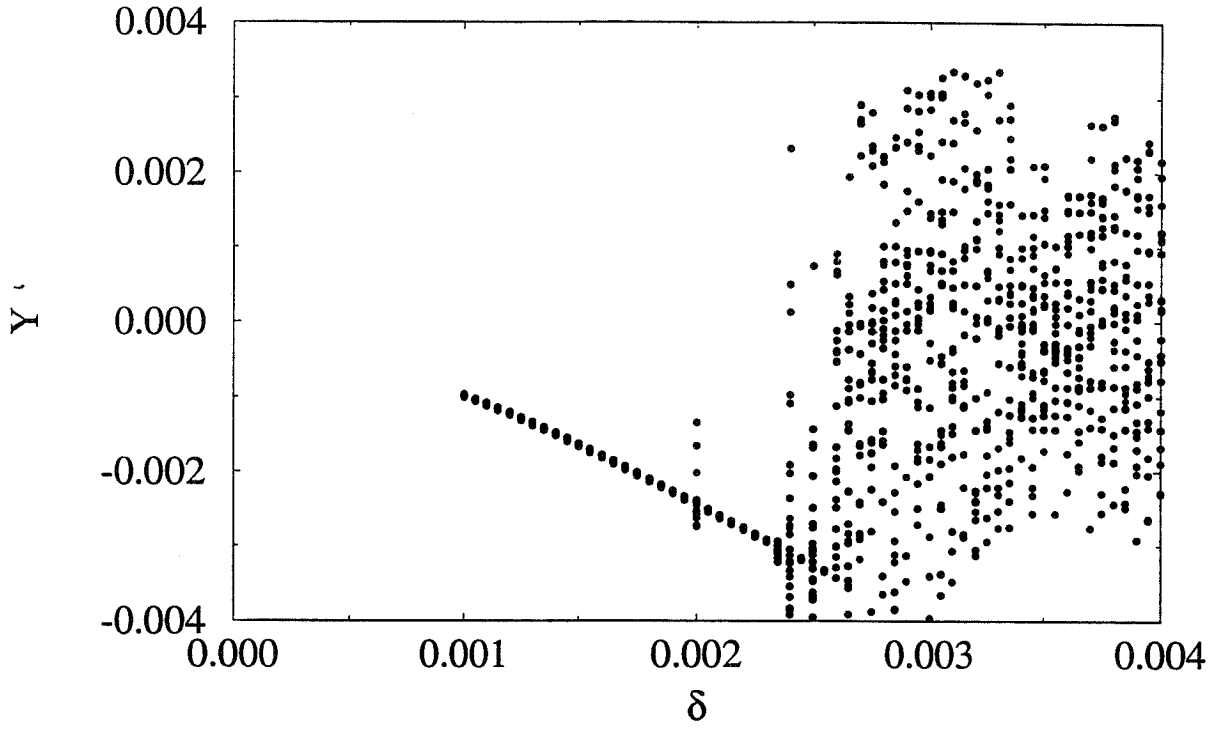

Figure 6.d: Bifurcation Diagram with Auxiliary Bearing Clearance as the Variable Parameter
$C_B = 250$, $K_B = 0.313e6$, $\omega = 1500$, $e = 0.0010$

ROTORDYNAMIC MODELLING AND RESPONSE CHARACTERISTICS OF AN ACTIVE MAGNETIC BEARING ROTOR SYSTEM

April M. Free and George T. Flowers

Department of Mechanical Engineering
Auburn University
Auburn, AL 36849

Victor S. Trent

Department of Electrical Engineering
Auburn University
Auburn, AL 36849

ABSTRACT

Auxiliary bearings are a critical feature of any magnetic bearing system. They protect the soft iron core of the magnetic bearing during an overload or failure. An auxiliary bearing typically consists of a rolling element bearing or bushing with a clearance gap between the rotor and the inner race of the support. The dynamics of such systems can be quite complex. It is desired to develop a rotordynamic model which describes the dynamic behavior of a flexible rotor system with magnetic bearings including auxiliary bearings. The model is based upon an experimental test facility. Some simulation studies are presented to illustrate the behavior of the model. In particular, the effects of introducing sideloading from the magnetic bearing when one coil fails is studied. These results are presented and discussed.

NOMENCLATURE

C = damping, N–s/m
C_L = clearance of auxiliary bearing, m
D = nominal gap thickness, m
$\mathbf{F}_X$ = external force vector acting on the rotor in X direction, N
$\mathbf{F}_Y$ = external force vector acting on the rotor in Y direction, N
G = gravitational acceleration, m/s^2
I = rotor inertia matrix
i = current, amp
K = stiffness, N/m
k = gain value
L = equivalent circuit length
M = mass, kg
m = total number of nodes
N = total number of modes considered
N_{B1} = node number at rotor left end
N_{B2} = node number at AMB
N_{B3} = node number at auxiliary bearing

N_{imb} = node number at imbalance location
N_T = number of turns of wire per coil
$\mathbf{Q}_X$ = rotor modal coordinate vector in X direction
$\mathbf{Q}_Y$ = rotor modal coordinate vector in Y direction
R_R = radius of rotor journal, m.
R_S = radius of auxiliary bearing bore, m.
t = time, s
t_f = fail time, s
v = voltage, volt
v_r = relative velocity at auxiliary bearing rotor/stator contact point
$\mathbf{X}_R$ = rotor physical coordinate vector in X direction
$\mathbf{X}_S$ = stator physical coordinate vector in X direction
$\mathbf{Y}_R$ = rotor physical coordinate vector in Y direction
$\mathbf{Y}_S$ = stator physical coordinate vector in Y direction
α = acceleration, rad/sec^2
δ = dynamic clearance
$\mathbf{\Gamma} = \Psi^T \mathbf{I} \Psi$
$\mathbf{\Phi}$ = rotor free-free modal displacement matrix
$\mathbf{\Psi}$ = rotor free-free modal rotation matrix
ψ = imbalance vector
μ_o = permeability of free space
μ_r = permeability of silicon steel
Ω = rotor operating speed, rad/s
τ = time constant
θ = angular position of the shaft
ζ = modal damping coefficient

Subscripts

a = first
B = auxiliary bearing
b = second
C = contact
g = gain constant
h = horizontal
l = left bearing
r = rate constant
v = vertical
x = x – direction
y = y – direction
bi = bias
1 = top magnet
2 = right magnet
3 = bottom magnet
4 = left magnet

Superscripts

a = current amplifier
c = controller
l = lead
p = sensor amplifier

INTRODUCTION

In recent years, the use of active magnetic bearings (AMB) for turbomachinery support has been an area of interest in both academia and in industry. Magnetic bearings provide the potential for significant improvements over other types of rotor supports, including elimination of wear, bearing friction-related energy losses and a means of actively suppressing rotor vibration. A critical feature of any magnetic bearing supported rotor system is auxiliary bearings to protect the soft iron core from rotor contact (and subsequent damage) during an overload or failure of the AMB. The present work is concerned with developing a suitable model and investigating the dynamic behavior of such a system.

EXPERIMENTAL TEST FACILITY

The model and control system development presented in this study is for an experimental test facility. The apparatus consists of a radial magnetic bearing that is supporting the right end of a rotor. The left end of the rotor is supported by a ball bearing suspended in a frame by four springs. A photograph and the corresponding schematic diagram are shown in Figure 1.

The apparatus has two basic components: the rotor shaft and the magnetic bearing. The shaft is made of steel and is 0.0098 meters in diameter and 0.4572 meters in length. A steel disk of diameter 7.62 cm, thickness 2.54 cm, and mass 0.810 kg is placed at the midpoint of the bearing span. Threaded holes on the disk allow for imbalance to be added to the system. The rotor is driven by a variable speed motor with a controller. Shaft vibration is measured using eddy current proximity displacement sensors fixed to measure displacement in both the vertical and horizontal directions.

The magnetic bearing is based upon a design described in Humphris, et al (1988). The basic parameters for the bearing are shown in Table 1. The bearing consists of four electromagnets equally spaced around a soft–iron core. A photograph and schematic diagram of the bearing are shown in Figure 2.

SIMULATION MODEL

A simulation model was developed for the rotor system described above. The model has three principal components – the rotor, magnetic bearing, and electronics. The governing equations for each are shown below.

The rotor is modelled using the free–free bending mode shapes and natural frequencies obtained through finite element analysis. The finite element code uses 11 stations and the first four modes (two rigid body and two flexible modes) are included in the simulation model. The rotor equations of motion can be expressed in terms of modal coordinates as

$$\ddot{\mathbf{Q}}_x + \Omega\Gamma\dot{\mathbf{Q}}_y + \omega_n^2\mathbf{Q}_x + \Phi^T\mathbf{F}_x = 0, \qquad (1.a)$$

$$\ddot{\mathbf{Q}}_y - \Omega\Gamma\dot{\mathbf{Q}}_x + \omega_n^2\mathbf{Q}_y + \Phi^T\mathbf{F}_y = 0, \qquad (1.b)$$

The auxiliary bearing consists of a ball bearing with a clearance between the rotor and the stator. The governing equations are

$$M_B\ddot{X}_B + C_{Bx}\dot{X}_B + K_{Bx}X_B = \mathbf{F}_{x,aux}, \quad (1.c)$$

$$M_B\ddot{Y}_B + C_{By}\dot{Y}_B + K_{By}Y_B = \mathbf{F}_{y,aux}, \quad (1.d)$$

where

$$\begin{aligned}
\mathbf{F}_{x,lin}(N_{b1}) &= \Phi_{N_{b1}}(K_{lx}\mathbf{Q}_x + C_{lx}\dot{\mathbf{Q}}_x) \\
\mathbf{F}_{y,lin}(N_{b1}) &= \Phi_{N_{b1}}(K_{ly}\mathbf{Q}_y + C_{ly}\dot{\mathbf{Q}}_y) \\
\mathbf{F}_{x,imb}(N_{imb}) &= \Omega^2\psi_6 cos\theta + \alpha\psi_6 sin\theta, \\
\mathbf{F}_{y,imb}(N_{imb}) &= \Omega^2\psi_6 sin\theta - \alpha\psi_6 cos\theta, \\
\mathbf{F}_{x,aux}(N_{b3}) &= \Phi_{N_{b3}}(\mathbf{F}_N cos\beta - \mathbf{F}_R sin\beta) \\
\mathbf{F}_{y,aux}(N_{b3}) &= \Phi_{N_{b3}}(\mathbf{F}_N sin\beta + \mathbf{F}_R cos\beta) \\
\mathbf{F}_{grav} &= \Phi^T MG \\
\mathbf{F}_N &= \phi K_c(\delta - \mathbf{D}).
\end{aligned}$$

If $v_r = 0$, then $\mathbf{F}_R$ = required static friction force to satisfy this condition. If $v_r \neq 0$ or if required static friction force $> \mu_s\mathbf{F}_N$, then $\mathbf{F}_R = \mu_k\mathbf{F}_N$.

$$\mathbf{F_x} = \mathbf{F}_{x,lin} + \mathbf{F}_{x,imb} + \mathbf{F}_{x,aux} - \mathbf{F}_{x,amb}$$

$$\mathbf{F_y} = \mathbf{F}_{y,lin} + \mathbf{F}_{y,imb} + \mathbf{F}_{y,aux} - \mathbf{F}_{y,amb} + \mathbf{F}_{grav}$$

where

$$\sin(\beta) = \frac{\mathbf{Y}_R - \mathbf{Y}_S}{\sqrt{(\mathbf{X}_R - \mathbf{X}_S)^2 + (\mathbf{Y}_R - \mathbf{Y}_S)^2}},$$

$$\cos(\beta) = \frac{\mathbf{X}_R - \mathbf{X}_S}{\sqrt{(\mathbf{X}_R - \mathbf{X}_S)^2 + (\mathbf{Y}_R - \mathbf{Y}_S)^2}},$$

$$\begin{aligned}
\delta &= \sqrt{(\Phi\mathbf{Q}_x - X_b)^2 + (\Phi\mathbf{Q}_y - Y_b)^2}, \\
\phi &= 1 \; if \; \delta > \Delta \\
&\quad\; 0 \; otherwise \\
\mathbf{Q}_x &= \Phi^T\mathbf{X}_r, \\
\mathbf{Q}_y &= \Phi^T\mathbf{Y}_r,
\end{aligned}$$

with

$$\begin{aligned}
\mathbf{X}_r &= \{X_{r1}, X_{r2}, \ldots, X_{rm}\}^T, \\
\mathbf{Y}_r &= \{Y_{r1}, Y_{r2}, \ldots, Y_{rm}\}^T.
\end{aligned}$$

The physical displacements of the rotor at the bearing and imbalance locations can be obtained using the following coordinate transformation:

$$X_{rk} = \sum_{i=1}^{N} \Phi_{ki} Q_{xi},$$

$$Y_{rk} = \sum_{i=1}^{N} \Phi_{ki} Q_{yi}, \qquad (k = N_{b1}, N_{b2}, N_{b3}, N_{imb})$$

The position of the shaft at the magnetic bearing location is measured using horizontal and vertical proximity sensors. They are modelled as linear first order systems.

$$\frac{dv_v^p}{dt} = \frac{k^p y - v_v^p}{\tau^p} \tag{2.a}$$

$$\frac{dv_h^p}{dt} = \frac{k^p x - v_h^p}{\tau^p} \tag{2.b}$$

The active control system is based upon a proportional–derivative (PD) control law and implemented using analog circuitry. The controller is modelled as

$$\frac{dv_v^c}{dt} = k_g v_v^p \tau^c + (k_g + k_r)\frac{v_v^p}{dt} - \tau^c v_v^c \tag{3.a}$$

$$\frac{dv_h^c}{dt} = k_g v_h^p \tau^c + (k_g + k_r)\frac{v_h^p}{dt} - \tau^c v_h^c \tag{3.b}$$

The control circuitry also includes a lead network. The governing equations are

$$\frac{dv_v^l}{dt} = \frac{1}{\tau_a^l} v_v^c + \frac{dv_v^c}{dt} - \frac{1}{\tau_b^l} v_v^l \tag{4.a}$$

$$\frac{dv_h^l}{dt} = \frac{1}{\tau_a^l} v_h^c + \frac{dv_h^c}{dt} - \frac{1}{\tau_b^l} v_h^l \tag{4.b}$$

Four current amplifiers (one for each coil) supply current to the magnetic bearing. They are modelled as

$$\frac{di_1^a}{dt} = -\frac{1}{\tau^a} i_1^a + \frac{1}{\tau^a} k_1^a v_v^l \tag{5.a}$$

$$\frac{di_2^a}{dt} = -\frac{1}{\tau^a} i_2^a + \frac{1}{\tau^a} k_2^a v_v^l \tag{5.b}$$

$$\frac{di_3^a}{dt} = -\frac{1}{\tau^a} i_3^a + \frac{1}{\tau^a} k_3^a v_h^l \tag{5.c}$$

$$\frac{di_4^a}{dt} = -\frac{1}{\tau^a} i_4^a + \frac{1}{\tau^a} k_4^a v_h^l \tag{5.d}$$

The forces supplied by the magnetic bearing to the rotor are assumed to be decoupled in the horizontal and vertical directions. The effects of flux saturation are included in the model based upon the approach described by Lewis (1993). The equations for these forces are

$$\mathbf{F}_{x,amb} = \mu_o A N_T^2 \left(\frac{i_2^2}{(2(D - x_{N_{B2}}) + \frac{L}{\mu_r})^2} - \frac{i_4^2}{(2(D + x_{N_{B2}}) + \frac{L}{\mu_r})^2} \right) \tag{6.a}$$

$$\mathbf{F}_{y,amb} = \mu_o A N_T^2 \left(\frac{i_1^2}{(2(D - y_{N_{B2}}) + \frac{L}{\mu_r})^2} - \frac{i_3^2}{(2(D + y_{N_{B2}}) + \frac{L}{\mu_r})^2} \right) \tag{6.b}$$

For design purposes, linearized models for the magnetic bearing forces are also needed. Linearization of (6.a) and (6.b) is performed about the nominal shaft position $y_{N_{B1}} = y_{N_{B2}} = 0$ and $x_{N_{B1}} = x_{N_{B2}} = 0$ and the nominal coil currents $i_1 = -i_3 = k_1^a v_1^{bi}$ and $i_2 = -i_4 = k_2^a v_2^{bi}$. The effects of flux saturation are not included. The current stiffnesses that result are:

$$K_1^i = \frac{\mu_o A k_1^a v_1^{bi} N_T^2}{2D^2} \tag{7.a}$$

$$K_2^i = \frac{\mu_o A k_2^a v_2^{bi} N_T^2}{2D^2} \tag{7.b}$$

$$K_3^i = \frac{\mu_o A k_1^a v_1^{bi} N_T^2}{2D^2} \tag{7.c}$$

$$K_4^i = \frac{\mu_o A k_2^a v_2^{bi} N_T^2}{2D^2} \tag{7.d}$$

The position stiffnesses that result are:

$$K_1^P = \frac{\mu_o A (k_1^a v_1^{bi})^2 N_T^2}{2D^3} \tag{8.a}$$

$$K_2^P = \frac{\mu_o A (k_2^a v_2^{bi})^2 N_T^2}{2D^3} \tag{8.b}$$

Parameter	Value	Units
K_{lx}, K_{ly}	17,510	N/m
C_{lx}, C_{ly}	2.0	N–s/m
K_C	87,557	N/m
C_C	0	N–s/m
K_B	17,510	N/m
C_{Bx}, C_{By}	2.0	N–s/m
M_B	0.033	kg
ψ_6	3.0 x 10^{-6}	kg–m
k^p	7.8 x 10^3	–
k_g	13	–
k_r	23	–
k^a	0.45	amp/v
τ^p	1.59 x 10^{-5}	–
τ_a^l	1.8 x 10^{-3}	–
τ_b^l	1.59 x 10^{-4}	–
τ^a	5.31 x 10^{-5}	–
A	3.42 x 10^{-4}	m^2
N_T	164	–
D	0.9 x 10^{-3}	m
μ_o	1.26 x 10^{-6}	–
v_1^b	4.2	volt
v_2^{bi}	1.9	volt
v_3^{bi}	1.0	volt
v_4^{bi}	1.9	volt

Table 1 Simulation Model Parameters

DISCUSSION

Using the rotordynamic model described in the preceding paragraphs, a study of the combined dynamics of a magnetic bearing supported rotor with auxiliary bearings was performed. The parameters used in this work were identified from experimental evaluation of the test rig and are shown in Table 1. All of the responses illustrated in the figures are for this base parametric configuration, unless otherwise indicated. Figure 4 shows the variation of system natural frequencies with rotor speed for the base parametric configuration (without auxiliary bearing contact). The rotor speed of 200 rad/sec was selected as a reasonable value near a critical speed in order to illustrate a worst case behavior of the system.

Figure 5 shows the rotor response under normal operating conditions. The horizontal and vertical responses are of the same amplitude and frequency at steady state. The response consists of a transient region of about 0.5 seconds in length followed by steady synchronous oscillations. The initial conditions are set so that the rotor contacts the auxiliary bearing during the transient phase of the oscillations. The rotor vibrates downward, contacts the auxiliary bearing, bounces several times, and then settles into a steady synchronous whirl of about 0.05 mm in amplitude.

Of particular interest in this study is the use of the remaining coils of the AMB (when one fails) to provide a sideloading force to reduce rotor vibration. The test configuration consists of allowing coil 2 to fail and investigating the effects of sideloading on the system. Coils 1 and 3 are kept in the same electronic configuration as if no failure had occurred. However, the voltage in coil 4 is set to a value that will pull the shaft horizontally over to the auxiliary bearing. Two basic scenarios for rotor control during failure are considered. Figures 6.a – 6.c illustrate the rotor behavior under the conditions for the first scenario, when the rotor speed is maintained at a constant value. For each case, the AMB fails at t_f= 0.5 seconds. There is some perturbation of the vertical motion of the rotor when the horizontal coil fails due to coupling of the horizontal and vertical motion (primarily) through the gyroscopic terms. However, the steady state vertical responses are not significantly affected. Figures 7.a – 7.c show the rotor behavior for the same failure conditions (with sideloading) as above for the second scenario, when the rotor is decelerated at a constant rate upon AMB failure. Again the response amplitudes tend to be lowest for smaller clearance values. It is observed that the responses may be quite high as the rotor contacts the auxiliary bearing, even with sideloading from the remaining coil. However, sideloading is shown to be quite effective in encouraging rotor contact that will dissipate the vibrational energy. The response amplitudes tend to decrease as the auxiliary bearing clearance is decreased. However from a practical perspective, there are definite design trade–offs that must be considered. If the clearance is too small, the rotor may strike the auxiliary bearing during normal operation of the magnetic bearing if the rotor is perturbed. This tends to unnecessarily shorten the life of the auxiliary bearing. If the clearance is too large, the rotor vibration (upon AMB failure) will be excessively high and may damage the rotor or the magnetic bearing structure.

The effect the sideloading voltage on the system dynamics is particularly interesting. The magnetic bearing forces are nonlinear functions of the dynamic clearance and the current. If one coil fails and the remaining coils are used to provide sideloading, the natural approach might seem to issue a constant command voltage, with the objective of having a constant sideloading force at steady state. However, the inherently unstable behavior of the magnetic bearing without active control coupled with the vibrational effects between the auxiliary bearing and the rotor produces a severely unstable response. A remedy is to command a voltage that is proportional to the horizontal shaft displacement. That is, $v^a = v_o^a(D + x_{N_{B2}})$, where v_o^a is a constant. With an ideal amplifier, any value of v_o^a can be used with such a system. However due to the delay in the dynamics from the time constant of the power amplifier, unstable behavior may also result if v_o^a is too large. Figure 8 shows the maximum v_o^a that can be commanded with stable behavior as a function of power amplifier

time constant. These results were developed by fitting a smooth curve through data points obtained by observing the behavior of the simulation model for various sideloading voltages and amplifier time constants. It must be concluded that power amplifier dynamics are a critical factor in the selection of appropriate levels of bearing sideloading.

CONCLUSION

A simulation model has been developed for a magnetic bearing supported flexible rotor system with auxiliary bearings including frictional effects. The model has been described in detail with experimentally obtained model parameters. The response characteristics for a variety of system configurations were presented and discussed, including the effects of sideloading. Some guidelines were given for the selection of appropriate levels of sideloading.

ACKNOWLEDGEMENT

This work was supported by the National Aeronautics and Space Administration under Grant No. NAG3–1507. The Government has certain rights in this material. Special appreciation is expressed to Dr. Albert F. Kascak of NASA/Lewis Research Center.

REFERENCES

Gondhalekar, V., and Holmes, R., "Design of a Radial Electromagnetic Bearing for the Vibration Control of a Supercritical Shaft," *Proceedings of the Institution of Mechanical Engineers*, Vol. 198C, No. 16, pp. 235–242.

Habermann, H., and Liard, G., "An Active Magnetic Bearing System," *Tribology International*, April, 1980, pp. 85–89.

Humphris, R.R., Kelm, R.D., Lewis, D.W., and Allaire, P.E., "Effect of Control Algorithms on Magnetic Journal Properties," *ASME Journal of Engineering for Gas Turbines and Power*, Vol. 108, October, 1986, pp. 624–632.

Ishii, T., Kirk, R.G., "Transient Response Technique Applied To Active Magnetic Bearing Machinery During Rotor Drop," *Rotating Machinery and Vehicle Dynamics*, Vol. 35, 1991, pp. 191–199.

Lewis, David W., "Electro and Permanent Magnet Materials," *Introduction To Magnetic Bearings: A Short Course*, July 27-28, 1993.

Shafai, B., Beale, S., LaRocca, and Cusson, E., "Magnetic Bearing Control Systems and Adaptive Forced Balancing," *IEEE Control Systems*, Vol. 14, No. 2, pp. 4–13.

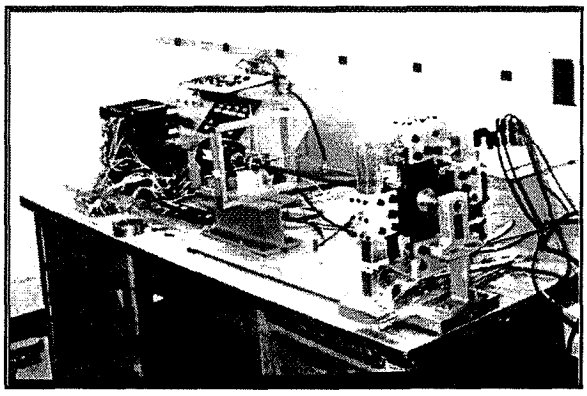

Figure 1.a Experimental Test Facility

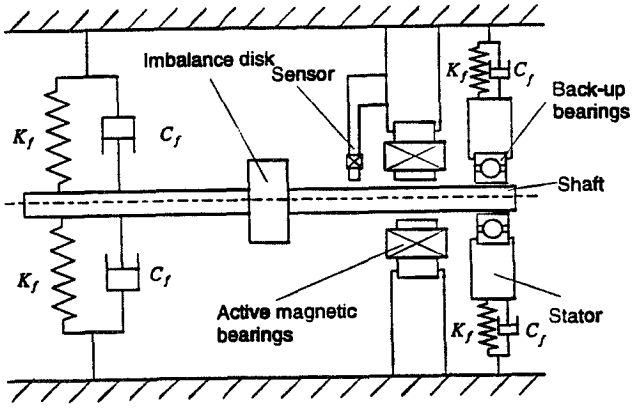

Figure 1.b Schematic Diagram of Experimental Test Facility

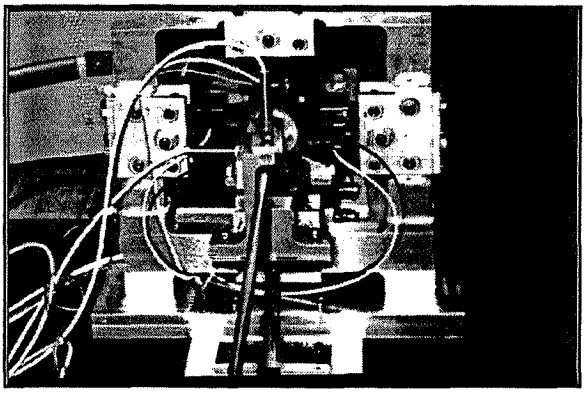

Figure 2.a Magnetic Bearing Assembly

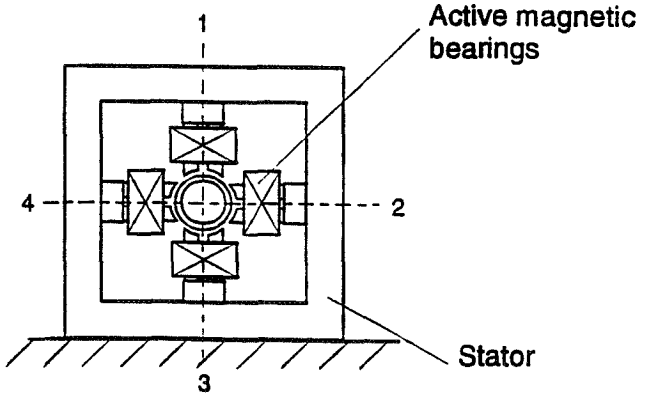

Figure 2.b Schematic Diagram of Magnetic Bearing

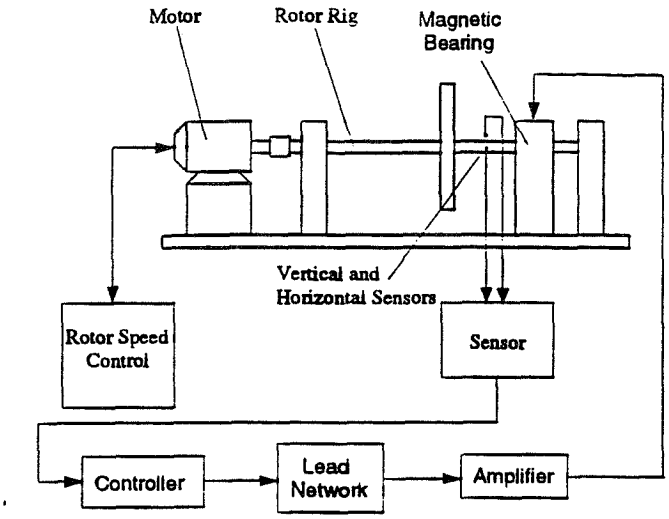

Figure 3 Block Diagram of Simulation Model

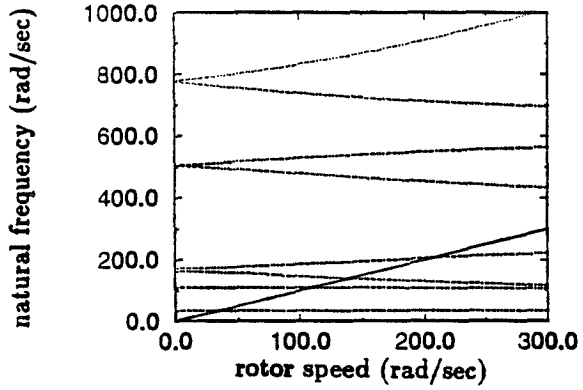

Figure 4 Rotor Natural Frequencies as a Function of Rotor Speed (for the parameters of Table 1)

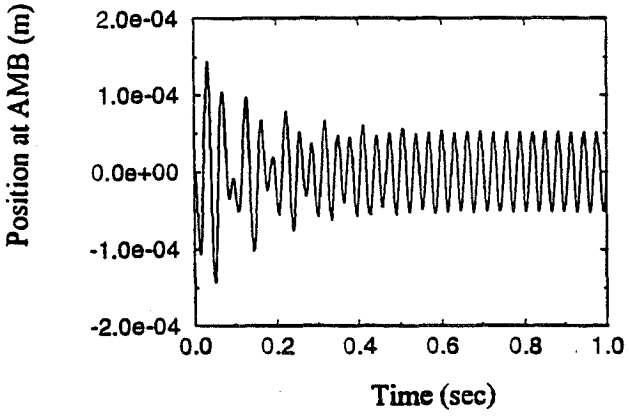

Figure 5 Rotor Response Without AMB Failure
$\Omega = 200\text{rad/sec}, C_L = \frac{D}{2}$

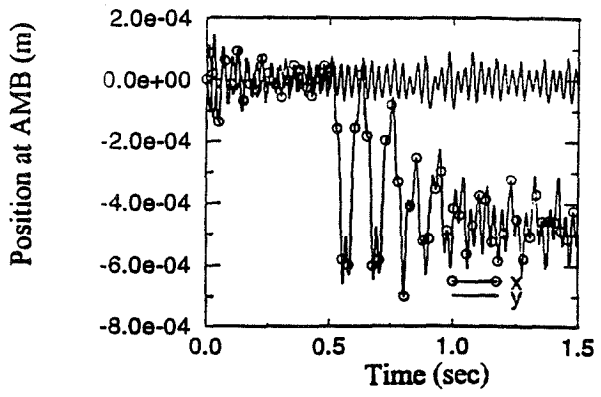

Figure 6.a Rotor Response With AMB Failure
$\Omega = 200\text{rad/sec}, C_L = \frac{2D}{3}$
$t_f = 0.5, \alpha = 0$

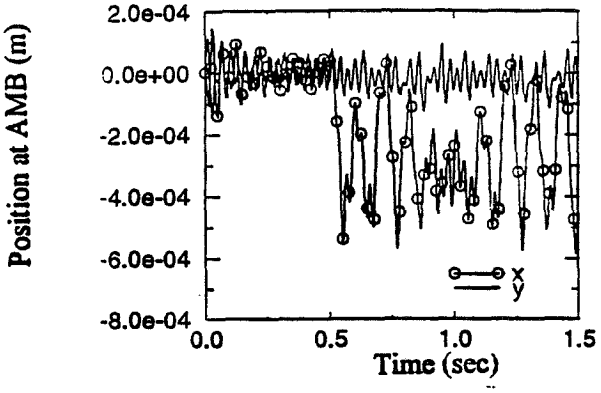

Figure 6.b Rotor Response With AMB Failure
$\Omega = 200\text{rad/sec}, C_L = \frac{D}{2}$
$t_f = 0.5, \alpha = 0$

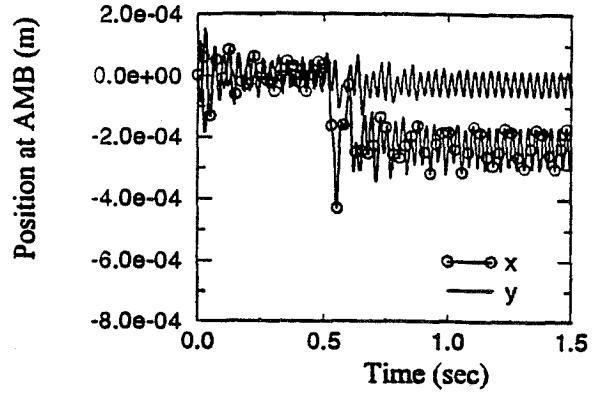

Figure 6.c Rotor Response With AMB Failure
$\Omega = 200\text{rad/sec}, C_L = \frac{D}{3}$
$t_f = 0.5, \alpha = 0$

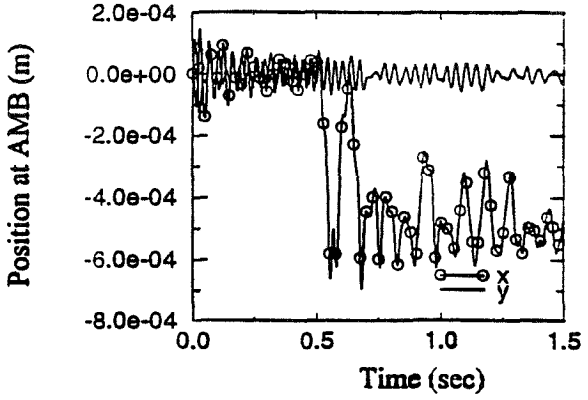

Figure 7.a Rotor Response With AMB Failure
$\Omega = 200\text{rad/sec}, C_L = \frac{2D}{3}$
$t_f = 0.5, \alpha = -100$

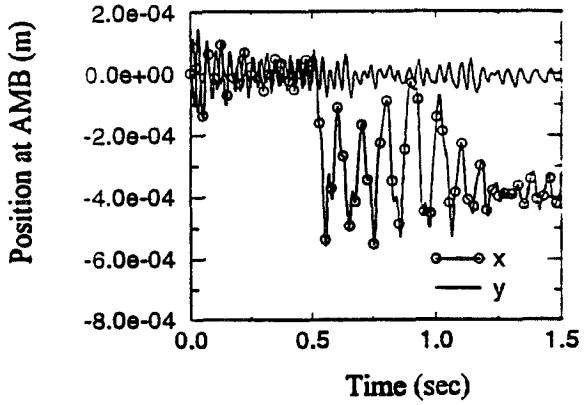

Figure 7.b Rotor Response With AMB Failure
$\Omega = 200\text{rad/sec}, C_L = \frac{D}{2}$
$t_f = 0.5, \alpha = -100$

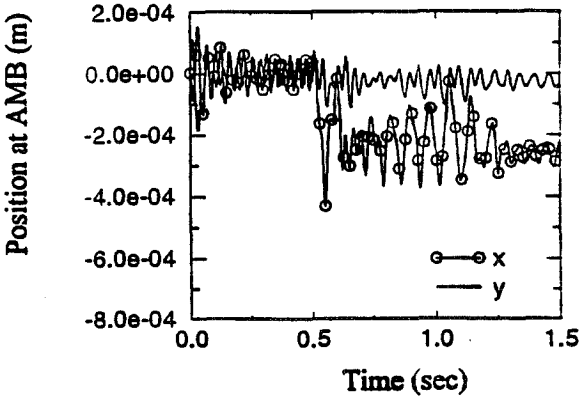

Figure 7.c Rotor Response With AMB Failure
$\Omega = 200\text{rad/sec}, C_L = \frac{D}{3}$
$t_f = 0.5, \alpha = -100$

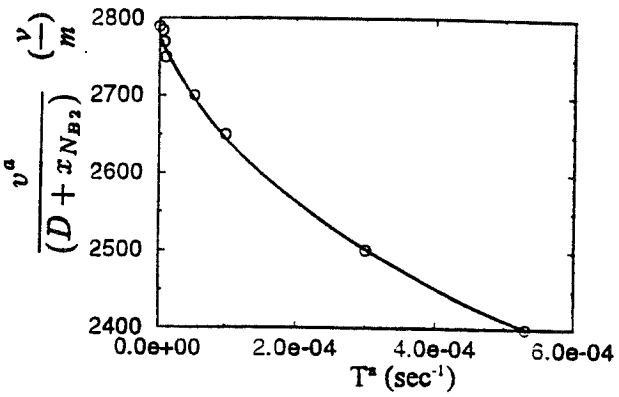

Figure 8 Maximum Sideloading Force as a Function of Power Amplifier Time Constant, τ^a (for parameters of Table 1)

NONLINEAR DYNAMICS OF A FOIL BEARING SUPPORTED ROTOR SYSTEM: SIMULATION AND ANALYSIS

Feng Li
G. T. Flowers

Department of Mechanical Engineering
Auburn University, AL 36849-5341

Abstract

Foil bearings provide noncontacting rotor support through a number of thin metal strips attached around the circumference of a stator and separated from the rotor by a fluid film. The resulting support stiffness is dominated by the characteristics of the foils and is a nonlinear function of the rotor deflection. The present study is concerned with characterizing this nonlinear effect and investigating its influence on rotordynamical behavior. A finite element model is developed for an existing bearing, the force versus deflection relation characterized, and the dynamics of a sample rotor system are studied. Some conclusions are discussed with regard to appropriate ranges of operation for such a system.

Nomenclature

$c_{x,y}$ = damping coefficient at x and y directions
d = foil bearing clearance, mm
f_b = bearing restoring force acting on shaft, N
I_a = rotor polar mass inertia matrix, kg-m^2
m = shaft and rigid disk mass, kg
m_e = imbalance mass, kg
n_f = number of foils
N = total number of nodes on shaft
N_{b1} = node number at left bearing
N_{b2} = node number at right bearing
N_{disk} = node number at disk on shaft
$p_{1,2}$ = foil bearing force coefficients
q_x = rotor modal coordinate vector in x direction, m
q_y = rotor modal coordinate vector in y direction, m
r_d = radius of rigid disk, mm
r_e = eccentricity of imbalance mass, mm
R_j = journal radius, mm
R_b = bearing radius, mm
t = foil thickness, mm
x = displacement of shaft at x direction, m
y = displacement of shaft at y direction, m
Ψ = rotor free-free modal rotation matrix
Φ = rotor free-free modal displacement matrix
Γ = $\Psi^T I_a \Psi$
ω = rotor speed, rad/s
ω_n = first critical speed, rad/s
ε = ratio of imbalance mass to total mass
$\varepsilon_{b1,b2}$ = bifurcation values of ε
ξ = damping factor
$\bar{\omega}_n$ = matrix of rotor free-free natural frequencies, rad/s
$\mu_{1,2}$ = mass modification coefficient

Introduction

The development of advanced types of high speed rotating machinery requires bearings that can withstand abusive environments for extended periods of time. Foil bearings offer a great deal of promise in this regard. Foil bearings have been applied successfully to wide range of light-duty, high-speed aerospace rotating machinery, auxiliary power units (APUs). They are presently employed in naval auxiliary power units (APUs) and numerous aircraft engines (e.g., Boeing 747, 757, and 767, DC-10, F-15, F16, and Falcon 2000) [Heshmat (1994)].

Active magnetic bearing (AMB) supported rotor systems require auxiliary bearings to support the rotor and provide protection for the soft iron of the magnets in the event of AMB overload or failure. Bushings or rolling element bearings with a clearance between the support inner race and the rotor have typically been used for such applications. Recently, foil bearings have been considered for use as auxiliary bearings. They

offer the opportunity to provide continuous support to the rotor without significantly impacting the ability of the AMB to actively control rotor vibration (due to the inherent relative softness of foil bearings) while eliminating the need for oil lubrication and the associated cooling systems. Such a configuration could be quite advantageous for use in critical applications, such as jet engines, where safety is a primary consideration.

There has been a great deal of research focussed on the dynamical behavior of foil bearings. Walowit, et al. (1973) first introduced a theoretical model to determine the static structural stiffness of foil bearings and performed an analysis of this model. In this analysis, the lubricant was assumed to be incompressible, the bearing was assumed to be an infinitely long, straight beam, and the friction forces due to foil/rotor contact were neglected. Bragin (1982) estimated the elastic characteristics of a foil sliding bearing with static loading using the foil packet model. Experimental results show that this idealized model makes it possible to determine the elastic reaction and stiffness of foil bearings. The foil packet, having low stiffness in comparison with the gas film, has the dominating effect on foil bearing elastic characteristics.

Based upon the above discussion, an important area of concern is the expected dynamical behavior of a rotor supported by foil bearings. In order to investigate such a system, a flexible rotor simulation model is developed and analyzed using both numerical and analytical approaches. Some interesting results and observations are presented and discussed.

Model Development

The simulation model used in this study consists of foil bearings coupled with a flexible rotor. The model is described below.

Foil Bearing Model

The initial reference configuration chosen for the foil prior to the journal insertion in bearing is shown in Figure 1. This configuration is not unique and may differ in an assembled state from the free form state due to foil interaction loading. The relationships of the geometry parameters of foil bearing, for example, the number of foils n_f, free foil length L_f, foil thickness t, bearing radius R_b, foil attachment angle φ, and foil radius of curvature R_{LI} are given in [Arakere and Nelson (1992)]. The geometry of the foil bearing used in this study are listed in Table 1.

Number of foils N_f	8
Bearing Radius, R_b	45.95 mm
Journal Radius, R_j	40.00 mm
Foil Radius, R_f	76.20 mm
Bearing Length L	106.7 mm
Foil Thickness t	0.229 mm
Material	Steel

Table 1 : Geometric parameters and material properties of foil bearing

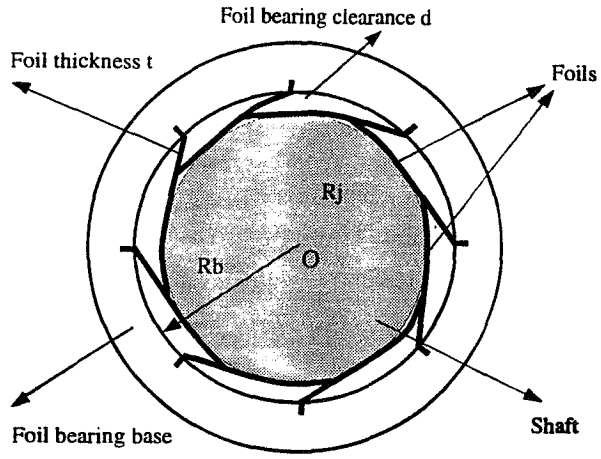

Figure 1 Foil bearing configuration

A finite element model of this foil bearing configuration is developed. The foils are modelled as elastic beams. There are several modelling issues that must be addressed in determining stiffness of foil bearing. These include how the foils interact, the impact of friction between the foils, and foil pre-loading. In order to address these problems, contact elements are defined between foils to simulate the mechanism of contact. Contact sliding and friction are considered in the analysis. To simulate the real case of shaft and bearings, the shaft is inserted into foil bearing, so that the foils are pre-loaded. The foil bearing force versus displacement characteristics, shown in Figure 2, are obtained by fitting a third order polynomial of the form ($f_p = p_1x + p_2x^3$) to the finite element analysis output

data. This function is used to simplify the analysis. For the foil bearing used in the current study (parameters listed in Table 1), p_1 is 7970.0 N/m, and p_2 is $1.496*10^{10}$ N/m^3. As can be seen from inspection of Figure 2, the approximation is quite good.

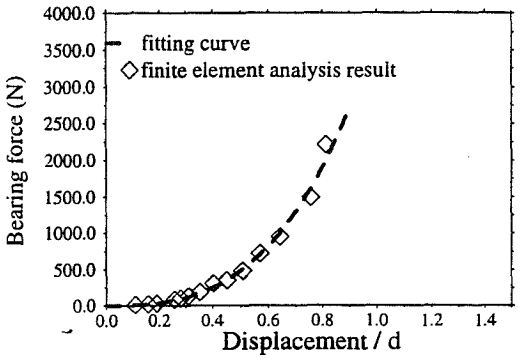

Fiigure 2 Variation of foil bearing force with displacement

Flexible Rotor Model and Analysis

The simulation study is based on the rotor/bearing configuration shown in Figure 3. It consists of a flexible rotor supported by foil bearings at both ends. A rigid disk with radius r_d is placed at the midpoint of the bearing span. The rotor is supported by two foil bearings at each end. The "z" direction is the spin axis. The geometry and material property parameters used in this study are listed in Table 2.

Length of shaft	620.0 mm
Radius of shaft	20.0 mm
Radius of rigid disk	100.0 mm
Mass of disk	2.0 kg
Mass of shaft	6.0 kg
Material	Steel

Table 2 : Geometric parameters and material properties of rotor system

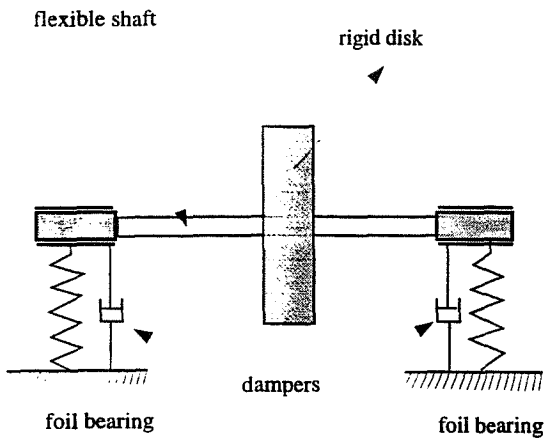

Figure 3 Schematic diagram of simulation model

The rotor shaft is modelled using the free-free bending mode shapes and natural frequencies obtained through finite element analysis. The finite element code uses 11 stations and the first four modes (two rigid body and two flexible modes) are included in the simulation model [Lawen and Flowers (1995)]. Based on these simplifications, the equations of motion for the system can be written as

$$\ddot{q}_x + \omega\Gamma\dot{q}_y + \bar{\omega}_n^2 q_x + \phi^T f_x = \phi^T f_{x,imb} \qquad (1)$$

$$\ddot{q}_y - \omega\Gamma\dot{q}_x + \bar{\omega}_n^2 q_y + \phi^T f_y = \phi^T f_{y,imb} \qquad (2)$$

where

$$f_x = \Phi_{N_{b1}}(p_1 q_x + p_2 q_x^3 + c_x \dot{q}_x) + \Phi_{N_{b2}}(p_1 q_x + p_2 q_x^3 + c_x \dot{q}_x) \qquad (3)$$

$$f_y = \Phi_{N_{b1}}(p_1 q_y + p_2 q_y^3 + c_y \dot{q}_y) + \Phi_{N_{b2}}(p_1 q_y + p_2 q_y^3 + c_y \dot{q}_y) \qquad (4)$$

$$f_{x,imb} = \psi\Omega^2\cos(\Omega t) \qquad (5)$$

$$f_{y,imb} = \psi\Omega^2\sin(\Omega t) \tag{6}$$

$$q_x = \Phi^{-1} x_r \tag{7}$$

$$q_y = \Phi^{-1} y_r \tag{8}$$

with

$$x_r = \{ x_{r1}, x_{r2}, \ldots, x_{rN} \}^T \tag{9}$$

$$y_r = \{ y_{r1}, y_{r2}, \ldots, y_{rN} \}^T \tag{10}$$

The physical displacements of the rotor at the right bearing, left bearing and rigid disk locations can be obtained by using coordinate transformations.

$$x_{rk} = \sum_{i=1}^{M} \Phi_{ki} q_{xi} \tag{11}$$

$$y_{rk} = \sum_{i=1}^{M} \Phi_{ki} q_{yi} \tag{12}$$

where M could be N_{b1}, N_{b2}, or N_{disk}.

Numerical Simulation Analysis

Numerical simulation is used to investigate the dynamical behavior of rotor system described above. ε is taken as 0.4%, rotor speed ω / ω_n is 4.93. Numerical simulation results, shown in Figure 4 - 9, show time response of the rigid disk in the horizontal and vertical directions, frequency domain analyses, and orbits.

Figure 4-6 show that the vibration in time, frequency domain and orbit of motion. In this case, the system has purely synchronous vibration without subharmonic component. Figure 7 and 8 show that a large 1/3 ω subharmonic response occurs besides the synchronous response in time and frequency domains. The amplitude of the subharmonic component, which is almost twice as large as the amplitude of the synchronous, dominates the vibration. Figure 9 shows the orbit of motion with large 1/3 ω subharmonic. In both of cases shown in Figure 4-6 and Figure 7-9, the rotor system has exactly the same parameters and rotor speed except the initial conditions. Comparison of vibration

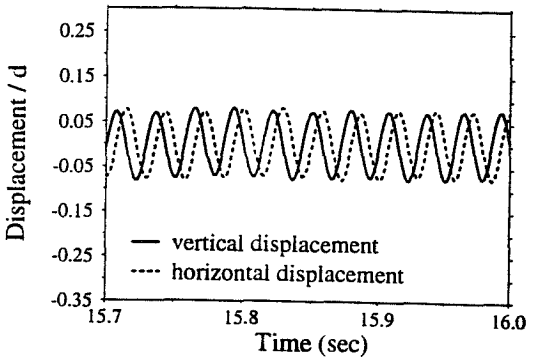

Figure 4 Purely synchronous time responses

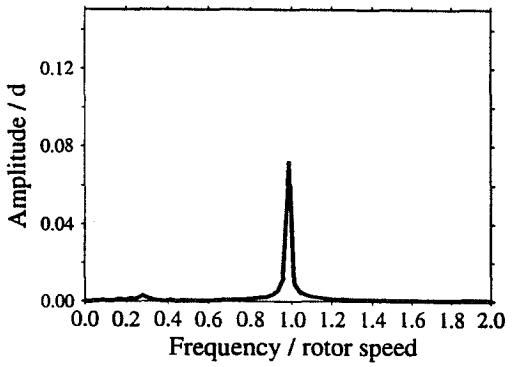

Figure 5 Purely synchronous frequency response

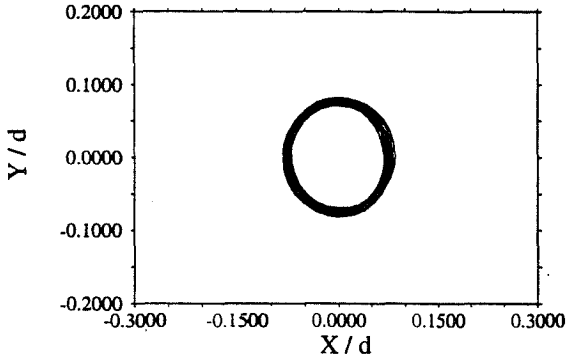

Figure 6 Purely synchronous trajectory

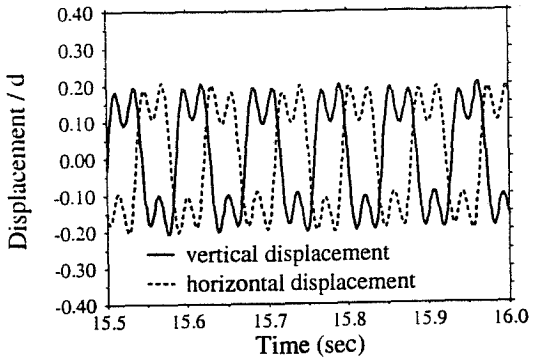

Figure 7 Time responses with a subharmonic component

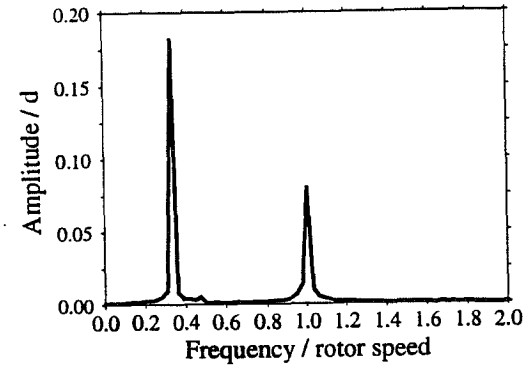

Figure 8 Frequency response with a subharmonic component

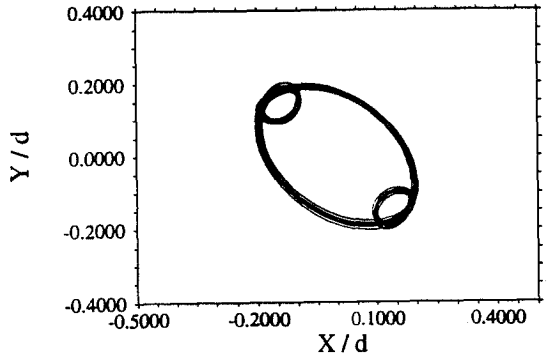

Figure 9 Trajectory with a subharmonic component

for these two cases shows that the rotor system supported by foil bearings has multiple response phenomena. It could be purely synchronous response or, it could have a combination of synchronous response and subharmonic component, depending upon the initial conditions. In the case of that system has purely synchronous vibration, the amplitude of vibration is much smaller than that of subharmonic case.

Harmonic Balance Analysis

The numerical harmonic balance approach is used to examine the synchronous and 1/3 ω subharmonic responses. The parameters are the same as in the previous study. Two case are examined : (1) the shaft is quite stiff (first two elastic natural frequencies are 400 and 1200 hz) and (2) the shaft is quite flexible (first two elastic natural frequencies are 100 and 300 hz). The results are shown in Figure 10.

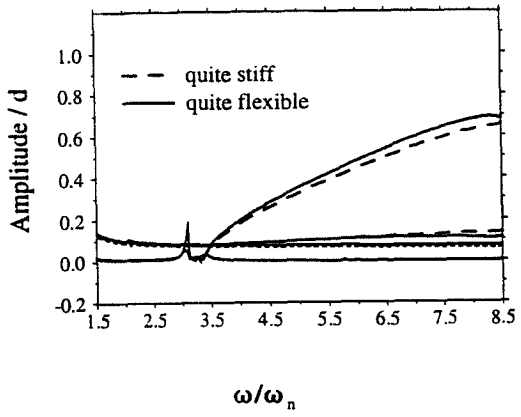

Figure 10 Variation of response amplitude with rotor speed for harmonic balance analysis

Figure 10 shows that the 1/3 ω subharmonic components occur when rotor speed (ω/ω_n) is larger then 3.0. The amplitude of subharmonic component is much larger than the amplitude of synchronous. It also shows that for the ranges of reasonable rotor speed ω/ω_n (1.5~8.5) and geometric configurations of shaft, the effect of rotor flexibility is not significant. It is concluded that the rigid rotor model described below adequately captures the dynamic behavior of such systems. In order to simplify the analysis and develop an understanding of the fundamental characteristics of

such systems, a rigid rotor model is now examined.

Rigid Rotor Model and Analysis

Based on the above discussions, the shaft is considered to be rigid. Furthermore, the masses of shaft and rigid disk are seem to be point masses. So, the rotor system has only two degrees of freedom of motion at vertical and horizontal directions. The bearing forces in the x and y direction are considered to be decoupled. So, the x and y equations are symmetric, and either of them can be selected to study without losing generality. The x equation is selected and is shown in (13).

$$\ddot{x} + 2\xi\omega_n\dot{x} + \omega_n^2 x + px^3 = \epsilon\omega^2 r_e\cos(\omega t) \qquad (13)$$

where

$$\omega_n = \sqrt{\frac{2p_1}{m}}\ ,\ p = \frac{2p_2}{m}\ ,\ \epsilon = \frac{m_e}{m} \qquad (14)$$

Harmonic Balance Analysis

The harmonic balance approach is used to investigate the dynamical behaviors of the rigid rotor system for the range of operating speed ($\omega/\omega_n \approx 1.5$-$8.5$). Based on the results of the above simulations, it is assumed that the response, x(t), takes the form

$$x(t) = A\cos(\omega t+\theta_1) + B\cos(\frac{1}{3}\omega t+\theta_2) \qquad (15)$$

where A and B are amplitudes of the synchronous and $1/3\,\omega$ subhamonic amplitudes, and θ_1 and θ_2 are the phase shifts associated with the synchronous and subharmonic components. The effect of support damping is specifically included in this analysis. Substitution of (15) into (13) yields the following relationships between the synchronous and subharmonic response amplitudes and rotor speed.

$$3pA^3+6pAB^2+\cos(3\theta_2-\theta_1)pB^3+4\Omega_1 A=4\epsilon r_e\omega^2\cos(\theta_1) \qquad (16)$$

$$8\xi\Omega_2 A+\sin(3\theta_2-\theta_1)pB^3=4\epsilon r_e\omega^2\sin(\theta_1) \qquad (17)$$

$$6pA^2B+3\cos(\theta_1-2\theta_2)pAB^2+3pB^3+4\Omega_3 B=0 \qquad (18)$$

$$8\xi\Omega_2 B + 9\sin(\theta_1-2\theta_2)pAB^2 = 0 \qquad (19)$$

where

$$\Omega_1 = \omega_n^2-\omega^2,\ \Omega_2 = \omega_n\omega\ ,\ \Omega_3 = \omega_n^2-\frac{1}{9}\omega^2 \qquad (20)$$

Equations (16) - (19) have two possible sets of solutions - one for B=0 and the other for B≠0. If B=0, equations (16) - (19) yield

$$B = 0 \qquad (21)$$

$$3pA^3 + 4\Omega_1 A = 4\epsilon r_e\omega^2\cos(\theta_1) \qquad (22)$$

$$2\xi\Omega_2 A = \epsilon r_e\omega^2\sin(\theta_1) \qquad (23)$$

From (22) and (23), θ can be canceled and an expression with only the synchronous response amplitude. A, the amplitude, can be obtained from

$$(3pA^3 + 4\Omega_1 A)^2 + (2\xi\Omega_2 A)^2 = 16\epsilon^2 r_e^2\omega^4 \qquad (24)$$

If B≠0, equations (25) - (28) can be simplified to yield

$$3pA^3+6pAB^2+\cos(3\theta_2-\theta_1)pB^3+4\Omega_1 A = 4\epsilon r_e\omega^2\cos(\theta_1) \qquad (25)$$

$$8\xi\Omega_2 A + \sin(3\theta_2-\theta_1)pB^3 = 4\epsilon r_e\omega^2\sin(\theta_1) \qquad (26)$$

$$6pA^2 + 3\cos(\theta_1-2\theta_2)pAB + 3pB^2 + 4\Omega_3 = 0 \qquad (27)$$

$$8\xi\Omega_2 + 9\sin(\theta_1-2\theta_2)pAB = 0 \qquad (28)$$

Equations (24) - (28) show that a rotor system supported by foil bearings can have two possible responses. One is purely synchronous, and the other is a combination of synchronous and subsynchronous components. The analytical results demonstrate the correctness of conclusions obtained from numerical simulation of the flexible model.

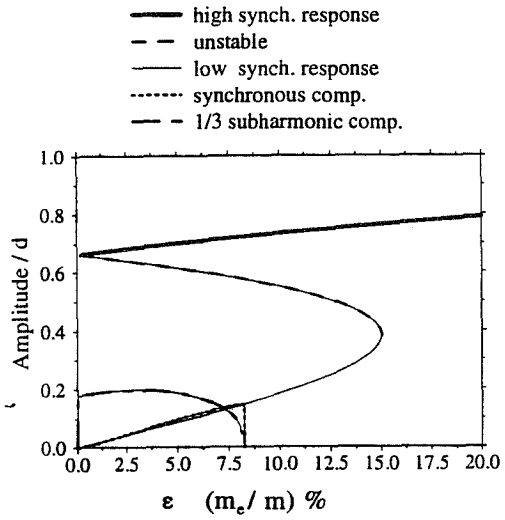

Figure 11 Variation of amplitude with imbalance

Figure 11 shows that the rotor system supported by foil bearings could have multiple responses depending on the value of ε. There are three possible responses, high synchronous, low synchronous, and a combination of synchronous and subsynchronous. If $\varepsilon < \varepsilon_{b1}$, the system could have multiple synchronous responses (high or low), or a combination of 1/3 ω subsynchronous and synchronous. The particular response the system actually takes depends on the initial conditions. If $\varepsilon_{b1} < \varepsilon < \varepsilon_{b2}$, the multiple response phenomena still exist (as in the situation for $\varepsilon < \varepsilon_{b1}$), except the subharmonic is of even order instead of odd order. Furthermore, if $\varepsilon > \varepsilon_{b2}$, the low synchronous response disappears. Determination of ω_h, ε_{b1} and ε_{b2} are important for rotor designers. Estimation of those values could be done by using the necessary and sufficient condition for real solution(s) of the quadratic and cubic equation. Finally, the closed form of estimation of these values are developed in this paper.

In order to explore these interesting phenomena, some assumptions must be made to simplify the analysis. First, damping is usually small, so it will be neglected. This results in $\theta_1=0$ and $\theta_2=0$. Based upon these assumptions, (15) becomes

$$x(t) = A\cos(\omega t) + B\cos(\frac{1}{3}\omega t) \tag{29}$$

Substitution of (29) into (13) yields

$$3pA^3 + 6pAB^2 + 3pB^3 + 4\Omega_1 A = 4\epsilon r_e \omega^2 \tag{30}$$

$$6pA^2B + 3pAB^2 + 3pB^3 + 4\Omega_3 B = 0 \tag{31}$$

Here, A, B, p, Ω_1, and Ω_3 have the same definitions as shown above.

Bifurcation Analysis

(1) Estimation of ε_{b2}

For estimation of ε_{b2}, only the synchronous response exists. So, let B=0, and substitute B=0 into (30). It yields

$$3pA^3 + 4\Omega_1 A = 4\epsilon r_e \omega^2 \tag{32}$$

Examination of (32) indicates that more than one real solution could exist if and only if $\Delta \le 0$ for (32). So,

$$\frac{1}{4}\left(\frac{4\epsilon r_e \omega^2}{3p}\right)^2 + \frac{1}{27}\left(\frac{4\Omega_1}{9p^2}\right)^3 < 0 \tag{33}$$

Assume, $\omega > \omega_n$, so $\Omega = \omega_n^2 - \omega^2 < 0$. Solving (33), ε_{b2} is given

$$\epsilon \le \frac{4}{9r_e}\left(1 - \frac{2p_1}{m(1+\mu_2)\omega^2}\right)\sqrt{\frac{m(1+\mu_2)\omega^2 - 2p_1}{2p_2}} = \epsilon_{b2} \tag{34}$$

where the total mass modification coefficient μ_2 due to the imbalance mass effect is

$$\mu_2 = \frac{4}{9r_e}\left(1 - \frac{2p_1}{m\omega^2}\right)\sqrt{\frac{m\omega^2 - 2p_1}{2p_2}} \tag{35}$$

(2) Estimation of ε_{b1}

Estimation of ε_{b1} is very similar to the estimation

of ε_{b2}, except that $B \neq 0$. Under the present situation, the rotor system could be characterized by (30) and (31). Using $B \neq 0$ condition, equation (31) can be simplified to yield

$$6pA^2 + 3pAB + 3pB^2 + 4\Omega_3 = 0 \qquad (36)$$

Because A and B << 1 in equation (30), the higher order terms of A and B can be neglected in order to obtain an estimation of A. So from equation (30), the estimation of A is given by if $\omega \neq \omega_n$.

$$A = \frac{\epsilon r_e \omega^2}{\Omega_1} \qquad (37)$$

Substitution of equation (37) into equation (36) yields the quadratic equation in B

$$3pB^2 + 3p\frac{\epsilon r_e \omega^2}{\Omega_1}B + 6p\left(\frac{\epsilon r_e \omega^2}{\Omega_1}\right)^2 + 4\Omega_3 = 0 \qquad (38)$$

In equation (38), B has real solutions if and only if $\Delta \geq 0$. So, it is shown that

$$\Delta = 9p^2\left(\frac{\epsilon r_e \omega^2}{\Omega_1}\right)^2 - 16p\left(6p\left(\frac{\epsilon r_e \omega^2}{\Omega_1}\right)^2 + 4\Omega_3\right) \geq 0 \qquad (39)$$

Solving (39) for ϵ, the bifurcation value ϵ_{b1} is given by

$$\epsilon \leq \frac{4}{3r_e\omega^2}\left(\omega^2 - \frac{2p_1}{(1+\mu_1)m}\right)\sqrt{\frac{(1+\mu_1)m\omega^2 - 18p_1}{42p_2}} = \epsilon_{b1} \qquad (40)$$

where the total mass modification coefficient μ_1 due to imbalance mass effect is

$$\mu_1 = \frac{4}{3r_e\omega^2}\left(\omega^2 - \frac{2p_1}{m}\right)\sqrt{\frac{m\omega^2 - 18p_1}{42p_2}} \qquad (41)$$

(3) Estimation of ω_b

Returning to equation (36), the subharmonic component could exist if and only if $\Delta \geq 0$ of the B quadratic equation (36). So, ω is given

$$\omega \geq 3\sqrt{\omega_n^2 + \frac{21A^2p_2}{8}} = \omega_b \qquad (42)$$

Equation (42) shows that $\omega_b \geq 3\omega_n$, and a 1/3 ω subharmonic could occur if $\omega \geq \omega_b$. This analysis result correlates well with the response observed in the flexible model numerical simulation. Comparisons of ε bifurcation values (ε_{b1} and ε_{b2}) to the corresponding values (obtained from numerical simulations of the flexible model) indicate that the relative error is in the range from 5% to 7%, which is quite reasonable.

Discussions On Variations of p_1 and p_2

In the above analysis, the foil bearing parameters (p_1 and p_2) are taken from the finite element analysis based the configuration listed in Table 2. It is of interest to consider the effect of variations of p_1 and p_2 on rotordynamical behavior. Figure 12 to Figure 15 show the higher, lower synchronous and 1/3 ω subharmonic changes versus p_1 and p_2, where p_{01} and p_{02} are the values of p_1 and p_2 used in the previous analysis.

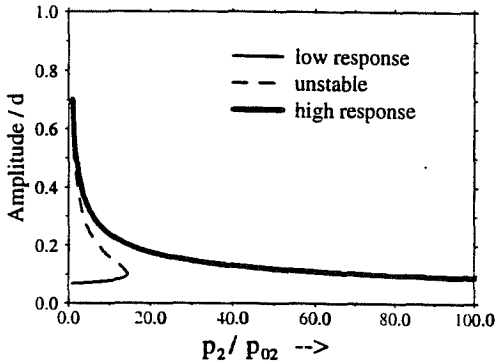

Figure 12 Variation of amplitude with p_2 (Purely synchronous)

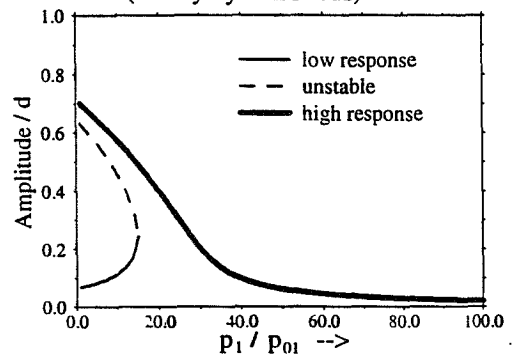

Figure 13 Variation of amplitude with p_1 (Purely synchronous)

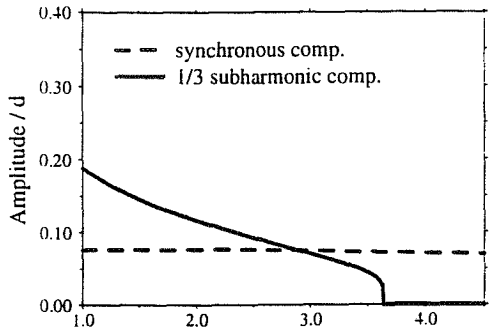

Figure 14 Variation of amplitude with p_2 (Subharmonic)

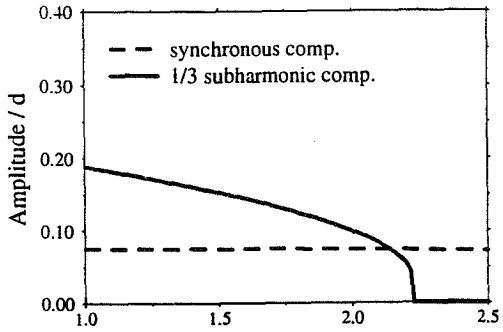

Figure 15 Variation of amplitude with p_1 (Subharmonic)

Figures 12 and 13 indicate, that in the case of purely synchronous vibration, the higher synchronous responses decrease as p_1 and p_2 increase. The lower synchronous responses increase first and then disappear as p_1 and p_2 increase. Figure 14 and Figure 15 show the coexistence of synchronous and 1/3 ω subharmonic, and indicate that the 1/3 ω subharmonic components decrease and disappear as p_1 and p_2 increase. Furthermore, decreases of the subharmonic responses are much more sensitive to parametric variations than are the synchronous responses.

Conclusions

A study of the nonlinear dynamical behavior of a foil bearing supported flexible rotor system has been presented. The simulation and analysis work has been discussed in some detail. The following results and conclusions have been obtained.

1. Very large 1/3 ω subharmonic response are found if the rotor speed is approximately larger than three times of the first critical speed ($\omega > \omega_h$). If the rotor speed is less than ω_h, the 1/3 ω subharmonic response will disappear. Closed form expression for ω_h is developed.
2. Multiple responses and bifurcation phenomena are shown. There are two particular values of imbalance mass ratio (ε_{b1} and ε_{b2}). If $\varepsilon < \varepsilon_{b1}$, the system could have multiple synchronous responses (high amplitude and low amplitude) only if synchronous responses are excited. It could also have responses with a combination of low synchronous and 1/3 subharmonic responses. The particular response the system actually takes is determined by the initial conditions. If $\varepsilon_{b1} < \varepsilon < \varepsilon_{b2}$, the system may also have multiple synchronous responses (high amplitude and low amplitude) only if synchronous responses are excited, or it may have responses with a combination of low synchronous and even order subharmonic components instead of 1/3 ω components. If $\varepsilon > \varepsilon_{b2}$, the system has only a single synchronous response. Also, closed form estimates of ε_{b1} and ε_{b2} are developed.
3. Variations of the linear and nonlinear coefficients of foil bearings have different impacts on the amplitudes of responses. If p_1 and p_2 increase, the high synchronous responses decrease. The low synchronous responses are not affected significantly. In the case of the existence of 1/3 ω subharmonic responses, the subsynchronous responses decrease much faster than high synchronous responses.

References

1. Bragin, A. N., Saprykin, I. S., and Balakin, N. I., 1982, "On Determining Foil Sliding Bearing Elastic Characteristics With Static Loading," Trenie i Iznos, Vol. 3, No.2, pp. 241-248.
2. Chihiro, Hayashi, 1953, Forced Oscillations in Non-linear Systems, Osaka, Japan, Nippon Printing and Publishing Company, Ltd..
3. Eshel, A., and Elrod, H. G., 1965, "The Theory of the Infinitely Wide, Perfectly Flexible, Self Acting Foil Bearing," *ASME Journal of Basic Engineering*, No.1, pp. 831-836.
4. Heshmat, H., and Ku, C. P. Roger, 1994, "Structural Damping of Self-acting Compliant Foil Journal Bearings, " *Transactions of the ASME*, Vol. 116, pp. 76-82.
5. Heshmat, H., 1994,"Advancements in the

Performance of Aerodynamic Foil Journal Bearing: High Speed and Load Capability," *ASME Journal of Tribology*, Vol. 116, No.2, pp. 287-292.
6. Lawen, James L., and Flowers, G. T., 1995, "Synchronous Dynamics of a Coupled Shaft / Bearing / Housing System With Auxiliary Support From a Clearance Bearing: Analysis and Experiment," to be published in the *ASME Journal of Engineering for Gas Turbines and Power.*
7. Oh, K. P., and Rohde, S. M., 1976, "A Theoretical Investigation of the Multileaf Journal Bearing," *ASME Journal of Applied Mechanics*, pp. 237-242.
8. Carpino, Marc, and Peng, Jih-Ping, 1994, "Theoretical performance of a hydrostatic foil bearing," *ASME Journal of Tribology*, Vol.116, No.1 pp. 83-89
9. Arakere, Nagaraj K., and Nelson, H. D, 1992, "An Analysis of Gas-Lubricated Foil-Journal Bearings," *STLE Tribology Transaction*, Vol.35, pp. 1-10.
10. Walowit, J. A., Murray, S. F., McCabe, J., Arwas, E. B., and Moyer, T., 1973, "Gas Lubricated Foil Bearing Technology Development for Propulsion and Power Systems," Air Force Aero Propulsion Laboratory, Wright-Patterson Air Force Base, Ohio, WPAFB Technical Report AFAPL-TR-73-92

INTERACTION DYNAMICS BETWEEN A FLEXIBLE ROTOR AND AN AUXILIARY CLEARANCE BEARING

James L. Lawen, Jr.*
General Electric Corporate Research and Development Center
Schenectady, NY

George T. Flowers
Department of Mechanical Engineering
Auburn University
Auburn, Alabama

ABSTRACT

This study investigates the application of synchronous interaction dynamics methodology to the design of auxiliary bearing systems. The technique is applied to a flexible rotor system and comparisons are made between the behavior predicted by this analysis method and the observed simulation response characteristics. Of particular interest is the influence of coupled shaft/bearing vibration modes on rotordynamical behavior. Experimental studies are also performed to validate the simulation results and provide insight into the expected behavior of such a system.

NOMENCLATURE

$_a$ = rotor polar mass inertia matrix, kg-m^2
ζ = stiffness, N/m
M_b = auxiliary bearing mass, kg.
N = total number of modes considered
N_{b1} = node number at leftmost bearing
N_{b2} = node number at rightmost bearing
N_{b3} = node number at auxiliary clearance bearing
$\}_x$ = rotor modal coordinate vector in X direction
$\}_y$ = rotor modal coordinate vector in Y direction
= time, s
ζ_b = amplitude of bearing vibration, m
ζ_r = amplitude of rotor vibration, m
ζ_b = auxiliary bearing physical coordinate vector in X direction, m
Y_b = auxiliary bearing physical coordinate vector in Y direction, m
X_r = rotor physical coordinate vector in X direction, m
Y_r = rotor physical coordinate vector in Y direction, m
V = structural damping coefficient, N/m
W = linear damping coefficient, N-s/m
Δ = radial clearance in auxiliary bearing, m
Ψ_r = rotor free-free modal rotation matrix
Φ_r = rotor free-free modal displacement matrix
$\Gamma = \Psi^T \mathbf{I}_a \Psi$
Ω = rotor operating speed, rad/s
ω_n = matrix of rotor free–free natural frequencies, rad/s
ψ = imbalance vector

Subscripts

bx = auxiliary bearing, x-direction
by = auxiliary bearing, y-direction
c = contact
xr = rightmost bearing, x-direction
xl = leftmost bearing, x-direction
yr = rightmost bearing, y-direction
yl = leftmost bearing, y-direction

INTRODUCTION

Auxiliary bearings for magnetic bearing supported rotor systems serve two basic missions. First, they protect the soft iron of the magnetic bearings during speed runup (through critical speeds) and overload. Second, they provide added rotor support

* Work performed while at Auburn University

luring critical operating conditions. A vital requirement is that the auxiliary bearings should perform heir roles without interfering with the rotor during ıormal operation of the system.

There has been quite a bit of work over the past lecades concerned with the dynamics of a rotor interacting with a clearance bearing. Some of the most ›rominent work in the area has been performed by Ehrich (1965, 1966, 1988), Bently (1974), Muszynka (1984), Childs (1979 and 1982), Choi and Noah 1987), and Kim and Noah (1989). The work of Kirk and Ishii (1993) figures prominently in the literature on this subject, with regard to auxiliary bearng applications. Schweitzer, et al. (1994) presents good review and discussion of issues related to the ouch-down dynamics of rotors on auxiliary bearings. Lawen and Flowers (1995) provides a more detailed eview of the relevant past literature on the subject.

While these studies have greatly enhanced the ınderstanding of the dynamics of rotors supported ›y auxiliary clearance bearings, there is still a need o develop a better understanding of the possible lynamics of such systems and to devise guidelines or the design of auxiliary bearings. With this idea n mind, motivation for the current work is due to study conducted by Black (1968). He examined he synchronous interaction of a rotor and stator ue to contact across a clearance annulus. By efining the rotor and stator displacements, $\bar{r}_r$ and $_s$ respectively, in terms of their polar receptances or transfer functions), the displacements can be xpressed in terms of the forces acting in the system s shown below:

$$\bar{r}_r = -\alpha_{11}\bar{P}_c + |\rho|e^{j\theta} \qquad (1.a)$$

$$\bar{r}_s = \beta_{11}P_c \qquad (1.b)$$

where α_{11} and β_{11} are the polar receptances of he rotor and stator respectively, P_c is the force due to ontact, and $|\rho|e^{j\theta}$ is the whirl radius of the rotor in he absence of contact due to imbalance. The radial learance, $\bar{R}$, can be defined in terms of the stator isplacement relative to the rotor during interaction s shown in (2).

$$\bar{R} = \bar{r}_r - \bar{r}_s \qquad (2)$$

Substituting (1.a) and (1.b) into (2) yields

$$\bar{R} + |\alpha_{11} + \beta_{11}|Pe^{j\eta} = |\rho|e^{j\theta} \qquad (3)$$

where η is the phase lead of $(\alpha_{11} + \beta_{11})$ relative to P as shown in (4).

$$(\alpha_{11} + \beta_{11}) = |\alpha_{11} + \beta_{11}|e^{j\eta} \qquad (4)$$

Obviously if the rotor whirl radius due to imbalance exceeds the radial clearance, $|\rho| > |R|$, then interaction occurs between the rotor and the stator due to contact. However, using vector triangles, Black also finds a criteria where interaction is possible even if $|\rho| < |R|$ as shown in (5).

$$\frac{\rho}{|P|} = \frac{-\cos(\eta) - \sqrt{\frac{\rho}{|R|} - \sin^2(\eta)}}{|\alpha_{11} + \beta_{11}|} \qquad (5)$$

For contact to occur, P, the contact force, must be positive which yields the following two conditions:

$$\eta < -90 \qquad (6.a)$$

$$|\sin(\eta)| < \frac{\rho}{|R|} \qquad (6.b)$$

These equations can be used to predict when interaction between stator and rotor is possible for $|\rho| < |R|$.

In essence, by defining the rotor and stator (bearing or bearing/housing) in polar receptance form and determining the phase lead, η, associated with the combined polar receptance, zones of interaction can be defined where rotor and stator coupling can occur even for rotor imbalance responses smaller than the radial clearance.

The present paper applies the synchronous interaction methodology devised by Black (1968) to the problem of auxiliary bearing design. The method is applied to a rotor and housing system modelled using modal coordinates for the structure, simulation and experimental studies are described, and the results compared and discussed. The implications for auxiliary bearing design are detailed.

ANALYSIS

Figure 1 illustrates the basic simulation model used for this investigation. It consists of a flexible rotor supported at both ends by magnetic bearings. A rigid disk with adjustable imbalance is placed at the midpoint of the bearing span. As a simplification, the magnetic bearings are modeled as spring and dashpot

ystems. Interaction with only a single auxiliary earing is considered.

The rotor is modeled using the free-free bending mode shapes and natural frequencies obtained hrough finite element analysis. Using this modal lata, the equations of motion for the flexible rotor nodel can be developed, as described in Ryan (1991).

Figure 2 shows the auxiliary bearing model used o study the effects of the bearing properties on he rotor response during coupled behavior between he flexible rotor and the auxiliary bearing. As simplification, the auxiliary bearing was modeled s an antifriction bearing with a clearance. The uxiliary bearing housing is represented as a mass ttached with springs to the bearing.

Using the methodology described above, potenial zones of coupling between the flexible rotor and he auxiliary bearing and between the flexible rotor, he auxiliary bearing, and the auxiliary bearing housng are determined. The basic approach is to determine the polar receptance of the rotor and the stator auxiliary bearing or auxiliary bearing/housing) and hen find the phase lead of the combined rotor-stator olar receptance. If the phase leads meets the criteia of (6.a) and (6.b), then interaction between the lexible rotor and stator is possible.

With this in mind, the equations of motion re written in complex notation using the following oordinates:

$$\bar{Q}_r = Q_x + jQ_y \tag{7.a}$$

$$\bar{R}_b = X_b + jY_b \tag{7.b}$$

The stiffness and damping terms for a particular ystem component, e.g. the left magnetic bearing, ere also equated in the horizontal and vertical irections, e.g. $K_l = K_{xl} = K_{yl}$. The resulting quations of motion are:

$$\begin{aligned} &\ddot{\bar{Q}}_r - j\Omega\Gamma\dot{\bar{Q}}_r + \omega_r^2\bar{Q}_r \\ &+\Phi_r^T\Phi_{r,Nb1}(K_l\bar{Q}_r + (\frac{V_l}{\Omega} + W_l)\dot{\bar{Q}}_r) \\ &+\Phi^T\Phi_{r,Nb2}(K_r\bar{Q}_r + (\frac{V_r}{\Omega} + W_r)\dot{\bar{Q}}_r) \\ &+\Phi_r^T F_{nl} = \Phi_r^T\bar{F}_{r,imb} \end{aligned} \tag{8.a}$$

$$M_b\ddot{\bar{R}}_b + (\frac{V_b}{\Omega} + W_b)\dot{\bar{R}}_b + K_b\bar{R}_b = \bar{F}_{nl} \tag{8.b}$$

F_{nl} and F_{imb} refer to the contacting and imbalance forces respectively.

Assuming a synchronous solution for the rotor and bearing,

$$\bar{Q}_r = Q_{ro}e^{j\Omega t} \tag{10.a}$$

$$\bar{R}_b = R_{bo}e^{j\Omega t}, \tag{10.b}$$

substitution of (10.a) and (10.b) into (8.a) and (8.b), yields the following polar receptances for the rotor-auxiliary bearing model:

$$\alpha_{11} = [\omega_n^2 - \Omega^2(I + \Gamma) + \Phi_r^T F_{supp}]^{-1} \tag{11.a}$$

$$\beta_{11} = [K_b - M_b\Omega^2 + j\Omega(\frac{V_b}{\Omega} + W_b)]^{-1} \tag{11.b}$$

where

$$\begin{aligned} F_{supp} = &\Phi_{r,Nb1}[K_l + j\Omega(\frac{V_l}{\Omega} + W_l)] \\ &+\Phi_{r,Nb2}[K_r + j\Omega(\frac{V_r}{\Omega} + W_r)] \end{aligned} \tag{11.c}$$

The receptances, α_{11} and β_{11}, reflect the equations of motion for the rotor and the auxiliary bearing being written in the form below.

$$\bar{Q}_r = \alpha_{11}\Phi_r^T(\bar{F}_{imb} - \bar{F}_{nl}) \tag{12.a}$$

$$\bar{R}_b = \beta_{11}\bar{F}_{nl} \tag{12.b}$$

It should be noted that the polar receptance given by (11.a) is in terms of the rotor modal coordinates. For the receptance in rotor physical coordinates at the auxiliary bearing location, N_{b3}, the following transformation must be performed.

$$\alpha_r = \sum_{i=1}^{N} \Phi_{N_{b3}}\alpha_{11} \tag{13}$$

The combined rotor-bearing polar receptance can then be written as follows:

$$\alpha_r + \beta_{11} = |\alpha_r + \beta_{11}|e^{j\eta} \tag{14}$$

where η is the phase lead of interest.

Therefore, (11.a), (11.b), and (13) are combined to form the combined polar receptance (14) for the auxiliary bearing interacting with the flexible rotor.

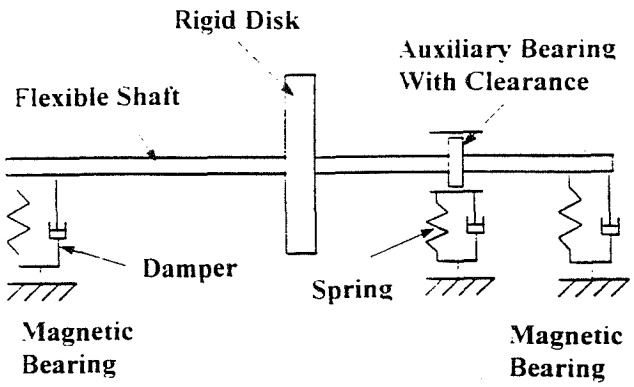

Figure 1 Schematic Diagram of Simulation Model

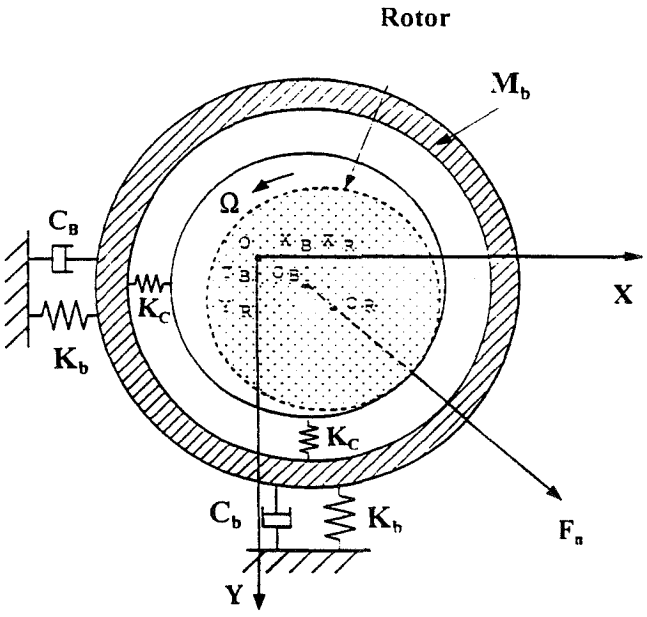

Figure 2 Auxiliary Bearing Model

The phase lead, η, associated with the combined complex polar receptances is then found over a range of operating speeds. If the conditions of (6.a) and (6.b) are met for rotor imbalance responses less than the clearance, then interaction between the rotor and auxiliary bearing is possible.

EXPERIMENTAL MODEL

Experimental tests were performed in order to validate the behavior predicted by the simulation model and to gain some insight into the dynamical responses that are to be expected. A photograph of the experimental test rig is shown in Figure 3. It has two basic components: a flexible shaft and an auxiliary clearance bearing rig. The shaft is made of steel and is 0.374 inches in diameter and 18.0 inches in length. It is supported at 1.0 inch from the right end by ball bearings suspended in a frame by four springs and at 1.0 inch from the left end by a bushing with a tight clearance. These supports represent the magnetic bearings. The stiffness of the left support is 17511 N/m for both the horizontal and vertical directions. It is used to somewhat isolate the rotor from the effects of the flexible coupling which attaches the rotor to the motor and to enforce low amplitude vibration at this location to protect the motor. The stiffness of the right support, for both horizontal and vertical directions, is 2539 N/m. This lower stiffness allows for significant vibration of the rotor in the speed range of the motor (0-10,000 rpm). A rigid disk with holes for placing imbalance screws is placed at the midpoint of the bearing span.

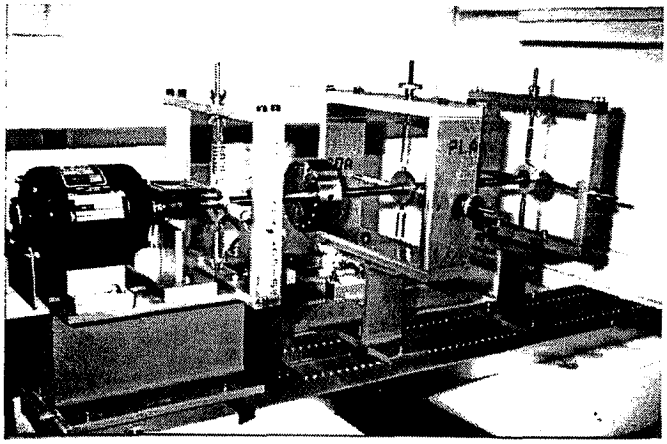

Figure 3 Photograph of Experimental Apparatus

The rotor is driven by an adjustable speed motor with feedback speed controller. Shaft vibration is measured using eddy current proximity displacement sensors fixed to measure displacement in the vertical and horizontal directions. During testing, the displacement signals of the shaft are sent to the signal analyzer where the frequency and amplitude components of the shaft response are recorded. The results are compared with those from the analytical studies. The auxiliary clearance bearing/housing assembly consists of a bushing suspended in a frame by four springs and is situated at the right end of the rotor.

DISCUSSION

In order to evaluate the effectiveness of the anal-

rsis technique described above, a series of parameer variation studies were performed. The nominal arametric configuration is shown in Table 1 and all he cases presented use these parameters unless otherwise indicated. These parameters are representative f reasonable values for the experimental test facility. The first four rotor modes (two rigid body and two lexible modes) are included in the simulation model.

The dynamic behavior of such a system is governed by shaft flexibility, auxiliary bearing stiffness, damping, and mass, imbalance, auxiliary bearing locations, bearing stiffness and damping, and auxiliary bearing clearance. The parameters over which the bearing designer has the most control are the auxiliary bearing stiffness and the clearance, which are the focus of the discussion below.

First, let us begin by considering the possible behaviors for different auxiliary bearing clearances. Figures 4.a – 4.e show some representative results for several values of bearing clearance. Figure 4.a shows the variation of η with the rotor speed. (Naturally, it is independent of the values of bearing clearance that are chosen.) Similarly, Figure 4.b shows the variation of $\frac{|\rho|}{\Delta}$ and $\sin\eta$ with rotor speed for the values of auxiliary bearing stiffness that are considered. Comparison of Figure 4.a with Figure 4.b indicate that the peaks in the η curve tend to occur near the respective combined rotor/stator critical speeds, as indicated by the amplitude peaks of the $\frac{|\rho|}{\Delta}$ and $\sin\eta$ curve in Figure 4.b. For rotor speeds below the first critical, interaction is not possible. For rotor speeds above the third critical, η approaches zero and interaction is possible for all rotor speeds for which $\sin\eta > \frac{\rho}{R}$, which is the entire remaining range of rotor speed shown. For each of the three values of clearance, there is a region between the first and second critical for which steady rotor/bearing interaction is impossible if the rotor imbalance response amplitude, ρ, is lower than the clearance. As the clearance is increased, this regime expands dramatically from a quite narrow band (196 to 247 rad/sec) to a rather broad range of rotor speeds (0 to 430 rad/sec). Inspection of Figures 4.c (rotor response amplitudes) and 4.d (bearing response amplitudes) reveals some interesting trends. Figure 4.d shows that interaction can occur over virtually the entire range of rotor speeds (except for the regime between the first and second critical speed as described above), which validates the behavior predicted using Black's interaction criteria. At the three critical speeds, the auxiliary bearings tend to attenuate the peak response amplitudes for all cases. Very little shift is seen in the location of the first critical speed as a result of interaction with the auxiliary bearing. These results agree well with experimental data for the region $0 \leq \Omega \leq 1000$ rad/sec, as shown in Figure 4.e.

Next, let us examine the effects of variations in auxiliary bearing stiffness on possible interactions between the rotor and the bearing. Some results for a variety of auxiliary bearing stiffnesses are summarized in Figures 5.a – 5.e. Figure 5.a shows the variation in η and Figure 5.b shows $\frac{|\rho|}{\Delta}$ and $\sin\eta$ for the range of rotor speed and the values of auxiliary bearing stiffness that are considered. Again, no interaction is possible at very low rotor speeds ($\Omega < 50$) and interaction can occur for all rotor speeds above the third critical speed ($\Omega > 1225$). In between these extremes, a variety of behaviors are possible depending upon the rotor speeds. In contrast with Figure 4.b, Figure 5.b indicates that $\sin\eta < \frac{|\rho|}{R}$ for almost the entire range of rotor speed. Unlike the previous case (for varying clearance values), the interaction dynamics here are dominated by the requirement that $\eta < -90$ degrees. Inspection of Figure 5.a indicates some interesting trends. For the lowest value of auxiliary bearing stiffness (K_b=88 N/m), interaction is possible over the entire range of rotor speed. As the auxiliary bearing stiffness is increased, there is again a range of rotor speed between the first and second critical speeds for which interaction is not possible. For the highest value of auxiliary bearing stiffness (K_b=2625 N/m), interaction is not possible for rotor speeds between 144 and 401 rad/sec. Figures 5.c (rotor response amplitudes) and 5.d (bearing response amplitudes) again validate the analysis results predicted using Black's synchronous interaction criteria. The auxiliary bearings attenuate the peak response amplitudes for all critical speeds. The first combined critical speed is increased by the presence of the auxiliary bearings (indicating dominance of the stiffness contribution from the auxiliary bearing), while the second and third combined critical speeds are reduced (indicating dominance of the mass contribution from the auxiliary bearing). These results are further validated by the experimental data for the region $0 \leq \Omega \leq 1000$ rad/sec, as shown in Figure 5.e.

CONCLUSIONS

Typically bearing support structures are designed considering only the stiffness and damping characteristics of the structure. For standard applications, this is an acceptable approach. However, the usage of auxiliary clearance bearings introduces an additional parameter, clearance, and an essentially nonlinear feature into the rotordynamics. In order to properly design such systems, it is necessary to develop a detailed understanding of the sorts of dynamical behavior that may be possible. Toward this end, the method of Black for the analysis of inter-

Parameter	Value	Units
K_{bx}, K_{by}	471	N/m
K_c	87,557	N/m
K_{lx}, K_{ly}	17,510	N/m
K_{rx}, K_{ry}	2,539	N/m
M_b	0.033	kg
V_{bx}, V_{by}	2,000	N/m
V_{lx}, V_{ly}	1,000	N/m
V_{rx}, V_{ry}	600	N/m
W_{bx}, W_{by}	0	N–s/m
W_{lx}, W_{ly}	0	N–s/m
W_{rx}, W_{ry}	0	N–s/m
ψ_1	3.0×10^{-6}	kg–m
ψ_{10}	2.5×10^{-5}	kg–m
Δ	5.0×10^{-5}	m

Table 1 Simulation Model Parameters

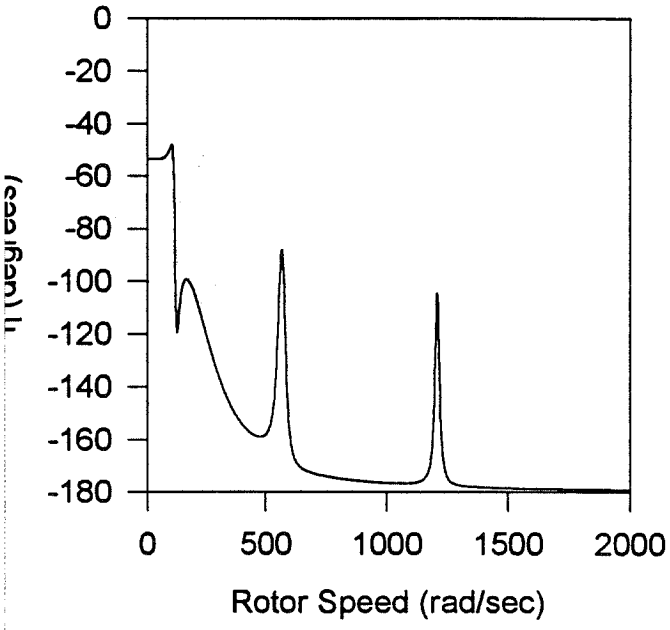

Figure 4.a Phase Lead for Varying Auxiliary Bearing Clearances

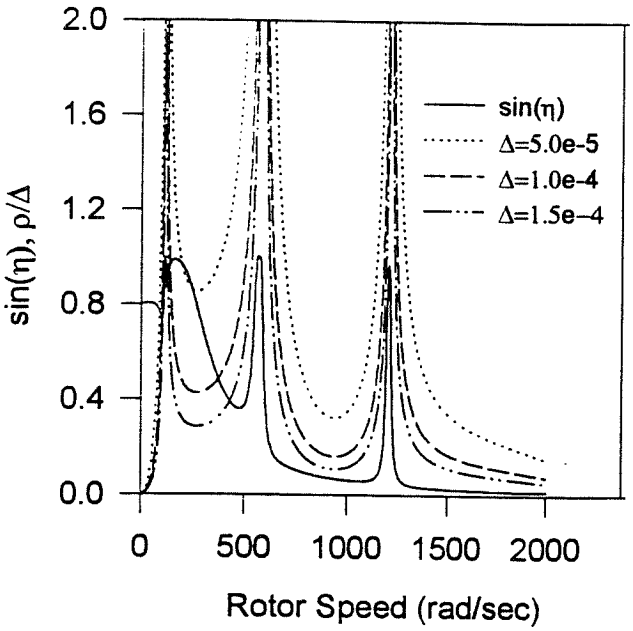

Figure 4.b Noncontacting Imbalance Response Amplitudes and sin(η) for Varying Auxiliary Bearing Clearances

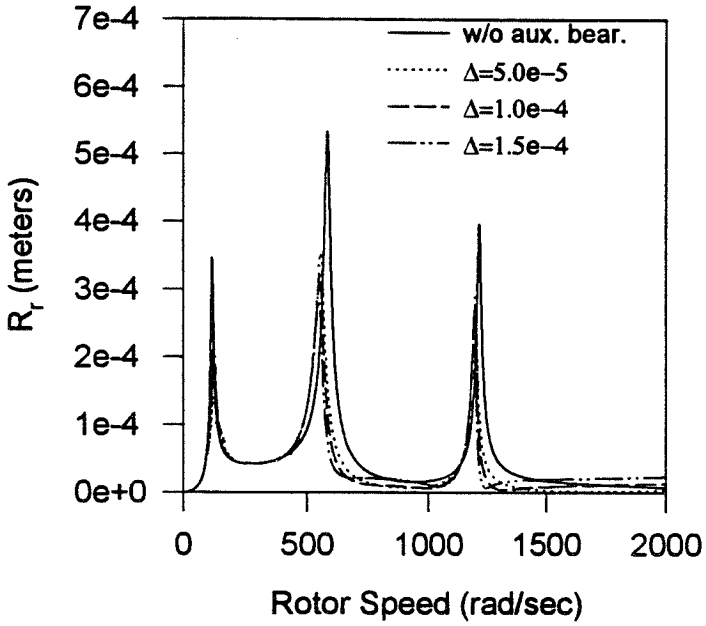

Figure 4.c Simulation Rotor Response Amplitudes for Varying Auxiliary Bearing Clearances

acting rotor/stator systems has been applied to the ase of a flexible rotor–bearing system, where the ro- or is modelled using modal coordinates. A simple lexible rotor system is studied, with simulation and xperimental studies being conducted for a variety of arametric configurations. These results have been resented and discussed. Regions of interaction have been detailed and the overall effects of various auxil- ary bearing clearance and stiffness values have been lescribed. Provided that the assumption of purely synchronous vibration is reasonably satisfied, Black's method for identifying regions of synchronous interaction is shown to be a versatile tool for the analysis of rotor systems with auxiliary clearance bearings.

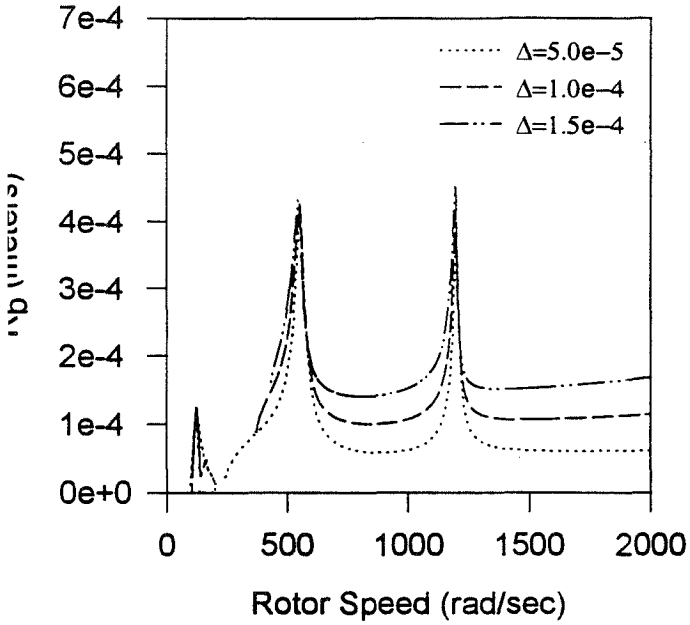

Figure 4.d Simulation Bearing Response Amplitudes for Varying Auxiliary Bearing Clearances

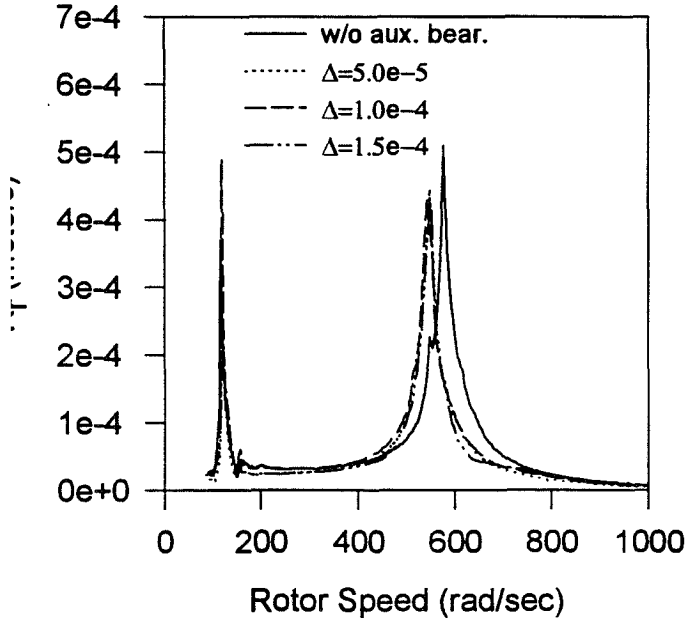

Figure 4.e Experimental Rotor Response Amplitudes for Varying Auxiliary Bearing Clearances

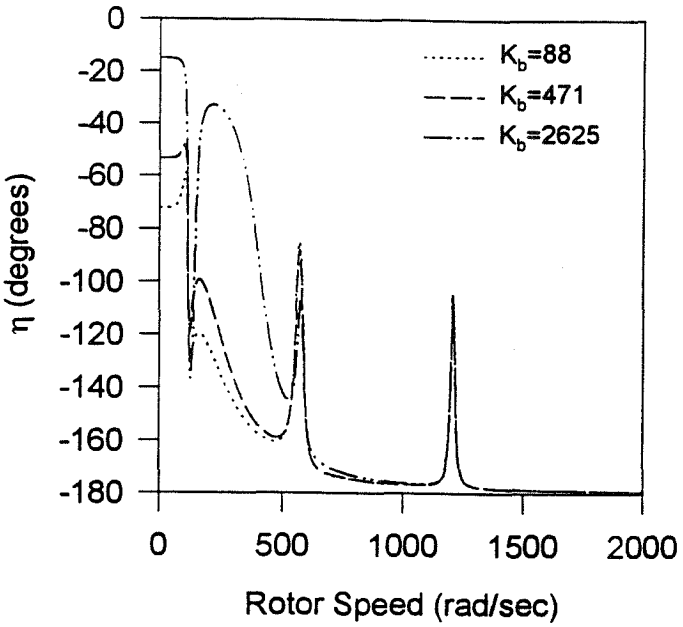

Figure 5.a Phase Lead for Varying Auxiliary Bearing Stiffness

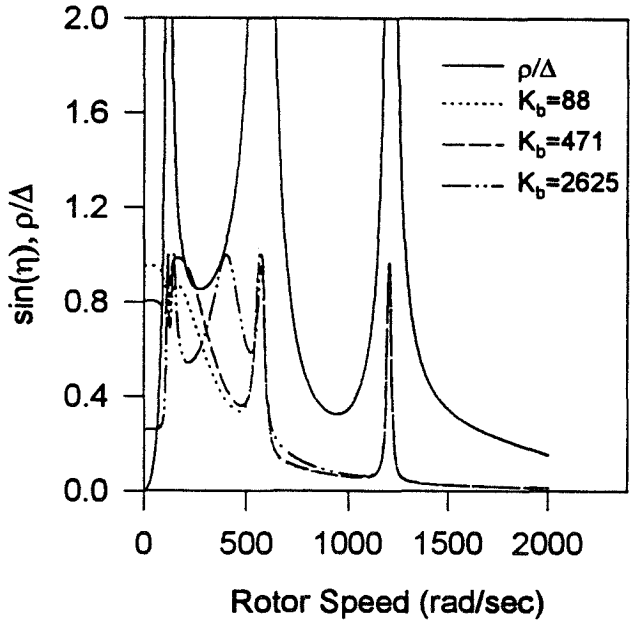

Figure 5.b Noncontacting Imbalance Response Amplitudes and sin(η) for Varying Auxiliary Bearing Stiffness

.CKNOWLEDGEMENT

This work was supported by NASA under Grant o. NGT-70312 and Grant No. NAG3-1507. The overnment has certain rights in this material. Apreciation is expressed to S.G. Ryan and A.F. Kascak ır their advice and assistance in this research effort.

REFERENCES

Black, H. F., 1968, "Interaction of a Whirling Rotor With a Vibrating Stator Across a Clearance Annulus," *Journal Mechanical Engineering Science*, Vol. 10, No 1, pp. 1–12.

Childs, D. W., 1982, "Fractional-Frequency Rotor Motion Due to Nonsymmetric Clearance Ef-

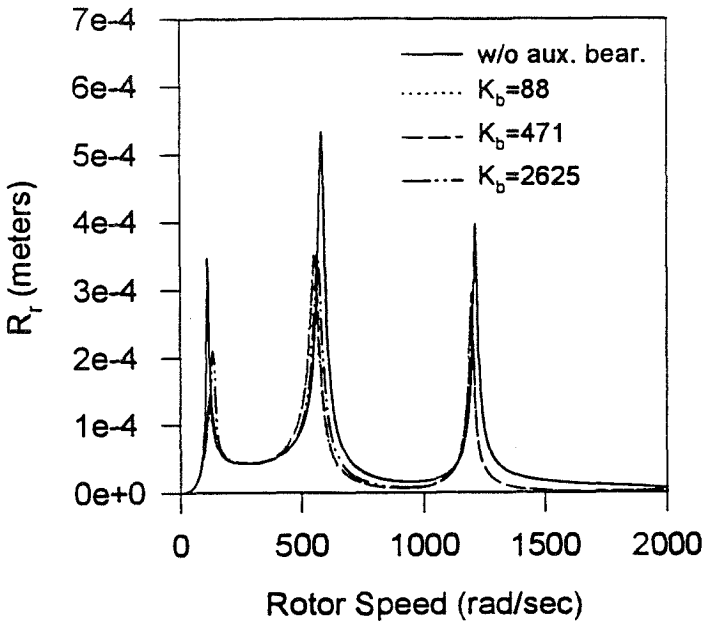

Figure 5.c Simulation Rotor Response Amplitudes for Varying Auxiliary Bearing Stiffness

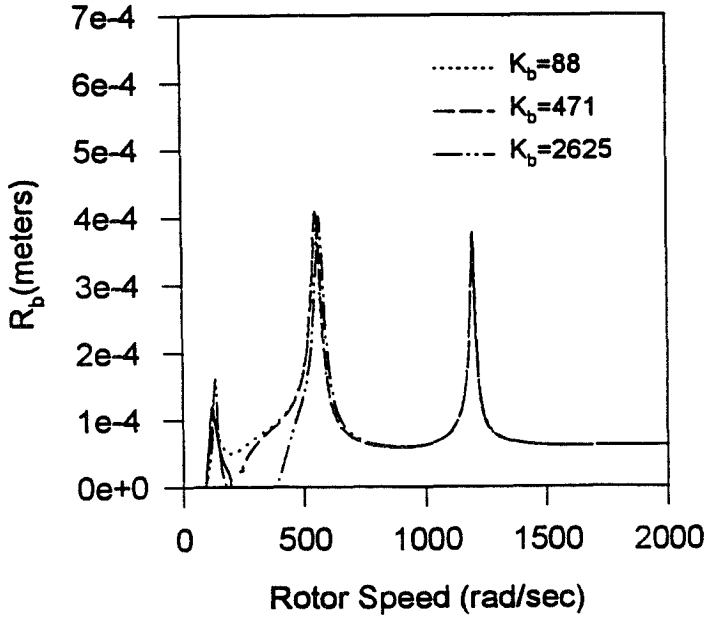

Figure 5.d Simulation Bearing Response Amplitudes for Varying Auxiliary Bearing Stiffness

fects," *ASME Journal of Engineering for Power*, Vol. 104, pp. 533–541.

Ehrich, F. F., 1965, "Bistable Vibrations of Rotors in Bearing Clearance," ASME Paper 65–WA/MD–1.

Ehrich, F. F., 1988, "High Order Subharmonic

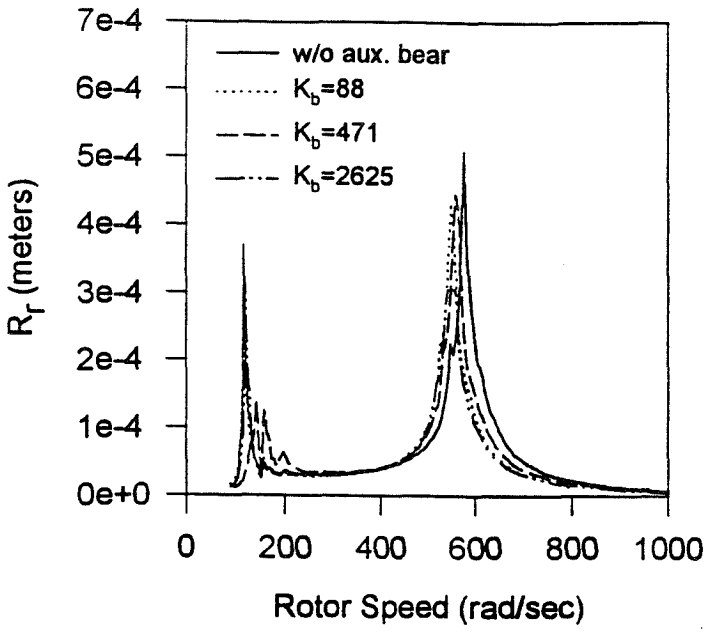

Figure 5.e Experimental Rotor Response Amplitudes for Varying Auxiliary Bearing Stiffness

Response of High Speed Rotors in Bearing Clearance," *ASME Journal of Vibration, Acoustics, Stress, and Reliability in Design*, Vol. 110, pp. 9–16.

Ishii, T., and Kirk, R. G., 1991, "Transient Response Technique Applied to Active Magnetic Bearing Machinery During Rotor Drop," *DE-Vol. 35, Rotating Machinery and Vehicle Dynamics, ASME*, pp. 191–199.

Kim, Y. B., and Noah, S. T., 1991, "Steady-State Analysis of a Nonlinear Rotor-Housing System," *Journal of Engineering for Gas Turbines and Power*, Vol. 113, pp. 550–556.

Lawen, James L., Jr., and Flowers, George T., 1995, "Synchronous Dynamics of a Coupled Shaft/ Bearing/Housing System With Auxiliary Support From a Clearance Bearing: Analysis and Experiment," presented at the *ASME International Gas Turbine Congress and Exposition*, Houston, Texas, June 5–8, 1995, ASME paper no. 95–GT–216.